ISSN 1512-3936
ISSN 2960-9682(Onlain)
DOI:https://doi.org/10.52340/building

№4(68) 2023

SCIENTIFIC-TECHNICAL JOURNAL

Tbilisi – 2023

B U I L D I N G

Responsible secretary T. Magradze (Georgia)
Tel: 64-39; 599 478422
E-mail: t.magradze@gtu.ge
Web-site: https:mshen-journal.ge

Indexed in Google Scholar

The magazine is published since 2006

Table of Content

DIAGNOSTICS OF TECHNICAL STATE OF HISTORICAL-CULTURAL MONUMENTS STRUCTURES BY COMBINING INSTRUMENTAL AND NUMERICAL METHODS

Makhaz Tsikarishvili, Gela Kipiani, Nino Tabatadze, Vakhtang Abashidze, Givi Dolidze
Georgian Technical University, Tbilisi 0170,Georgia.
m.tsikarishvili@gtu.ge

Abstract

In the work is developed the diagnosis of the technical state of the historical and cultural monuments structures by combining of instrumental and numerical calculation methods that is carried out on the basis of laboratory, non-destructive control methods and the creation of design models (functional or imitative) at conducting numerical experiments. The methodology of the complex approach to solving the problems related to the maintenance of resource, safety, durability and strength of the monument structure are also stated. The presented methodology envisages the creation of an automated complex in order to periodically check the technical state of the monument.

The analysis of the obtained data provides the basis for the evaluation of the technical state of the monument that provides for the collecting of the structural solution of various reinforcements in a unified base. If necessary, an appropriate amplification scheme should be selected. Finally, we will obtain an assessment of the technical state of historical-cultural monuments, by combining instrumental and numerical methods. All this will give us a noticeable technical and economic effect.

Key words: monument, instrumental examination, model, diagnostics

Introduction

In the period of global, technical, and ecological problems, the refinement and development of methods for diagnosing the mode of deformation of the historical-cultural monuments structures are especially relevant.

Cultural heritage and its material components, historical-cultural monuments - represent an integral part of the Earth's ecosystem, an informational resource of intellectual potential, the preservation of that is necessary for future generations. It is a source of spiritual food, culture, art, knowledge, and experience for future generations. The primary task, with the preservation of monuments, is the study of the given heritage and information. The modern method of assessing the mode of deformation of monuments requires the improvement of the combination of instrumental and numerical methods of diagnosis that gives the possibility to us to manage the state of the monument. It is also necessary to develop a system for the registration, collection, systematization, and storage of the received information for its analytical processing.

Based on all the above-mentioned, the problem is very relevant.

The aim of the paper is to develop the concept of perfecting the methodology for diagnosing the technical state of historical-cultural monuments by combining instrumental and numerical methods.

Main part

The historical-cultural monuments are considered as a system object "monument- environment" and include information in recent years, in the practice of restoration of historical-cultural monuments, there is a trend of complex assessment of their technical state in relation to changing environmental conditions. Therefore, it has become quite reasonable to consider the object of restoration as an element of a complex natural-technical system "monument-environment", in that architectural monument would be imagined as a subsystem, containing some interconnected structural and architectural elements.

We have made an analysis of the structural solutions of the monuments in order to carry out a complex examination of the technical state of the historical-cultural monument and to formulate recommendations in the right direction for conducting the restoration.

Based on the analysis, a classification of structural solutions was created, instrumental measurement methods were used to study the causes of damage and deformations.

In the works [1,2,3,4,5,6,7], the structural types of monuments are considered and the analysis of structural solutions is carried out, on the example of several historical and cultural monuments in Georgia, such as: Alaverdi Monastery, Tsughrugasheni Cathedral, Safari St. Saba Temple, Nikosi Church complex of the Deity, Sanagire Basilica (Gurjaani district), "Eastern" complex (Shikhiani), located on Abo-Tbileli Street #1.

Fig. 1. Shikhiani "Easter" temple

From the considered works of Georgian and foreign scientists [4,5,8, 9] it would be seen that they give preference to construct an experimental model and testing it on a vibro table, or by numerical methods, by construction of design model, processing schemes for reinforcing structures.

Based on the literature review, it is determined that conducting the experiment requires a long time and high material expenses, and the construction of the design model and the calculation using only numerical methods does not give the desired results. Therefore, we considered it is necessary to improve the existing methodology by combining experimental and numerical methods.

For the restoration-reconstruction of historical-cultural monuments, it is appropriate to consider the features of their structures and the working principles of individual elements as independent structures, determining their deformability and bearing capacity.

The features of the types of arched structures of the historical-cultural monuments in Georgia are considered, on the example of the structures of the historical-cultural monuments.

We have considered different types of the most common structures: cylindrical dome (Fig. 2), cross dome (Fig. 3), closed dome (Fig. 4) and closed arches (Fig. 5).

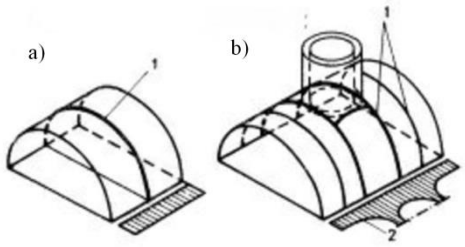

Fig. 2. Cylindrical dome

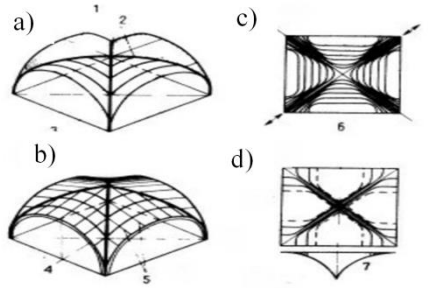

Fig. 3. Cross dome

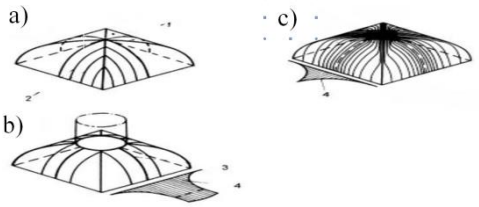

Fig. 4. Closed dome

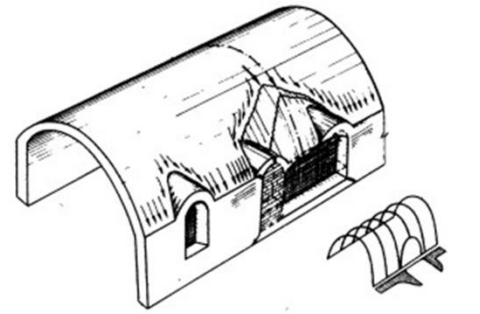

Fig. 5. Closed arches

The considered examples showed that the rigid element gives the possibility to significantly damaged arch systems to maintain their original shape for certain time even in the absence of their "supporting restraint".

The shape of dome or arch, in that arbitrary section under load works in accordance with the most rational mode, are symmetrically compressed, is the most rational shape.

In practice, most of the arches were built for technological and operational reasons, as well as from purely aesthetic considerations, are not rational. Their cross-sections are asymmetrically compressed or undergo different types of stress.

The height of the compressed zone of the cross-section is the main indicator, both in terms of stability and in terms of the arch structure ability. This applies to arches made of brick and stone. For any non-centrally compressed section, the height of the compressed zone is approximately equal to twice the distance from the point of application of the normal force to the nearest edge of the section, i.e.

$$h_c=(\frac{h}{2}-e)2,$$

where h_c - is the height of the compressed zone; h - is the total height of the section; $e=\frac{M}{N}$ - is the eccentricity of application of normal force with respect to the center of the section.

By decreasing the height of the compressed cross-sectional area, the streses increases, while at the same time the stability of the arch contour decreases. This attitude is expressed by the formula.

$$\sigma = \frac{N}{F_c \ \varphi},$$

In this formula F_c - is the area of the compressed cross-section; φ - is a coefficient that includes the off-center compression of the cross-section.

The minimum height of the compressed zone, at that the structure still maintains equilibrium (stability) depends on various factors, specifically: the value of the load and the normal compressive force N, the dome span, the quality of the construction material, and others. The design theoretical height of the compressed cross-sectional area would sometimes be controlled by measuring (probing) the depth of connecion areas.

Each type of structure is characterized by a specific type of deformation, which is included in the characteristics of the working scheme. Along with the change of the working scheme and the condition of the construction material, the deformation expression and deformability change.

The characteristic location of cracks in cylindrical, cross, and closed domes with respect to main types of arches and main types of deformations is determined.

The sensor system gives the possibility to control the increase in stress and the occurrence of deformations in the structures of buildings or the deviation of its main elements from the vertical, horizontal displacement on a defined horizon, to estimate the amount of pressure on the ground of the object, the amount of wind load on the upper levels, to control the geological and hydrogeological condition of the building base.

Exceeding the allowable operational loads or negative impacts that lead to the loss of stability of the structure will generate an alarm signal. On the diagnostic scheme, the accident zone may be allocated, and the type of impact specified.

The concept of perfecting the method of diagnosis of the mode of deformation of the structures of historical-cultural monuments by a combination of experimental and numerical methods has been developed that is presented in the form of a block diagram of hardware-computer diagnostics of the stressed-deformed state of the historical-cultural monument (Fig. 6).

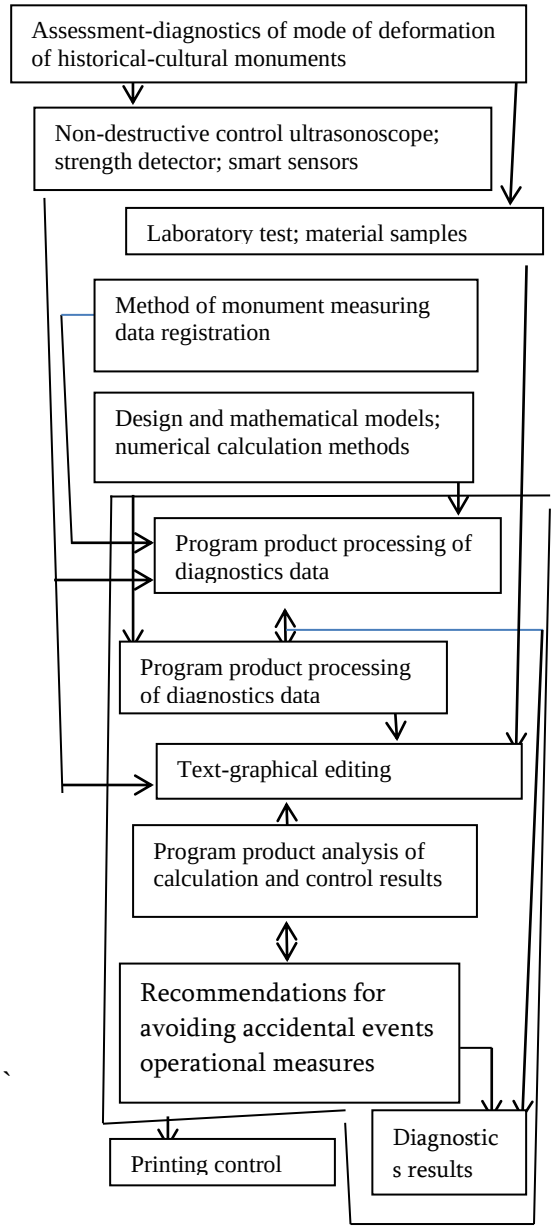

Fig. 6. Block diagram of hardware-computer diagnostics of the historical-cultural monument mode of deformation

Diagnostics of the historical-cultural monuments mode of deformation by combining experimental and numerical methods is a methodology that includes a complex of hardware-computer diagnostics and combines non-destructive, modern methods of control, laboratory testing of the used material and realization of the obtained results by numerical methods (e.g. finite element method), based on the principle of entering the received data into the reporting model.

The study of the Shikhiani "Easter" temple structures was carried out with the developed methodology. The data of the visual and instrumental examination of the technical state of the load-bearing

structures are presented. After drawing up and calculating the design models of the objects under examination, the analysis of the results of the calculation was carried out, after which the enhanced model was calculated, and a comparative analysis was made. In the paper are presented both the results of the calculation and the reinforcing schemes of the damaged structure in an illustrated form, which are stated below.

Design model of Shikhiani temple and its calculation design program SAP2000 fragments

Design model of Shikhiani temple and its analysis Fragments of CAE program SAP2000

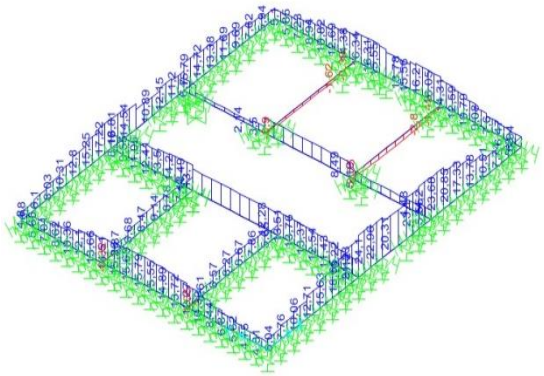

Fig. 7. Diagram of of stresses redistribution on foundation in the case of clay ground, SAP2000

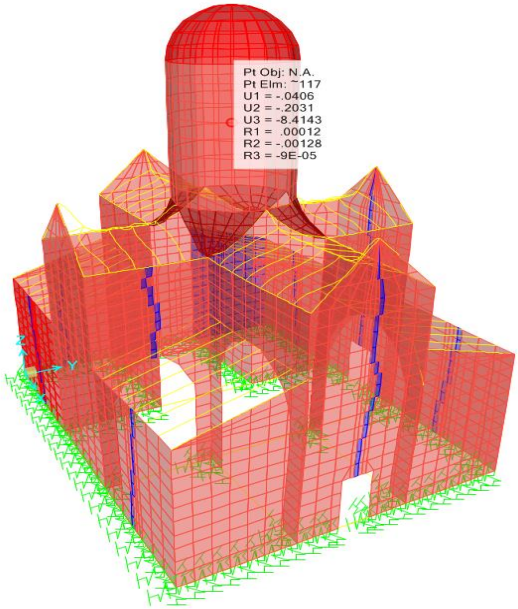

Fig.8, a. Displacements at wind load, SAP2000

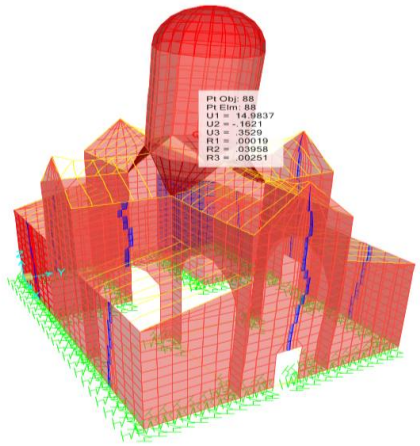

Fig. 8, b. Displacements at earthquake, SAP2000

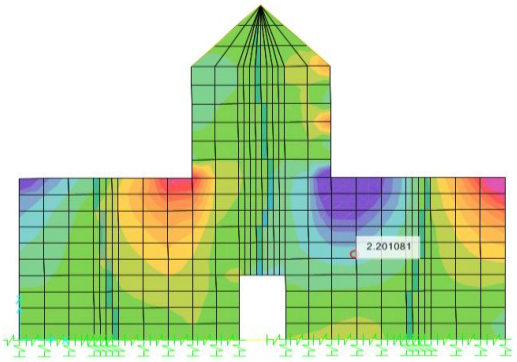

Fig. 9, a. Cracks distribution on west façade prior model reinforcement, SAP2000

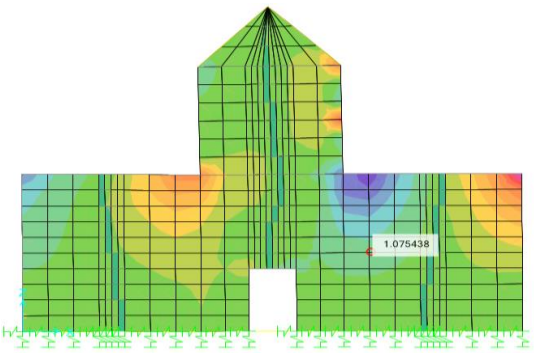

Fig. 9, b. Cracks distribution on west façade in reinforced model, SAP2000

The stress permissible limit for such type buildings is presented as 1,1, that is accepted from norms for for masonry and reinforced masonry structures (SNiP II-22-81).

On the structure (dark color on the structure, SAP2000 Critical locations are shown). From calculation is clear that stresses in reinforced model satisfy the proper norms.

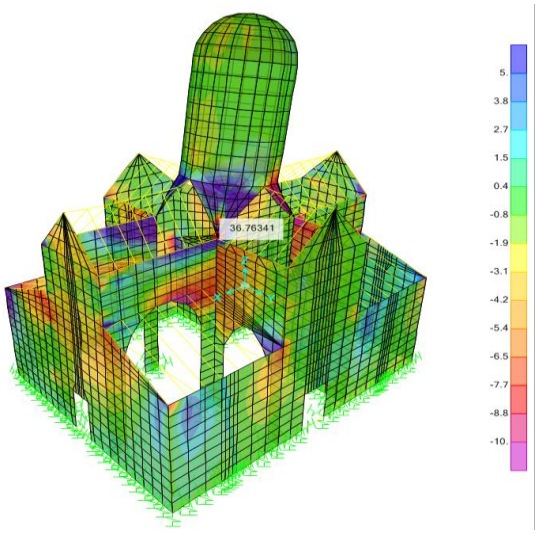

Fig. 10, a. Stresses distribution on whole structure of model under reinforcement, SAP2000

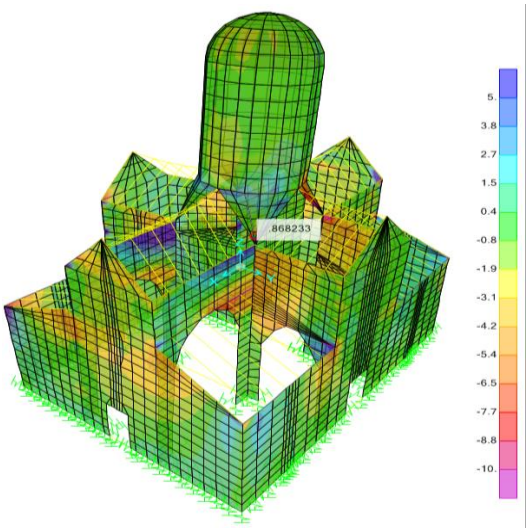

Fig. 10, b. Stresses distribution on whole structure of reinforced model, SAP2000

The models are calculated using the finite element method in the "SAP2000" program, in accordance with acting in Georgia norms. Design schemes are built according to architectural and structural projects. Permanent, temporary and wind loads are modeled on buildings and calculated according to wind pulsation effects. The impact of the seismic force on the structure is also considered, taking into account the relevant norms.

Buildings were calculated by stresses combination.

The maximum displacement obtained by the wind load for the Shikhiani "Easter" temple is 20 mm, which is permissible, considering the relevant norms, and as a result of the seismic impact, we get the maximum displacement, in value - 146 mm, which is quite a large displacement.

The analysis of the results of the calculation showed us that horizontal deformations under static load in some elements of the building are not allowed.

The analysis obtained from the results of the calculation requires structural reinforcing of the monument.

Conclusions

1. The structural solutions of the existing historical-cultural monuments are analyzed, their classification is made (for example, cylindrical dome, cross dome, closed dome and closed arches), the architectural monument is presented as an element of a complex natural-technical system "monument-environment" that contains mutual connecting structural and architectural elements.
2. The block diagram of hardware-computer diagnostics of the historical-cultural monument mode of deformation has been developed, in which the methodology of the monument state examination is provided, combining experimental and numerical methods.
3. The technical state of the historical-cultural monument - Shikhiani "Easter" temple building was studied using the developed methodology.

Reference

[1] M. Tsikarishvili, N. Tabatadze, M. Vardiashvili, A. Katamidze - Ecological and technical monitoring of Georgian historical-cultural monuments, Scientific-technical Journal "Mshenebloba" N3(34), 2014, pp. 18-24.

[2] M. Tsikarishvili, N. Tabatadze, M. Vardiashvili, I. Garibashvili - Analysis of structural solutions of existing on territory of Georgia historical-cultural monuments, Scientific-technical Journal "Mshenebloba" N3(38), 2015, pp. 44-53.

[3] M. Tsikarishvili, U. Dzodzuashvili, N. Tabatadze, M. Vardiashvili - Analysis of building monitoring systems, Scientific-technical Journal "Mshenebloba" N3(38),2015, pp. 117-128.

[4] N. Tabatadze – Research of deformability of historical-cultural monuments structures, Scientific-technical Journal "Mshenebloba" N4(43), 2016, pp. 81-84;

[5] M. Tsikarishvili, N. Tabatadze – Control of historical-cultural monuments mode of

deformation and creation of diagnostics organizational structure, Scientific-technical Journal "Mshenebloba" N1(44), 2017;
[6] N. Tabatadze – Perfection of historical-cultural monuments structures yrchnical state diagnostics by combination of experimental and numerical methods, Collection of GTU Scientific Works, N3(505)-2017.
[7] N. Tabatadze. Analysis of historical-cultural monuments structural solutions, Collection of fbstracts of Georgian Technical University students 83 Open International Scientific Conference, p.7.
[8] J. HOŁA, K. SCHABOWICZ, State- of-the-art non-destructive methods for diagnostic testing of building structures – anticipated development trends, Wrocław University of Technology, Wybrzeże Wyspiańskiego 27, 50-370 Wrocław, Poland, 2010, p. 6-7;
[9] Paulo B. Lourenço, Rob van Hees, Francisco Fernandes, Barbara Lubelli, Character i zation and damage of brick masonry; ISISE, Department of Civil Engineering, University of Minho, Azurém, P 4800-058 Guimarães, Portugal;

DEHYDRATION OF THE CRUSHED MOUNTAIN ROCK MASS - ADDITIVE FOR IMPROVING THE STRUCTURE OF CONCRETE OBTAINED BY GRINDING

Razhden Skhvitaridze, Tamaz Batsikadze, Malkhaz Turdzeladze, Davit Bedukadze, Akaki Skhvitaridze, Levan Baramadze

Georgian Technical University, Tbilisi 0170, Georgia.
davidbedukadze@gmail.com

Abstract

The influence of the concrete additive obtained by dehydration-grinding of the mass of crushed mountain rocks brought by landslides from the massifs of the mountains of Georgia on its strength has been studied. It is established that without reducing the strength, it replaces an average of 20% of cement in concrete, thereby: reducing CO_2 emission and footprint ("Carbon footprint") and the cost of concrete; reduces the size and number of voids and pores in concrete; does not increase the water/cement ratio in concrete; prevents negative events caused by free lime (CaOtav.) added to concrete with cement;

Keywords: concrete, innovative admixture, dehydration, clays, argillites, portlandite, prevention, pozzolanization, rehydrogenation, pores and voids.

Introduction

By utilization of the mass of debris mountain rocks brought by landslides from the mountains, or excess soil formed on construction sites: dehydration-grinding.

Dehydration by retaining silicate mineral structure (Know-how).

It is ground so that the average size of the filler grains is greater than the maximum of cement used in concrete, less than the minimum of sand. During hardening of concrete, rehydro-liming occurs with the formation of structural crystal hydrates.

The tobermorite, stratlingite, generated in filler, together with cement ettringite form fiber-needle-flaky habit clusters by modifying the structure of cement concrete with 3D self-nano-reinforcement, by reducing the anisotropy of strength - by increasing of stability to loads with variable direction- magnitude.

of Georgian clays by thermal dehydration in cement concrete technologies, which will create the preconditions for cement concrete pozzolanization by rehydro-liming, so the study of the basics of this process is actual.

Main part

Concrete void filler (According to EN 206-1:2013, type II addition), is ready for use as an ingredient in concrete as a Type II admixture **[1].**

Even in the 21 century, cement and concrete made from it are products in high demand. By 2023, global cement production has reached 4.0 billion tons, and concrete has reached 10.0 billion m^3. According to the calculation, for every 1 person living on earth, [(4.0/8.0) billion t] there is 0.5 t of cement and (10.0/8.0 billion m^3) 1.2 m^3 of concrete produced.

Problem 1. During the production of 1 ton of cement clinker, the "carbon footprint" released at 1500 ^{0}C is equal to 0.8 t of CO_2 on average. **[2].** In turn, if the cost of cement in traditional concrete = 300-400 kg/m^3, then "Carbon footprint" = 240-320 kg/m^3, i.e. (240-320) x 1.2 = 288-384 kg/m^3 per person, which is a very large amount and should be reduced.

Concrete according to EN 206-1:2013 **[1]** is made of cement containing grains of 0-90 μm, fine filler with grains of 0-5000 μm - sand, coarse aggregate containing grains of 6(6000 μm)-40(70) mm (gravel), mixed with water.

According to BS EN 197-1:2011 **[3]**, cement is mainly prepared by ultrafine grinding in separators or mills, and also - mainly on the basis of clinkers fired using the "dry method";

Problem 2. The amount of CaO_{free} in the clinker fired by the "dry method" = 2-3 mass % - which then passes into the concrete and causes negative results: the unstable mineral portlandite $Ca(OH)_2$ is formed in the hardened concrete mass, which

reduces the stability of the concrete. This problem needs to be solved!
bending strength R_c /R_b >10, and 20 times higher than tensile - RJR. >20. It is an anisotropy of strength. The mineral portlandite $Ca(OH)_2$ (CH in CCN notation) is responsible for it, which is formed in cement from cement minerals . The strength of aggregates in cement-concrete is on average 6-7 on the Mohs scale, of the cement stone - 4-5, and of Ca(OH)z- 2-3. Cement-concrete collapses at the cement/filler boundary during bending loads, because the weakest compound Ca(OH)z is accumulated there, as confirmed by Stark eta!. (2001). In addition, during sulphate corrosion of Ca(OH)z by the action of SOi• penetrated from the outside into the cement concrete, late but inevitably reducing the bending and compression strength of structure, it forms the expansive mineral ettringite C3AC3SH 32 (CCN) with fiber-needle-flaky habitus.

$Ca^{2+}+SO_4^{2-}+2H_2O=CaSO_42H_2O$ (1)

$3CaS0_4+3Ca0•Al_20_3+32H_20=3CaO•Al_20_3.3CaSO_4$ $32H_2O$ {C3AC3SH32(CCN)} (2)

In the 21th century increasing of market demand and structure stability and prevention of cement concrete anisotropy is realized by: metal reinforcement - macro reinforcement , as well as by fibers -volume 'dispersed 3D micro reinforcement'.

In the 20 ph century, in some countries, in order of cement economy and intensification of cement concrete hardening process started mixing of highly active filler metakaolin – Al_20_3 •$2Si0_2$ obtained by thermal treatment of kaolin clay, in the cement composition, as Kakali eta! 2001, as well as Kovo 2011), as well Mansour eta! (2012), confirmed. The basis for the use of metakaolin in cement-concrete is the property of mineral kaolinite Al_20_3•$2Si0_2$•$2H_20$: in result of heating above 550^0•C the kaolinite structure dehydrates and at 700^0C irreversibly forms the mineral metakaolin Al_20_3 •$2Si0_2$ which according to Tailor H.F.W., acting with $Ca(OH)_2$ of cement concrete causes pozzolanization , i.e. a reaction of binding to SiO_2 and Al_20_3 . Calcium hydro silicate $CaO•SiO_2•H_2O$ (CCN) and calcium

hydro aluminosilicate stratlingite C_2ASH (CCN) are formed in cement concrete. Scientific novelty of the research is: the initial hypothesis formed based on Roman/Georgian construction traditions, as well as using the analysis of references : cement concrete strength anisotropy and building and structure instability can be prevented by: dehydration maintaining of habit of the main constituent mineral of aqueous aluminosilicate rock (e.g. clay); mixing of obtained modifiers in cement concrete; pozzolznization with rehydro-liming with portlandite Ca(OH)z; 3D nano-reinforcement of the interfacial transition zone in cement concrete- with an increase in bending strength.

Problem 3. When assessing the quality of concrete, they consider only defects caused by mistakes made in the process of manufacturing concrete products **[4].** They do not consider technological deviations in the production of cement and concrete. In particular, the maximum sizes of ultra-finely ground cement grains in separator mills do not exceed 40-50 μm, and the minimum sizes of fine aggregate sand grains used in concrete are slightly less than 140 μm. Therefore, there is a shortage of 50-140 μm cement-sand grains in modern concrete **(Fig. 1.)** and the so-called "Filling defects in concrete", which is finally reflected in the mass of concrete and the formation of macro-sized voids on the surface **(Fig. 2.);**

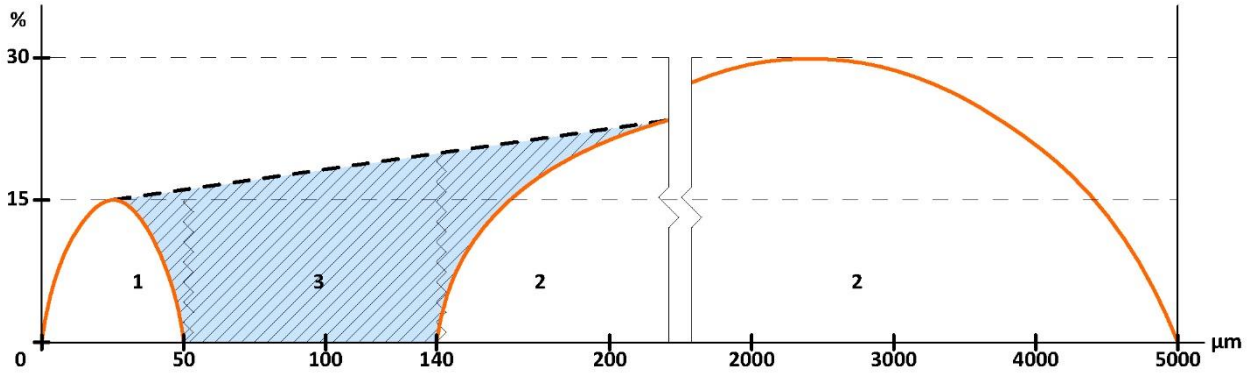

Fig.1. Granulometry of grains of Cement and Sand in a concrete mix
1 – Cement; 2 – Sand; 3 – Deficiency of 50-140μm grains of Cement and Sand in the concrete mixture.

Fig.2. Macro-sized voids on the concrete surface

Problem 4. In mountainous countries, mountain rivers are characterized by periodic flood regime. A typical structural landslide **[5]** is created, which brings clay-like mass containing silica (SiO_2) and alumina (Al_2O_3) turned into mud from the mountains to the location of accumulation with a capacity of no less than 200 m^3/s. In particular, in Georgia, the Duruj River brings it down from the Caucasus mountains every year and "collects" it in the valley above Kvareli as a mass containing no less than 0.5 ml/m^3 of stone-gravel clay-shale. It is necessary to take out and utilize the mass of crushed mountain rocks brought from the mountains by torrents from the river bed, because otherwise devastating negative events and consequences are expected for the city of Kvareli.

During the construction of foundations, tunnels and other facilities, an excess amount of clay soil containing silica (SiO_2) and alumina (Al_2O_3) is inevitably generated, which must be removed and utilized **[6].**

To determine the temperature range in which the clay transforms into a modified form, DTG was carried out, the curves of which are shown in Figure 3.

According to DTG data, the endothermic effect at 100-150 oc is present on all curves, which corresponds to the removal of physically bound water. In the temperature range 650-850 °C, an endothermic effect is observed, which is obviously associated with the dehydration of the crystal lattice of clay minerals and their transition to an amorphous form - metakaolin. The peak of this endothermic effect at a relatively low temperature (718 °C) is observed in Gardabani clay, which indicates a high tendency to temperature activation - modification, and therefore all our further studies were carried out only on Gardabani clay.

To determine the temperature changes in the mineral composition, Gardabani clay was heated

in a laboratory muffle furnace at temperature 550, 600,
700 and 800 oc with a holding time of 1 hour.
Calcined samples were subjected to X-ray phase
analysis. The x-ray diffraction patterns (Fig. 4) clearly show the phase changes of the clay with an increase in the firing temperature. On the diffractogram a (original clay) the clay mineral chlorite is presented
(14.65, 7.55, 4.46, 3.74) A. With an increase in the firing temperature (b, c, d, e), the amount of chlorite decreases, and X-ray amorphous phase appears (in the form ofbulge).

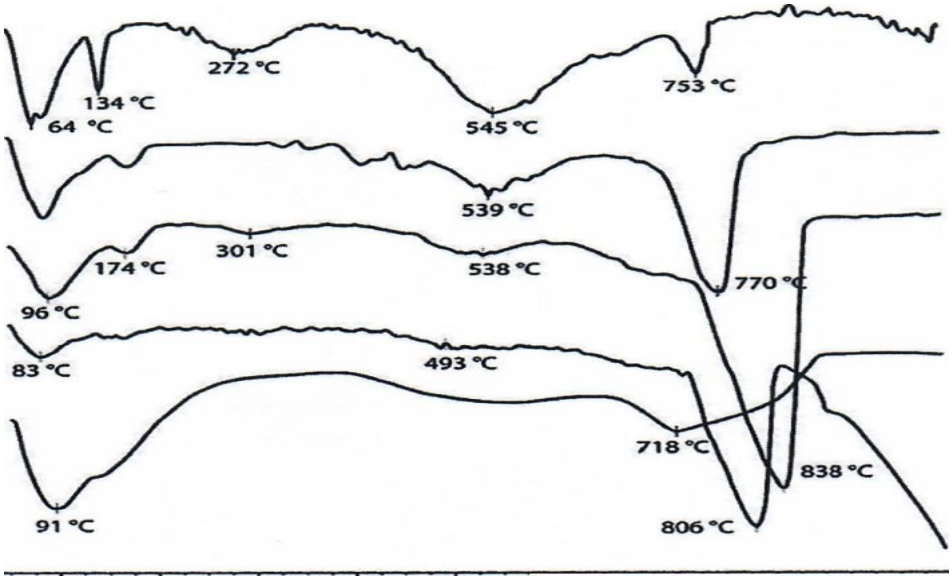

Fig. 3. Clay DTG curves: a– Duruji, b – Teleti, c– Metekhi, d -Miriani, e – Gardabani.

It is obvious that during the heat treatment of clay rocks from 550 °C, dehydration of clay minerals begins and metakaolin appears, i.e. fired clay acquires pozzolanic properties to bind Ca(OH)2 into calcium silicate hydrates.
The ability to bind $Ca(OH)_2$, i.e. the determination of the pozzolanic activity of the modified additives was carried out according to GOST R 56593-2015 by the absorption of $Ca(OH)_2$ from its aqueous solution, recalculated into CaO.
The additive is considered highly active when the amount of CaO absorbed exceeds 70 mg/g, moderately active when the amount of CaO absorbed is in the range of 30-70 mg/g and considered low active when less than 30 mg/g of CaO is absorbed.
Gardabani clay heat treated at different temperatures, showed the best absorption ofCaO from the lime solution at all stages of the test. The reactivity of heat treated clayey rocks to $Ca(OH)_2$ is explained by the fact that at 600-800 °C the kaolinite mineral $Al_20_3•2Si0_2•2H_20$ - is dehydrated and transformed into an active anhydride - metakaolin (Al_2O_3 •$2Si0_2$).
Based on the results of this study, it is possible to determine promising local rocks, which, when developing a temperature modification regime in order to increase pozzolanic activity, are able to significantly reduce the proportion of clinker in the composition of Portland cement and the proportion of the cement in the composition of cement concrete, without reducing mechanical strength. Such a rock is, Gardabani clay -heat treated at 700 °C.

Startup idea. To create a pozzolanic property **[**capable of hydraulic reaction with $Ca(OH)_2$, or containing $\mathbf{SiO_2}$ or $\mathbf{nAl_2O_3 * m\ SiO_2}$**]** for filling voids caused by the lack of 50-140 μm grains in concrete. Which with the "presence" of 50-140 μm grains ensures the elimination of structural voids in the concrete mass and surface, due to the modification of unstable $Ca(OH)_2$ into water-stable compounds by the pozzolanization reaction - "doesn't exist anymore":

$5Ca(OH)_2 + 6SiO_2\ n\ H_2O + 4H_2O = 5CaO * 6SiO_2 * n9H_2O$ [C-H-S (1)] (3)

$Ca(OH)_2 + nAl_2O_3 * mSiO_2 + zH_2O = CaO * nAl_2O_3 * mSiO_2 * zH_2O + H_2O$ (4)

Start-up offer. In order to prevent the problem of lack of 50-140 μm cement-sand grains in concrete and the presence of $Ca(OH)_2$, the filler will be made by utilizing the mass of debris mountain rocks brought by the mountain mudflow, or excess soil generated at construction sites: by dehydration-grinding.

Mountain rocks or soil must contain either at least 25% silica (SiO_2) and at least 5-12% alumina (Al_2O_3), or at least 30-40% **$nAl_2O_3 * mSiO_2 * pH_2O$** type aluminium silicate.

Innovative. Prepared according to the outline presented in Fig. 4: by dehydrating the mountain rocks containing clays brought down from the mountains, or the soil containing argillites formed on the construction site, preserving the mineral structure (heat reament possible in all types of ovens at a temperature not more then 800 ^{0}C), after which it goes through a grinding process so that the average size of the filler grains (D_{filler}) should exceed the maximum of cement used in concrete (D_{cement}>40 μm) and should be less than the minimum of sand (d_{sand} <140 μm). This condition is achieved by grinding in such a way that the residue on sieve № 014 does not exceed 5 mass %.

Table 1. Oxide composition of the used mountain rocks

Name:	Chemical Composition mas%:										
	SiO_2	Al_2O_3	Fe_2O_3	FeO	MgO	CaO	MnO	R_2O	Low	H_2O	Total
clay shale	59,23	18,02	4,58	2,41	2,31	1,01	0,38	5,10	4,90	2,06	100,00
argillite	56,77	22,07	0,89	5,54	2,59	0,67	0,08	3,80	5,37	2,22	100,00

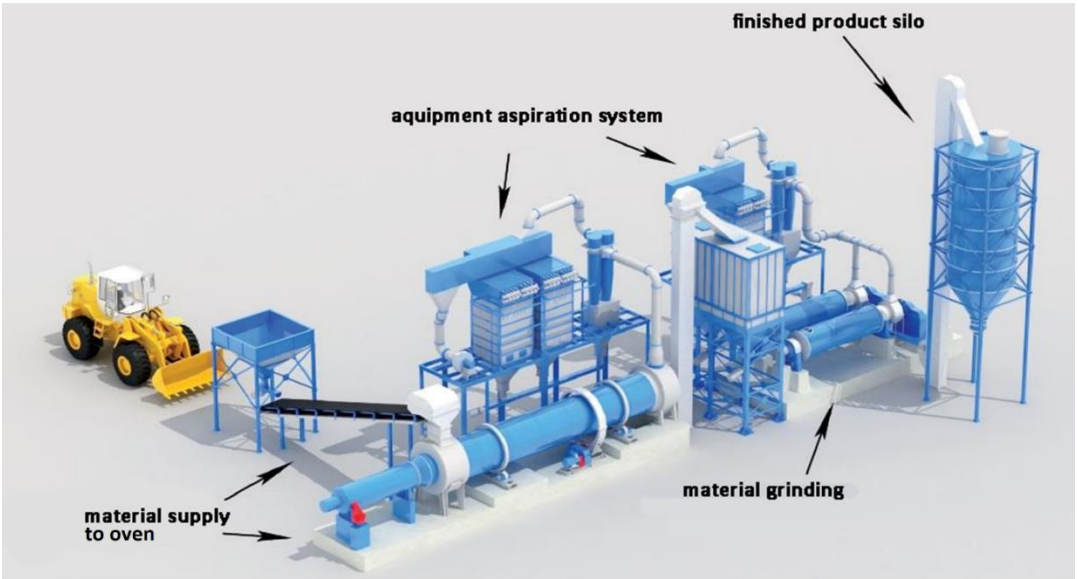

Fig.4. Technological Line for the Production of Filler

The result is that the filler:

- **It is highly ecological and less energy intensive.** The carbon footprint is reduced by reducing the CO_2 emission in the environment during the production of the filling, as only 30.0 kcal/kg of heat and 0.0058 kg/kg of conditional heat are spent on dehydration. 1100 kcal/kg of heat and 0.292 kg/kg of conditional heating are spent on making clinker.

- In traditional concrete manufacturing technology, on average 20% (10-30%) of the cement mass will be replaced by concrete void filler - while maintaining the design strength, which will reduce the carbon footprint from 240-320 kg/m^3 to 192-256 kg/m^3.

- The cost of concrete also decreases. If 1t of cement costs $80.0, and 1t of filler costs $20.0, then the cost of cement in 1m^3 of unfilled B30 class concrete will be $80.0*0.4t/$m^3$ = $32.0/$m^3$, and the cost of cement-filling in filled B30 class concrete will be $80.0*0.32 $/$m^3$=25.6$/m^3. The cost of 1m^3 B30 grade concrete decreased by $6.4/$m^3$.

- **The practical value of the innovative filler** is that it prevents the deficiency of 50-140 μm grains and the presence of **$Ca(OH)_2$** in concrete and is **highly economical**; The market value of the well-known "Filler" is 25-30 $/t, and the innovative filling is within 20-25 $/t;

- The volume of the Georgian concrete market exceeds 7.0 million m^3. In case of mixing 20 mass % innovative filler in all manufactured concrete, commercial/economic effect: 7.0 mln.m^3 * 5$=5.6 mln.$.

- Defects in the form of cracks and voids will no longer occur in the concrete product(s). In Georgia, the builder's time and money will no longer be spent on their prevention, which will speed up the construction process. It will contribute to the sustainable development of the economy in general.

Innovative Concret void filler- is a pinkish-brownish-blackish powder.

The grain-particle sizes are 40-140 μm; specific surface 2300 - 2700 cm^2/g; true density 2.7 g/cm^3; bulk density 800 kg/m^3; Water requirement <25%; Pozzolanic activity 40 – 80 mg CaO/1g active mineral additive. The sale can be carried out either packed in bags of 25-40-50 kg capacity, "big-bags", or in bulk form;

Shelf life without deterioration of properties is 1 year.

The technological readiness level exceeds **TRL-5** and is ready for **Pilot** testing.

Conclusion

supplement will prevent the problems and defects caused by the lack of 50-140 μm grains in the concrete mixture: it will improve the flowability of the concrete mixture, and it will reduce the size and number of macro-sized voids and pores in the mass and surface of the hardened concrete.

- When the concrete hardens, rehydro-liming will occur, with the formation of structural crystal hydrates. This is an innovation [7]

- prevention of negative events caused by free CaO added to concrete by cement.

Reference

[1]. GOST R. 57345-2016/(EN 206-1:2013. Concrete – Part !: Specification, performance, production and conformity, IDT);

[2]. European Commission. Integrated Pollution Prevention and Control. Reference Document on Best Available Techniques in the Cement and Magnesium Oxide Manufacturing Industries.May 2010". http://eippecb.jrc.ec.europa.eu

[**3].** BS EN 197-1:2011 Cement Composition, specifications and conformity criteria for common cements;

[4]. 7 Types of Construction Defects in Reinforced concrete. https://theconstructor.org/concrete/construction - defects - concrete – structures/8472/#.

[5]. Ivo Baselt a, Gustavo Queiroz de Oliveira a , Jan-Thomas Fischer b , Shiva P. Pudasaini c,d, Evolution of stony debris flows in laboratory experiments. Geomorphology 372 (2021) 107431. https://doi.org/10.1016/j.geomorph.2020.107431 Evolution of stony debris flows in laboratory experiments (uni-bonn.de);

[6]. National Waste Management Strategy for 2016-2030 (in Georgian).

https://www.gov.ge/files/55440_55440_810817_convert-jpg-to-pdf.net_2016-05-05_14-41-01.pdf;

[7]. R.Skhvitaridze, E.Shapakidze, I.Gejadze, M.Abazadze, M.Turdzeladze, T.Cheishvili, A.Skhvitaridze. "PHYSICAL-CHEMICAL PRINCIPLES OF CLAY MODIFYING INTO FILLER, POZZOLANIZATION THROUGH REHYDRO-LIMING, FOR CEMENT CONCRETE RESISTANCE TO THE NATURAL DISASTERS". Acta Geodynamica et Geomaterialia. Vol.18., No. 4(204), 503-510, 2021. **DOI**:10.13168/AGG.2021.0036. journal homepage: https://irsm.cas.cz/acta.

This work was supported by Shota Rustaveli National Science Foundation of Georgia (SRNSFG) [grant number AR-22-2064.]

CONSISTING OF SMALL OSCILLATION COEFFICIENTS / HIK/ MATRIX REDUCTION, FROM POSITIVE ELEMENTSON THE CONTAINED MATRIX

Gela Kipiani, Ana Tabatadze, Irma Garibashvili
Georgian Technical University, Tbilisi 0170, Georgia
gelakip@gmail.com

Abstract

The issues of studying linear oscillations of a discrete mechanical system based on analytical mechanics, which are included in the field of teaching theoretical mechanics and construction mechanics, are presented. The development of modern techniques is impossible without considering oscillatory processes, which is why every work in the theory of oscillations is important.

Keywords: oscillation, theory, mechanical system, motion.

Introduction

Such movement of the system, which is repeated with respect to some average location (in particular, with respect to the equilibrium location of the system) is called oscillation. Oscillation theory is currently a widely developed independent discipline with its complex mathematical apparatus. Vibration of buildings and machines, electromagnetic oscillations in radio equipment and optics, sound and ultrasonic oscillations, oscillations affecting the nervous-psychic state of a person and so on, all these seem to us to be different, but the methods of mathematical physics combine them under one name - oscillation.

Back in classical mechanics, when Galileo, Huygens and Newton studied the movement of a mathematical pendulum, the beginnings of modern oscillations were observed. Oscillatory processes in systems with constant parameters (linear systems) were formulated in the works of Lagrange, later he received the name of the theory of linear oscillations. These oscillations are described by linear differential equations with constant coefficients.

For many scientists, linear differential equations (linear oscillations) have become a powerful tool for scientific research. For example, A.N. Krilov and his students developed the theory of linear oscillations and successfully used it to solve such problematic problems as ship rocking, gyroscope theory, and artillery problems. Artillery tasks.

They were not used in the first stage of the study of oscillations by the method of linearization (Ostrogradsky, Helmholtz, Rayleigh). At the same time, the fact that in the last century there was a mathematical apparatus, by the generalization of which it was possible to study non-linear oscillations, at least oscillations quite close to linear ones. An oscillation quite close to linear is called an oscillation whose corresponding differential equation contains a small parameter e, for which, by assigning a zero value, we get an ordinary linear differential equation. Astronomers, while studying two- and three-body problems, were the first to consider nonlinear equations containing small parameters. [1-14]

In the formation of the theory of oscillations, the fundamental role was played by the works of van der Pol, some about oscillations, etc. Andronov's study of autocurrents in non-linear systems. It should also be noted that L. Works of Mandelstam, where a general approach to the study of oscillatory processes is developed.

Main part

Determine the estimable inequalities for each approximation error. To do this, let's prove the theorems about the limits of the basic frequency, with the assumption that

$$h_{ik} \geq 0,\ h_{ik} = h_{ki},\ \lambda_i^{(0)} \geq 0. \qquad (1)$$

1. Theorem. The square of the fundamental frequency is placed Between $\frac{\lambda_i^{(m-1)}}{\lambda_i^{(m)}}$

the smallest and largest values of the ratio, i.e.

$$\min \frac{\lambda_i^{(m-1)}}{\lambda_i^{(m)}} < P_1^2 < \max \frac{\lambda_i^{(m-1)}}{\lambda_i^{(m)}}. \qquad (2)$$

Approval. Let's write (1) the equation of the inverse form for the first form

$$U_{1i} = P_1^2 \sum_{k=1}^{s} h_{ik} U_{1k}\ ,\ (i = 1, 2, ..., s).$$

We multiply both sides of the equation by and then sum with respect to the $\lambda_i^{(m-1)}$ index the index, we get: $\sum_{i=1}^{s} U_{1i}\lambda_i^{(m-1)} = P_1^2 \sum_{i=1}^{s} \lambda_\ell^{(m-1)} \sum_{k=1}^{s} h_{ik}U_{1k} =$

$= P_1^2 \sum_{k=1}^{s} U_{1k} \sum_{i=1}^{s} h_{ik}\lambda_i^{(m-1)} = P_1^2 \sum_{k=1}^{s} U_{1k}\lambda_k^{(m)}$.

Here we will use equation (1). We write the above equation in the following form

$$\sum_{i=1}^{s} U_{1i}\left[\lambda_i^{(m-1)} - P_1^2\lambda_i^{(m)}\right] = 0 . \qquad (3)$$

In order to positive P_1^2 - was more for it At the greatest value of the ratio $\frac{\lambda_i^{(m-1)}}{\lambda_i^{(m)}}$, all terms of (3) are required to be negative, and if P_1^2 is less $\frac{\lambda_i^{(m-1)}}{\lambda_i^{(m)}}$ At the smallest value, then each term of (3) must be positive. Both cases are impossible due to the equality of (3) to zero, so inequality (1) musthold.

2.Theorem. The smallest value less $\frac{\lambda_i^{(m-1)}}{\lambda_i^{(m)}}$ increases with the increase of - m, and the largest value decreases, their difference can be made smaller than any small value for sufficiently large m.

2.Approval. According to (2), we can write for the mentioned ratio:

$$\frac{\lambda_i^{(m-1)}}{\lambda_i^{(m)}} = \frac{\sum_{k-1}^{s} h_{ik}\lambda_k^{(m-2)}}{\sum_{k-1}^{s} h_{ik}\lambda_k^{(m-1)}} . \qquad (4)$$

The right fraction of (4) is placed between the smallest and largest values of the positive fractions.

$$\frac{\lambda_1^{(m-2)}}{\lambda_1^{(m-1)}}, \frac{\lambda_2^{(m-2)}}{\lambda_2^{(m-1)}}, \ldots, \frac{\lambda_s^{(m-2)}}{\lambda_s^{(m-1)}} . \qquad (5)$$

The smallest value of ratio (4) is greater than the smallest value of (5), and the largest value of (5) is less than the largest value of (5), i.e.

$$\min\frac{\lambda_i^{(m-0)}}{\lambda_i^{(m-1)}} < \min\frac{\lambda_i^{(m-1)}}{\lambda_i^{(m)}} <$$

$$P_1^2 \max\frac{\lambda_i^{(m-1)}}{\lambda_i^{(m)}} < \max\frac{\lambda_i^{(m-2)}}{\lambda_i^{(m-1)}} .$$

which proves the validity of the theorem.

3.Theorem. The square of the fundamental frequency satisfies the P_1^2 inequality

$$\min\frac{\lambda_i^{(m-1)}}{\lambda_i^{(m)}} < P_1^2 < \frac{\sum_{i=1}^{s} \lambda_i^{(0)}\lambda_i^{(m-1)}}{\sum_{i=1}^{s} \lambda_i^{(0)}\lambda_i^{(m)}} . \qquad (6)$$

We will not present the proof of this theorem here. If we choose the starting form conveniently, then inequality (6) will be simplified. For example, if we take it as the starting form $\lambda_1^{(0)} = \lambda_2^{(0)} = \cdots = \lambda_s^{(0)} = 1$, then

$$\min\frac{\lambda_i^{(m-1)}}{\lambda_i^{(m)}} \le P_1^2 \le \frac{\sum_{i=1}^{s} \lambda_i^{(m-1)}}{\sum_{i=1}^{s} \lambda_i^{(m)}} . \qquad (7)$$

Other inequalities for estimating the lower and upper bounds of the fundamental frequency were established by P.F. Papkovich and S.M. Berstain.

Let's determine the main frequency, in case of asymmetric loading of a three-pole coil of constant cross-section (Fig. 1). Q_1 =100 kg, Q_2 = 60 kg, Q_3 = 80 kg, ℓ_1 = 100 cm; ℓ_2 =200 cm, ℓ_3 =150 cm, a_1= b_1 =50 cm, a_2 = b_2 = 100 cm, a_3= b_3 = 75ð, E= 2 · 10^6 kg/cm^2, I= 63,62 cm^4.

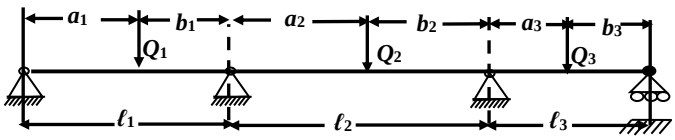

fig. 1. constant cross section triple beam

We calculate the coefficients of influence α_{ik} by formulas [9]

$$\alpha_{11} = \frac{a_1^2 b_1}{3EI}\left[\frac{b_1}{\ell_1} - \frac{(\ell_1 + a_1)(\ell_2 + \ell_3)}{F}\left(1 - \frac{a_1^2}{\ell_1^2}\right)\right];$$

$$\alpha_{12} = \frac{a_1 a_2 b_2 \ell_1 [\ell_2(\ell_2 + a_2) - 2(\ell_2 + \ell_3)(\ell_2 + b_2)]}{6EI\ell_2 F}$$

$$\left(1 - \frac{a_1^2}{\ell_1^2}\right)$$

$$\alpha_{13} = \frac{a_1 a_3 b_3 \ell_1 \ell_2 (\ell_3 + b_3)}{6EI\ell_3 F}\left(1 - \frac{a_1^2}{\ell_1^2}\right);$$

$$\alpha_{22} = \frac{a_2 b_2}{6EI}$$

$$\left\{\frac{2a_2 b_2}{\ell_2} - \frac{b_2[2(\ell_3 + b_3)(\ell_2 + b_2) - \ell_2(\ell_2 + a_2)]\left(1 - \frac{b_2}{\ell_2^2}\right)}{F}\right.$$

$$+ \left. + \frac{a_2[2(\ell_1 + b_2)(\ell_2 + a_2) - \ell_2(\ell_2 + b_2)]\left(1 - \frac{a_2}{\ell_1^2}\right)}{F}\right\}; \quad (8)$$

$$\alpha_{23} = \frac{a_2 b_2 b_3 \ell_3 [\ell_2(\ell_2 + b_2) - 2(\ell_1 + b_2)(\ell_2 + a_2)]}{6EI\ell_2 F}$$

$$\left(1 - \frac{b_3^2}{\ell_3^2}\right)$$

$$\alpha_{33} = \frac{a_1^2 b_1}{3EI}\left[\frac{a_3}{\ell_3} - \frac{(\ell_1 + \ell_2)(\ell_3 + b_3)}{F}\left(1 - \frac{b_3^2}{\ell_3^2}\right)\right]$$

where $F = 4(\ell_1 + \ell_2)(\ell_2 + \ell_3) - \ell_2^2$.

For the example in question α_{11} = 129,8·10^{-6}; α_{12} = –96,95·10^{-6}; α_{13} = 21,81·10^{-6}; α_{21} = α_{12}; α_{22} = 611,7·10^{-6}; α_{23} = –174,5·10^{-6}; α_{31} = α_{13}; α_{33} = 405,5·10^{-6}.

Equation written in inverse form

$$\lambda_i = P^2 \sum_{k=1}^{s} h_{ik}\lambda_k ,$$

where $h_{ik} = \alpha_{ik}\sqrt{m_i m_k}$, (*i*, *k* = 1, 2, 3In our case, it will take the form;

$$\lambda_1 = P^2(13,231\lambda_1 - 7,655\lambda_2 + 1,988\lambda_3)\cdot 10^{-6}$$
$$\lambda_2 = P^2(-7,655\lambda_1 - 37,412\lambda_2 - 12,323\lambda_3)\cdot 10^{-6} \quad (9)$$
$$\lambda_3 = P^2(1,988\lambda_1 - 12,323\lambda_2 + 33,06\lambda_3)\cdot 10^{-6}$$

If we introduce a new quantity

$$\mu_1 = \lambda_1; \quad \mu_2 = -\lambda_2; \quad \mu_3 = \lambda_3. \quad (10)$$

Then we will get a system with positive coefficients regarding to μ_i

$$\mu_1 = P^2(13,231\mu_1 + 7,655\mu_2 + 1,988\mu_3)\cdot 10^{-6};$$
$$\mu_2 = P^2(7,655\mu_1 + 37,412\lambda_2 + 12,323\mu_3)\cdot 10^{-6}; \quad (11)$$
$$\mu_3 = P^2(1,988\mu_1 + 12,323\mu_2 + 33,06\mu_3)\cdot 10^{-6}.$$

The coefficients of this system satisfy the symmetry condition and are all positive, so we can use the theorems about the fundamental frequency. There will be a matrix consisting of coefficients.

There will be a composite

$$\text{matrix}\,\|h_{ik}\| = \begin{Vmatrix} 13,231 & 7,655 & 1,968 \\ 7,655 & 37,412 & 12,323 \\ 1,988 & 12,323 & 33,06 \end{Vmatrix}\cdot 10^{-6}.$$

If we take it as the starting form $\mu_1^{(0)} = \mu_2^{(0)} = \mu_3^{(0)} = 1$, then $\lambda_i^{(1)} = \sum_{k=1}^{s} h_{ik}\lambda_k^{(0)}$

We get the first approximation from the formula: $\mu_1^{(1)} = h_{11} + h_{12} + h_{13} = 22,874\cdot 10^{-6}$; $\mu_{(2)}^{(1)} = 57,39\cdot 10^{-6}$,

We get the first approximation:

$\mu_1^{(1)} = h_{11} + h_{12} + h_{13} = 22,874\cdot 10^{-6}$;

$\mu_{(2)}^{(1)} = 57,39\cdot 10^{-6}$,

$$\mu_3^{(1)} = 47,371\cdot 10^{-6}.$$

The ratio of the amplitudes will be (divided by) $\mu_1^{(1)}$ 1:2, 509:2, 071 Second approximation:

$$\mu_{(1)}^{(2)} = 36,554\cdot 10^{-6}; \mu_{(2)}^{(2)} = 127,043\cdot 10^{-6}, \mu_{(3)}^{(2)} = 101,373\cdot 10^{-6},$$

The ratio of amplitudes will be 1:3, 475:2, 773.

Third approximation:

$\mu_{(1)}^{(3)} = 45,345\cdot 10^{-6}$; $\mu_{(2)}^{(3)} = 171,834\cdot 10^{-6}$; $\mu_{(3)}^{(3)} = 136,485\cdot 10^{-6}$;

And the ratio of amplitudes is 1:3,789:3.01. The main frequency of the second approximation will be 140.5<p1<145.1, and the third approximation will be 142.2<p1<143.2.

By transforming (10), it turned out to be possible to reduce the system (9) to positive coefficients on the system (4) without changing the roots of the eternal equation, due to the fact that there is a correspondence between the number of sign changes of h_{ik} coefficients and the number of

changes in the amplitudes of the first form of oscillation. Such a correspondence always exists if the coefficients of h_{ik} in the eigen form decomposition $h_{ik} = \sum_{n=1}^{s} \frac{U_{ni}U_{nk}}{P_n^2}$; ($i$, k = 1, 2, ..., s).

The sign of the coefficients h_{ik} and hence the sign of the amplitudes of the first eigen form are determined by the sign of the sum corresponding to the lowest frequency. This becomes possible when the second frequency is much higher than the first (in most cases it is). If these frequencies are close to each other, then the correspondence of signs between the coefficients and the amplitudes of the first form may be violated. In this case, the method given in the example about reducing to a system with positive coefficients is not directly applicable to the given system. But even here we can determine the correspondence between the signs. let's change it $\lambda_i = p^2 \sum_{k=1}^{s} h_{ik}\lambda_k$ equations h_{ik} by coefficients (m – 1) with row iteration (m = 1,2,3...; $h_{ik}^{(0)} = h_{ik}$), so changed by equations

$$\lambda_i = P^{2m} \sum_{k=1}^{s} h_{ik}^{(m-1)}\lambda_k \qquad (12)$$

For the quite biggest m

$$h_{ik}^{(m-1)} = \sum_{n=1}^{s} \frac{U_{ni}U_{nk}}{P_n^{2m}}.$$

According to the smallest frequency of the row, the corresponding sign determines the signs of the coefficients of (12) and analysis. Condition (1) will be fulfilled for this system, which is why we will use theorems about the fundamental frequency. Let's note that we got the fundamental frequency in the 2m-power, and the amplitudes of the first form in absolute values.

Let's consider an example, let's say that the matrix consisting of the coefficients of the system equations has the form:

$$\|h_{ik}\| = \begin{Vmatrix} 1,94 & 0,15 & -0,57 & -20,13 \\ 0,15 & 0,90 & -0,89 & -0,03 \\ 0,57 & -0,89 & 1,01 & 0,21 \\ -20,13 & -0,03 & 0,21 & 0,16 \end{Vmatrix}$$

Positive coefficients of the given system by putting the following on the system:

$$\lambda_1 = \mu_1, \quad \lambda_2 = \mu_2, \quad \lambda_3 = -\mu_3, \quad \lambda_4 = -\mu_4.$$

And for the system whose matrix is

$$\|h_{ik}\| = \begin{Vmatrix} 81,30 & -8,58 & -16,91 & -8,04 \\ -8,58 & -3,67 & -7,24 & -3,45 \\ -16,91 & -7,24 & -4,56 & -2,22 \\ -8,04 & -3,45 & -4,28 & 3,39 \end{Vmatrix} \cdot 10^{-5}$$

We cannot use the subtraction method directly, the coefficients of the first iteration are calculated by the formula: $h_{ik}^{(1)} = \sum_{k=1}^{s} h_{ik}\lambda_k$ (i, k = 1, 2, ..., s),

$$\|h_{ik}^{(1)}\| = \begin{Vmatrix} 7033,9 & -575,89 & -1216,01 & -613,77 \\ -575,89 & 151,41 & 213,06 & 86,01 \\ -1216,01 & 213,06 & 365,02 & 161,76 \\ -613,77 & 86,01 & 163,76 & 92,96 \end{Vmatrix} \cdot 10^{-10}.$$

Now if we insert here: $\lambda_1 = \mu_1$, $\lambda_2 = -\mu_2$, $\lambda_3 = -\mu_3$, $\lambda_4 = -\mu_4$.
We will get an equivalent system with positive coefficients.

Conclusions

The theorem is proved when the square of the basic frequency lies between the smallest and largest values. As the ratio increases, when it is not significant, it decreases, their difference can be made small. The fundamental frequency of a three-pole coil of constant cross-section under unsymmetrical loading is determined.

Reference

1. Kvitsian Tariel. Theoretical mechanics course. dynamics. Publishing House "Technical University" Tbilisi, 2019 - 474 p.

2. Gorjoladze I. Kifiani c. Buksianidze A. Theoretical mechanic's course. dynamics. Publishing House "Technical University" Tbilisi, 2008 -542 p.

3. Khvingia M. Fundamentals of applied theory of mechanical vibrations and machine dynamics. Tbilisi, "Ganat-Leba", Tbilisi 1981, 455 p.

4. Gorgidze A. Course of theoretical mechanics (dynamics). Tbilisi, "Education", 1972.

5. Vekua n. Theoretical mechanics. Article II. Tbilisi.: "Education", 1970.

6. Machaidze E., Kifiani G. Compiled theory of calculation of thin-walled spatial systems, "Technical University" publishing house, Tbilisi, 2006 -369 p.
7. Gegelashvili T. Kifiani c. "Linear Oscillations of a Discrete Mechanical System". Eureka Publishing House, Tbilisi, 1993, 241 p.

8.Zdenek P Bazant, Luigi Cedolin. Stability of Structures (Elastic, Inelastic, Fracture, and Damage Theories) Dover Publications, Inc. Mineola, New York.2003-1011p.
9.Лунц У.Б.О Поперечных колебаниях валов,ОНТИ,НКТП,1985.
10.Бабаков И.М. Теория колебании. М.: «Наука», 1968.
11.Кузьмин П.А. Малые колебания и устойчивость движения. М.: «Наука», 1973.
12.Мигулин В.В., Медведев В.И. и др. Основы теорий колеба-ний. М.: «Наука», 1978.
13.Пановко Я.Г. Введение к теорию механических колебаний. М.: «Наука», 1991.
14.Тимощенко С.П., Янг Л.Х., Уивер У. Колебания в инженер-ном деле. М.: Машиностроение. 1985

BEARING CAPACITY OF FOUNDATION AND SETTING OF THE BOILER NEAR THE VERTICAL WALL

Giorgi Lutidze, Nina Areshidze, Kote Iashvili, Nino Bakhtadze
Georgian Technical University, Tbilisi 0170, Georgia
george.pato@gmail.com

Abstract

The paper discusses the task setting and analytical solution for the quantitative evaluation of the bond and tensile properties of a defined layer of soil. It also examines the impact of a foundation with a distributed load in the vicinity of a vertical pile wall when the entire soil rests on non-compressible (rocky) soil. The assumption in this analysis is that the vertical wall of the pile is strengthened by bracing structures but is allowed to move vertically within the ground. The components of the stress state are obtained using the Riber-Philon trigonometric series method. Formulas for determining vertical and horizontal deformations are also provided. Hank's physical equations are employed to establish the relationship between stresses and deformations, taking into account the effect of σ_m on the shear modulus G(σ_m) and the bulk deformation modulus K(σ_m). This relationship is incorporated into the system of Hooke's equations when G=const and K=const. Through the analysis of the obtained results, it becomes possible to estimate base-soil deformations, considering its non-linear properties, and to assess the uneven settlement of the building's foundation.

Keywords: stress-deformed state of the base-soil, Riber-Philon trigonometric series, Hank's physical equations, volumetric and shear deformations, foundation adhesion, base-soil bearing capacity, edge of the pot

Introduction

A complex non-uniform stress-deformed state is created in the array of the vertical soil wall strengthened by the bracing of the boiler. While we have a distributed load near the boiler enclosure, additional normal and shear stresses occur in the ground array. In such case, when predicting the stress-deformed state, it becomes essential to account for the nonlinear properties of the soil, especially in the context of foundations for buildings and structures located in proximity to boilers. It is necessary to estimate both volumetric and displacement deformations, as well as the relative difference in the resulting joint.

When analyzing existing foundation calculation methods, it becomes evident that the calculation model that closely aligns with the actual performance of foundation-soil interactions is one that factors in both the width and depth of the deformation area. In this paper, problem we address is massive soil layer of defined capacity, which rests on a non-compressible soil, in this layer we have a boiler with a vertical wall, near the fence of which we have a foundation with distributed load. Also, the stress-deformed state caused by the soil's own weight was studied through Riber-Faillonin's trigonometric series, the stress-deformed state caused by the soil's self-weight was studied under the conditions of compressive compression.

The relationship between stress and deformations is described by Hank's [1] physical equations, which enable us to consider both linear and non-linear base-soil models. These equations define linear deformation as the sum of volume and shear deformations (ε_Z=ε_ν 〖+ε〗 _γ).

Many scientists worked on short-term and long-term prediction methods of foundations. Garsevanov [5], K. Egorov [4], N. Citovich [2], S. Tymoshenko [6], V. Florin [3], Z. Ter-Martirosian [8] and others [9-10]. The relevance and practical value have those methods that can quantitatively evaluate the soil's adhesion and traction capacity, taking into account the elastoplastic properties of the soil. In this way, we can determine the relationship between stresses and deformations, and obtain graphs of double curvature in its gradual and progressive part. Similar graphs have been obtained by N. Citovich [2], I. Zaretskyi [7], Ter-Martirossian [8] during laboratory research on the deformation of clay soils. When performing the calculations of the connection of buildings and structures near the edge of the boiler, it is necessary to consider the elastic-plastic behavior of the foundation-soils, because zones of additional plastic deformations occur in the foundation. Moreover, it is important to take into account the change of the deformation modulus in the depth of the foundation for a soil capacity of

more than 5 m (Klein's model [20]), which makes it possible to correctly calculate the connection of the foundation based on the elastic-plastic properties of the soil at the edge of the embankment. It should be noted that the calculation models, which make it possible to describe the elastic-plastic and elastic-viscous properties of the soil by constructing double curvature graphs. Foreign scientists are trying to find new methods based on the results of field tests, the problems of predicting the junction of soil arrays using computer software packages and numerical modeling of the task.

Main part

The distributed load on the horizontal section with width b=2a and distance c from the retaining structure of the vertical wall is considered, when the entire base-soil rests on the non-compressible layer. It is assumed that the vertical wall is reinforced with rectangular cross-section profiles made up of curved profiles, but the vertical displacement of the soil is allowed (Fig. 1). It is known that for this task the ground stress components are determined as a quarter plane with the help of Riber-Philon trigonometric series.

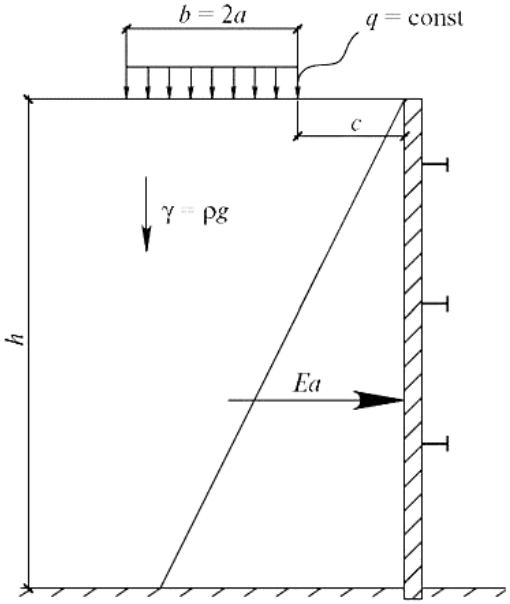

fig. 1 Calculation scheme Soil layer with capacity h resting on non-compressible base, stationary construction of reinforcement of the vertical wall of the boiler, distributed load q=const with strip width b=2a and distance c from the boiler wall.

$$\sigma_y(x,y) = \frac{qa}{l} + \frac{4q}{\pi}\sum_{m=1}^{\infty}\frac{\sin\frac{m\pi a}{l}}{m}\frac{\left[\left(\frac{m\pi h}{l}ch\frac{m\pi h}{l}+sh\frac{m\pi h}{l}\right)ch\frac{m\pi(y-h)}{l}-\frac{m\pi(y-h)}{l}sh\frac{m\pi(y-h)}{l}sh\frac{m\pi h}{l}\right]}{sh\frac{2m\pi h}{l}+\frac{2m\pi h}{l}}\cos\frac{m\pi x}{l}; \quad (1)$$

$$\sigma_x(x,y) = \frac{qa}{l}\frac{\nu}{1-\nu} + \frac{4q}{\pi}\sum_{m=1}^{\infty}\frac{\sin\frac{m\pi a}{l}}{m}\frac{\left[\left(\frac{m\pi h}{l}ch\frac{m\pi h}{l}+sh\frac{m\pi h}{l}\right)ch\frac{m\pi(y-h)}{l}-\frac{m\pi(y-h)}{l}sh\frac{m\pi(y-h)}{l}sh\frac{m\pi h}{l}\right]}{sh\frac{2m\pi h}{l}+\frac{2m\pi h}{l}}\cos\frac{m\pi x}{l}; \quad (2)$$

$$\tau_{xy}(x,y) = -\frac{4q}{\pi}\sum_{m=1}^{\infty}\frac{\sin\frac{m\pi a}{l}}{m}\frac{\left[\frac{m\pi h}{l}ch\frac{m\pi h}{l}sh\frac{m\pi(y-h)}{l}-\frac{m\pi(y-h)}{l}ch\frac{m\pi(y-h)}{l}sh\frac{m\pi h}{l}\right]}{sh\frac{2m\pi h}{l}+\frac{2m\pi h}{l}}\sin\frac{m\pi x}{l}; \quad (3)$$

$$\sigma_m(x,y) = \frac{1+\nu}{3}\left[\frac{qa}{l}\frac{1}{1-\nu} + \frac{8q}{\pi}\sum_{m=1}^{\infty}\frac{sin\frac{m\pi a}{l}}{m}\frac{sh\frac{m\pi a}{l}\,ch\frac{m\pi(y-h)}{l}}{sh\frac{2m\pi h}{l}+\frac{2m\pi h}{l}}cos\frac{m\pi x}{l}\right]; \quad (4)$$

Based on the system of equations (1-4), the value is obtained as the sum of the equally distributed load q intensity 2c width band and -q intensity 2a width band. Hank's system of physical equations, which allows determining the linear and non-linear relationship between stress and strain, looks like this:

$$\varepsilon_x = \chi(\sigma_x - \sigma_m) + \chi^*\sigma_m, \quad y_{xy} = 2\chi\tau_{xy}; \quad (5)$$
$$\varepsilon_y = \chi(\sigma_y - \sigma_m) + \chi^*\sigma_m, \quad y_{yz} = 2\chi\tau_{yz}; \quad (6)$$
$$\varepsilon_z = \chi(\sigma_z - \sigma_m) + \chi^*\sigma_m, \quad y_{zx} = 2\chi\tau_{zx}; \quad (7)$$
$$\chi = \frac{\gamma_i}{2\tau_i} = \frac{f(\tau_i,\sigma_m,\mu_\sigma)}{2\tau_i}; \quad (8)$$
$$\chi^* = \frac{\varepsilon_m}{\sigma_m} = \frac{f^*(\tau_i,\sigma_m,\mu_\sigma)}{2\tau_i}; \quad (9)$$

Hank's equations when χ=1/2 G and χ^*=1/K where G=E/2(1+ν) and K=E/(1-2ν) go into the system of Hooke's equations.

For the definition of non-linear volumetric deformations, the approach proposed by academician S. By Grigorian:

$$\varepsilon_m(\sigma_m) = \varepsilon^*(1 - e^{-\alpha\sigma_m}) \quad (10)$$

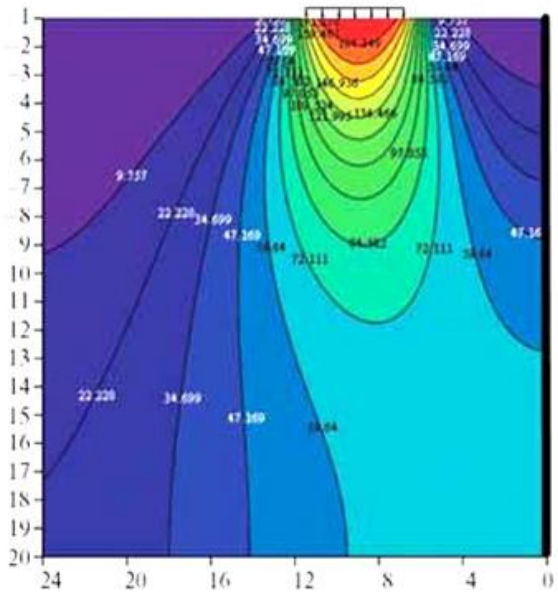

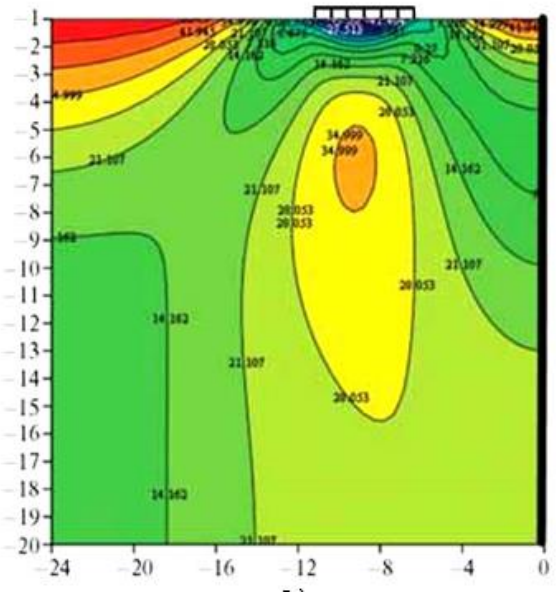

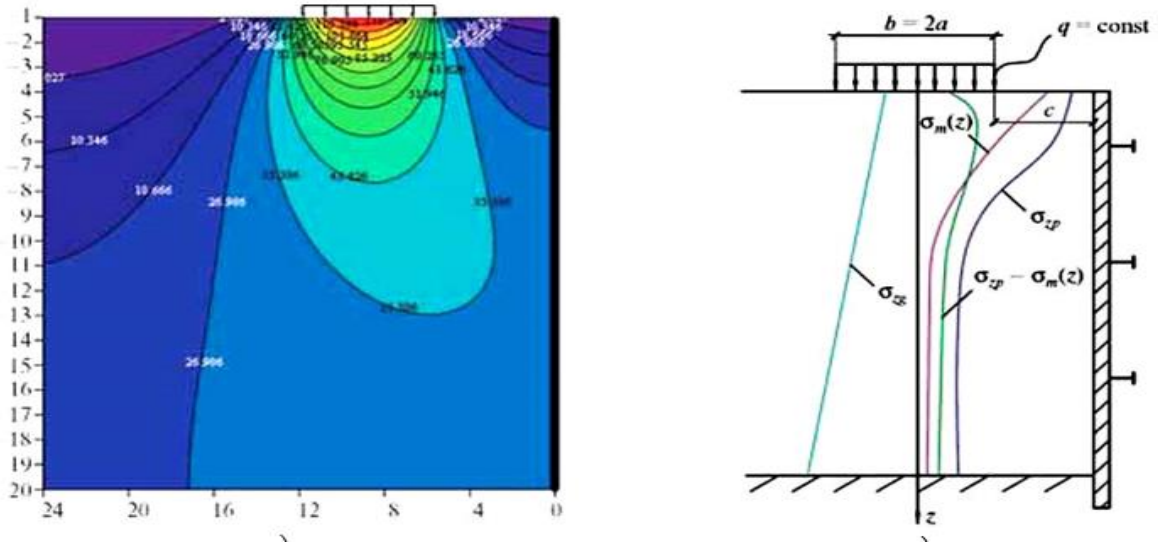

fig. 2. Stress isolines when q=200 kPa, C=6 m, b=2a=6 m: a) vertical σ_m; b) Horizontal σ_x c) Average stress σ_m d) Calculation scheme for determining ground displacement and volumetric deformation based on Hank's physical equations.

The elastic modulus of volumetric deformation can be calculated if we compare the image of ε_m to σ_m:

$$\frac{\varepsilon_m}{\sigma_m} = \frac{1}{K} = \frac{\varepsilon^*(1-e^{-\alpha\sigma_m})}{\sigma_m}; \quad (11)$$

$$K = \frac{\sigma_m}{\varepsilon_m} \quad (12)$$

when σ_m→∞; ε_m→ε^*, and when α=0, ε^*=ε_m we get a linear relationship K=ε_m/σ_m. In order to describe the elasto-plastic properties of shear-bonded soils, the following relation was used for soils:

$$\gamma_i = \frac{\tau_i}{G^0}\frac{\tau_i^*}{\tau_i^*-\tau_i} \quad (13)$$

where γ_i is the intensity of angular deformation.

τ_i- the effective value of the voltage

τ_i^*- the threshold value of the voltage intensity

G^0- shear modulus at the initial section of the γ_i-τ_i curve

$$\tau_i^* = (\sigma_m + \sigma_g)tg\varphi + c_i \quad (14)$$

where φ_i,c_i are the limiting parameters of strength, determined by (τ_i-σ_m) linear from addiction; σ_g- natural voltage.

The shear modulus is calculated by the formula:

$$G = G^0\left(1 - \frac{\tau_i^*}{\tau_i^*-\tau_i}\right) \quad (15)$$

Analytical calculations made on the computer allowed us to determine the voltage components on the entire plane. Fig. 2 presents the obtained results. In the simplest case, in the case of linear dependence of stresses and deformations, the relationship between G and K can be determined by an analytical solution for the z(x=0) axis. Then we can write the formulas (11) and (12) in the case of the linear model, the initial data q=200 kPa were used. c=6 m. ν=0.27, K=40 MPa, G_e=50 MPa.

In order to take into account, the non-linearity of the deformation of the soil layer, we should use Hank's equation in the calculation:

$$\varepsilon_z = \frac{\sigma_z-\sigma_m}{G(\sigma_m,\ \tau_i/\tau_i^*)} + \frac{\sigma_m}{K} \quad (16)$$

By inserting (σ_m,τ_i) and K(σ_m), we get nonlinear equations:

$$\varepsilon_{z,\nu} = \varepsilon^*(1 - e^{-\alpha\sigma_m}) \quad (17)$$

$$\varepsilon_{z,\gamma} = \frac{\sigma_z-\sigma_m}{2G(\sigma_m,\tau_i/\tau_i^*)} \quad (18)$$

where τ_i=(σ_1-σ_3)/√3=(σ_z-σ_x)/√3 (on axis x=0); τ_i^*=(σ_m+σ_g)tgφ+c_i,σ_zp, σ_xp are determined by expressions (1)-(4).

From the analysis of equations (17)-(18), it follows that the exponent of volume deformation ε_(z,ν), σ_z will have a decreasing character with the increase, and σ_m→∞ ; Then ε_(z,ν)→ε^*. At the same time, when σ_z increases, the value of ε_(z,γ) will initially increase linearly and then go into an intensive growth process, and since τ_i→τ_i^*; ε_(z,γ)→∞. Therefore, the total value of the deformation will have a double curvature, i.e. in the initial section τ_i<τ_i^* ; The decreasing

character of ε_z, after τ_i→τ_i^* goes into progressive deformation Fig. 3.

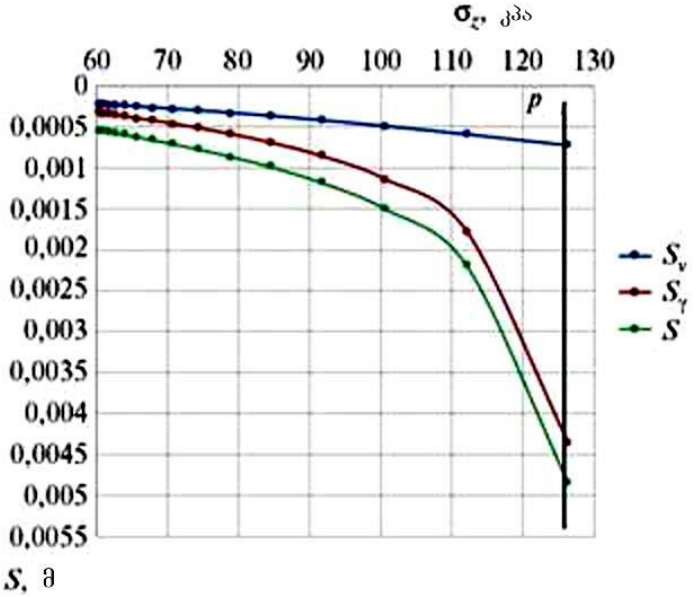

fig. 3. The graph of the vertical movement of the soil layer calculated by formulas (17) and (18) (thickness of the soil layer H=15 m)

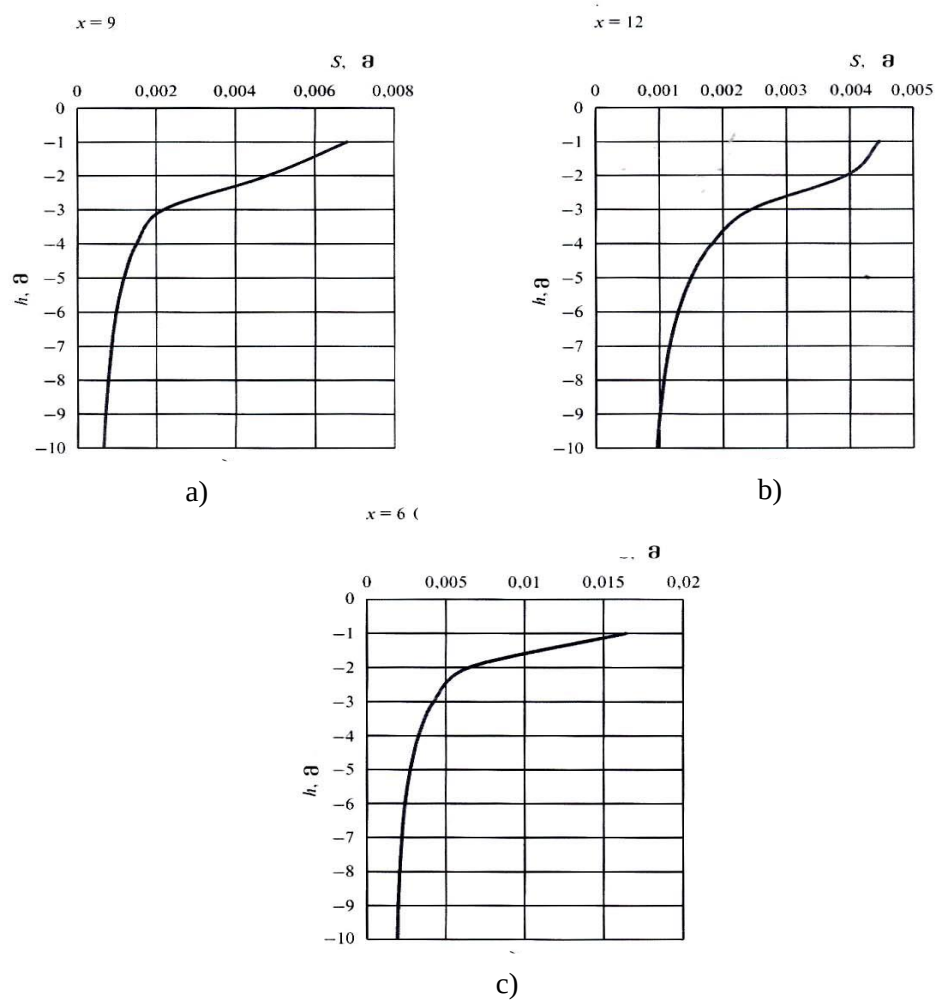

fig. 4. Graphic representation of axial deformation on different vertical (x>0)

The total deformation of the base with the power of the base H=15 m for different X>0 can be determined by the following integral:

$$S = \int_0^h \varepsilon_{z,\nu_i}(dz) + \int_0^h \varepsilon_{z,\gamma_i}(dz) = S_\nu + S_\gamma$$

(19)

Calculation of total base deformations ε_z=ε_(z,ν)+ε_zγ on different verticals when x > 0 with soil mechanical parameters ε^*=0.016, α=0.015, ν=0.3, G_e=50 MPa, φ=25^0 and c= 15 kPa is presented in fig. 4. On

From the analysis of the obtained results, it follows that the total deformation on the left side of the foundation (x = 12) is S_left=11 mm, on the right side of the foundation (x = 6) - S_right=44 mm; In the center of the foundation (x = 9) - S_center=16 mm. In this way, an uneven fit of the sides of the foundation ΔS/l=0.0055 is observed, which is caused by the close location of the foundation to the face of the boiler.

Conclusion

By generalizing the obtained results, the following conclusions can be made:

1. The selected geomechanical model of the base (geometric parameters, initial and boundary conditions), as well as the calculation scheme of the soil environment (linear and non-linear and rheological) and the system of equations (Hank's physical and Hooke's system of equations) have a significant impact on the character of the stress-strain curve, as well as on the base-soil traction ability.
2. The calculation model used in this paper, together with the elastic-plastic model during displacement and the nonlinear model during volumetric soil deformation, allowed us to represent the linear deformation of the soil in Hank's physical equations in the form of the sum of linear deformation volumetric and displacement exponents.
3. The calculation model of the base when limiting the horizontal movement of the ground (ε_x=0) near the boundary of the vertical pile leads to a decrease in deformation ε_z and an increase in σ_z.
4. Calculation of deformations showed that under the foundation near the vertical pile, which is affected by the distributed load, uneven joints definitely appear. In the considered case, the ratio was ΔS/l=0.0055, which significantly exceeds the standard value.

It should be noted that during new construction, the quantitative assessment of the tension-deformation of foundations is one of the priority tasks in the design of building foundations.

Reference

1. Hencky H. Zur Theorie plastischer Deformationen und der hierdurch im Material hervorgerufenen Nachspannungen. *ZaMM*. 1924; 323-334.
2. Tsytovich N.A. *Soil mechanics*. Moscow, Stroyizdat Publ., 1963; 638.
3. Florin V.A. *Fundamentals of soil mechanics.* Moscow, Gosstroyizdat Publ., 1961; 543.
4. Egorov K.E. About the deformation of the base of the finite thickness. *Soil Mechanics and Foundation Engineering*. 1961; 1.
5. Gersevanov I.M., Macheret Y.A. About an infinite long beam on elastic soil loaded with force. *Hy- draulic Engineering*. 1935; 15-23.
6. Timoshenko S.P., Gud'er Dzh. *Theory of elasti-city*. Moscow, Nauka Publ, 1975; 576.
7. Zaretskiy Yu.K., Karabaev M.I. Influence of the sequence of construction of nearby high-rise buil- dings on precipitation and roll of foundation slabs. *MGSU* [Proceedings of the Moscow State University of Civil Engineering]. 2006; 51-56.
8. Ter-Martirosyan Z.G., Ter-Martirosyan A.Z. *Soil mechanics for high-rise buildings having sophisti- cated underground substructures: study guide*. Moscow, ASV Publ., 2020; 912.
9. Karaulov A.M., Korolev K.V., Galter D.S. Limiting pressure of the round stamp upon the basis in the constrained conditions. *News of Higher Educational Institutions. Construction*. 2018; 720, 23-30.
10. Kudriavtcev S.A., Paramonov V.N., Kazharskii A.V., Goncharova E.D. Calculated evaluation of shoring of deep excavation in the restrained urban conditions. *Japanese Geotechnical Society Special Publication*. 2016; 2(79):2722-2725. DOI: 10.3208/jgssp. TC305-10
11. Kleyn G.K. Taking into account the heterogeneity of discontinuous deformations and other mechanical properties of soils when calculating structures on a solid foundation. *Collection of works of MISI.* 1956.

USE OF PLASTIC POTENTIAL IN THE THEORY OF FLUIDITY

Tamaz Batsikadze, Nugzar Murgulia, Jumber Nizharadze
Georgian Technical University, Tbilisi 0170, Georgia
j.nizharadze@gtu.ge

Abstract

In general case, plastic potential functions have been used to solve problems of the fluidity process. Equations in principal stresses are obtained for the components of the plastic deformation increment tensor when the scalar function $g(\sigma_{ij})$) is replaced by the Mises plasticity function $f(\sigma_{ij})$.

On the basis of the fluidity theory, expressions of plastic deformation parameters for plates made of isotropic and anisotropic material are compiled. The case where the forces acted in the plane of anisotropy was considered. When forces were applied in a direction perpendicular to the plate plane, the specimen was pre-tested in tension in that direction.

Finally, for all six components of the plastic deformation increment, the corresponding relations were derived.

Keywords: plastic deformation increment, plastic potential, incompressible body, isotropic and anisotropic bodies, fluidity.

Introduction

The use of the Lévy-Mises's equations to solve particular, relatively simple problems of fluidity theory gives good results and agrees with experimental data, which is not the case for more general cases. The authors of this article seek to utilize the plastic potential to solve such problems.

The plastic potential is a scalar function of stress (e.g., $g(\sigma_{ij})$), partial derivative of which by σ_{ij} allows us to derive equations for the components of the increment of the plastic deformation tensor

$$d\varepsilon_{ij}^{p} = \frac{\partial g(\sigma_{ij})}{\partial \sigma_{ij}} d\lambda' \text{ or}$$

$$\frac{d\varepsilon_{ij}^{p}}{\partial g(\sigma_{ij})/\partial \sigma_{ij}} = \cdots d\lambda'(1)$$

where $d\lambda'$ - positive constant, since otherwise it would appear that negative strain is associated with positive stresses, which would be absurd.

Main part

In the article [4] we considered the problem of obtaining the equations of fluidity theory using the plastic potential.

In the presented work, we make the task more difficult. The plastic potential function $f(\sigma_{ij})$ (by which we change the plastic condition), is always chosen to be symmetric for all three stress invariants, so that it does not depend on the chosen system or principal stresses. Let's build a drawing (Fig. 1), which shows the increment of plastic deformation in three-dimensional space.

Thus, we actually obtain a new problem. Let us denote the principal increments of plastic deformations on the axis σ_1 through ε_1^p and consider with respect to the axes σ_2 and σ_3 – $d\varepsilon_2^p$ *and* $d\varepsilon_3^p$, which also represent the components of the vectors of plastic deformation increment caused by the $(\sigma_1; \sigma_2; \sigma_3)$ stresses.

For further calculation it will be convenient to place this vector on the surface of the plastic cylinder. In this case its direction will be the same as the direction of the external normal of the surface $g(\sigma_{ij})$ at a point $(\sigma_1; \sigma_2; \sigma_3)$. This phenomenon is explained by the fact that the ratios of the directional cosines with respect to the surface of the cylinder, are determined by the methods of Descartes' geometry.

$$\frac{\partial g}{\partial \sigma_1} : \frac{\partial g}{\partial \sigma_2} : \frac{\partial g}{\partial \sigma_3}$$

We have been able to depict the theory of fluidity in a geometric way, which comes from the consideration of the plastic potential. Thus

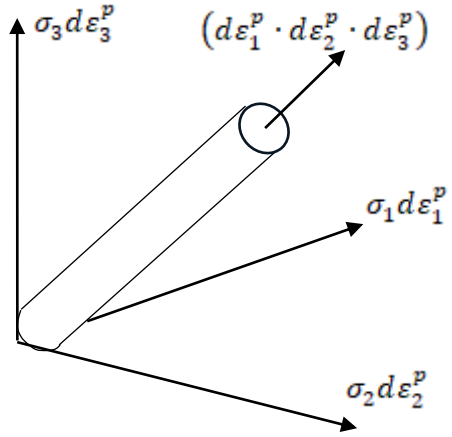

Fig. 1

$$d\varepsilon_1^p : d\varepsilon_2^p : d\varepsilon_3^p = \frac{\partial g}{\partial \sigma_1} : \frac{\partial g}{\partial \sigma_2} : \frac{\partial g}{\partial \sigma_3} \quad (3)$$

In this case the function g, based on the incompressibility condition, must satisfy the condition

$$d\varepsilon_1^p + d\varepsilon_2^p + d\varepsilon_3^p = \frac{\partial g}{\partial \sigma_1} + \frac{\partial g}{\partial \sigma_2} + \frac{\partial g}{\partial \sigma_3} = 0$$

Mises' plastic condition fulfills this requirement.

It turns out that there are only six different directions of normal, which correspond to the six surfaces of the sides of the prism. Only the maximum stress having the maximum absolute value is used in the case of the given above stress distribution $(\sigma_1; \sigma_2; \sigma_3)$ (e.g., $(\sigma_1 - \sigma_3)$), from this $g(\sigma_{ij}) = (\sigma_1 - \sigma_3)$ and we get

$$d\varepsilon_1^p : d\varepsilon_2^p : d\varepsilon_3^p = \frac{\partial(\sigma_1 - \sigma_3)}{\partial \sigma_1} : \frac{\partial(\sigma_1 - \sigma_3)}{\partial \sigma_2} : \frac{\partial(\sigma_1 - \sigma_3)}{\partial \sigma_3} \quad (4)$$

We come to the following conclusion: (4) shows the only position that is possible for plastic deformation only in the plane of σ_1 and σ_3. Plastic strain increments are equal in value and opposite in direction.

Let's move on to the next problem. We use the plastic potential to consider the plastic fluidity of anisotropic materials. Just as for isotropic materials, the function $f(\sigma_{ij})$ is a plastic potential. To find the increment of deformation, its partial derivative by σ_{ij}

$$\frac{\partial f}{\partial \sigma_x} = G(\sigma_x - \sigma_z) + H(\sigma_x - \sigma_y) \quad (5)$$

and accordingly [4], we will have

$$\frac{d\varepsilon_x^p}{G(\sigma_x - \sigma_z) + H(\sigma_x - \sigma_y)} = d\lambda \quad (6)$$

These images also satisfy the incompressibility condition.

$$d\varepsilon_x^p + d\varepsilon_z^p = 0$$

When the elastic deformation increments are smaller than the plastic deformation increments, the upper index can be removed i.e., we will be dealing with a perfectly rigid Lévy-Mises's plastic material. If the cut-out sample in the plane (x, y) is stretched in the x -axis direction, which is the anisotropy axis, we get

$$d\varepsilon_x^p : d\varepsilon_y^p : d\varepsilon_z^p = G + H \div (-H) \cdot \div (-G)$$

Let us denote by r the ratio of thickness deformation with width deformation

$$r_x = \frac{d\varepsilon_y^p}{d\varepsilon_z^p} = \frac{H}{G}$$

The index x indicates that the sample is cut along the axis x

If the sample is cut out along the axis y, then

$$r_y = \frac{d\varepsilon_x^p}{d\varepsilon_z^p} = \frac{H}{F}. \quad (7)$$

We have considered the case where the load acts in the direction of the anisotropy axis. In order to obtain the required anisotropy parameters in the plane of the plate, it is necessary to test the specimen in tension in at least one more direction. If a plate made of anisotropic material is subjected to forces perpendicular to its (x, y) planes, then it is obvious that τ_{yz} and τ_{zy} will be equal to zero. Suppose we cut the sample at some angle to the x-axis and stretch it. In this case, based on the equilibrium condition

$$\sigma_x = \sigma cos^2\alpha; \qquad \sigma_y = \sigma sin^2\alpha;$$
$$\tau_{xy} = \sigma sin\alpha \cdot cos\alpha.$$

Where, σ is the tensile yield stress.

$$\begin{aligned} d\varepsilon_x^p &= [(G+H)cos^2\alpha - Hsin^2\alpha]\sigma d\lambda; \\ d\varepsilon_y^p &= [(F+H)sin^2\alpha - Hcos^2\alpha]\sigma d\lambda; \\ d\varepsilon_z^p &= -[Fsin^2\alpha + Gcos^2\alpha]\sigma d\lambda; \\ d\gamma_{xy}^p &= N(sin\alpha \cdot cos\alpha)\sigma d\lambda; \end{aligned} \quad (8)$$

Thus, consideration of the deformation geometry led us to the following conclusions:

1) The deformation increment $d\varepsilon^p_{\alpha+\frac{\pi}{2}}$ in the direction of the plate width is determined by the expression

$$d\varepsilon^p_{\alpha+\frac{\pi}{2}} = d\varepsilon^p_x sin^2\alpha + d\varepsilon^p_y cos^2\alpha - 2\gamma^p_{xy} sin\alpha \cdot cos\alpha \quad ;$$

Therefore

$$r_a = \frac{d\varepsilon^p_{\alpha+\frac{\pi}{2}}}{d\varepsilon^p_z} = \frac{d\varepsilon^p_x sin^2\alpha + d\varepsilon^p_y cos^2\alpha - 2\gamma^p_{xy} sin\alpha \cdot cos\alpha}{d\varepsilon^p_z}; \qquad (9)$$

$$r_a = \frac{H + (2N - F - G - 4H) sin^2\alpha \cdot cos^2\alpha}{F sin^2\alpha + G cos^2\alpha}$$

2) in sheet metal, the rolling direction is usually the direction of the anisotropy axis, and the x-axis is taken in this direction. This conclusion makes it possible to present (9) in another form:

$$r_x = r_{0^\circ} = \frac{H}{G}; \quad r_y = r_{90^\circ} = \frac{H}{F}; \quad r_{45^\circ} = \frac{2H-(F+G)}{2(F+a)} \qquad (10)$$

that is

$$\frac{N}{G} = \left(r_{45^\circ} + \frac{1}{2}\right)\left(1 + \frac{r_{0^\circ}}{r_{90^\circ}}\right) \qquad (10')$$

where, r_{0°, r_{45°, r_{90° are values of r in the rolling direction and at directions of an angle of 45° and 90°.

3) In the course of analysis, we assumed that the ratio of the anisotropy parameters did not change during the process. In practice, this tolerance needs to be checked separately for each material, since it should not be thought that the behavior of each anisotropic material and even more behavior of each alloy during the same process will be the same.

For example, the anisotropy parameters do not actually change for aluminum and steel, while the value of magnesium alloy depends significantly on the degree of deformation. For metal sheets, the value of r is generally measured when the longitudinal deformation exceeds 5%. In such a case, it is reasonable to assume that the elastic deformations are small and therefore the volume does not change. Therefore, longitudinal and transverse deformations are measured, and the deformation in the thickness direction, based on the difficulty of its measurement (due to the smallness of the sheet thickness), is calculated by the formula

$$r = \frac{ln\left(W_0/W\right)}{ln\left(t_0/t\right)} = \frac{ln\left(W_0/W\right)}{ln\left(Wl/W_0 l_0\right)} \qquad (11)$$

Here. W, t and l are current values of length, width, and thickness, and W_0, t_0 and l_0 – initial parameters. Let us adapt the above analysis to an anisotropic, hardened material.

The anisotropic state changes as a rule, while a material experiences plastic deformation. If we assume that these changes are small during testing, then we should think that in the case of a material with large initial anisotropy, the theoretical and practical results should be the same. We are guided by this consideration when we consider that the prior to a test isotropic material remains the same under plastic deformation conditions. On this basis, if the state of anisotropy is constant, then fluidity stresses should increase strictly proportionally when metal strengthens and anisotropy parameters should decrease in the same way, and their ratio should be unchanged. While conducting the experiment these ratios are measured rather than the absolute value of each parameter.

As mentioned above, the deformation ratio for some materials may be unchanged, but for some others it may not. Therefore, the application of the theory of anisotropy always requires caution. With all of the above in mind, Mr. Hill.R proposed the concept of equivalent stress and the formula that we will use in the laboratory testing process in the future

$$\overline{\sigma} = \sqrt{\frac{3}{2}\left[\frac{F(\sigma_y-\sigma_z)^2+G(\sigma_z-\sigma_y)^2+H(\sigma_x-\sigma_y)^2+2L\cdot\tau_{yz}^2+2M\cdot\tau_{zx}^2+2N\cdot\tau_{xy}^2}{F+G+H}\right]} \quad (12)$$

This formula will allow us to consider the parameters of anisotropy, and not their absolute value.

Let's move on to the work of plastic deformation. Increment of the work of plastic deformation per unit volume of a rigid-plastic body

$$dW = \sigma_{ij\cdot}\cdot d\varepsilon_{ij} = \sigma_{ij\cdot}\cdot\frac{\partial f}{\partial\sigma_{ij}}d\lambda \quad (13)$$

In the case of a rigid-plastic material, from (7) we obtain

$$\begin{aligned} Gd\varepsilon_y - Hd\varepsilon_z &= (FG+GH+HF)(\sigma_y-\sigma_z)d\lambda;\\ Hd\varepsilon_z + Fd\varepsilon_x &= (FG+GH+HF)(\sigma_z-\sigma_x)d\lambda; \end{aligned} \quad (14)$$

$$Fd\varepsilon_x + Gd\varepsilon_y = (FG+GH+HF)(\sigma_x-\sigma_y)d\lambda;$$

Let's take into account equality $dW = \overline{\sigma}\cdot\overline{d\varepsilon} = d\lambda$.

$$\overline{d\varepsilon} = \frac{d\lambda}{\overline{\sigma}} = \sqrt{\frac{3}{2}}(F+G+H)^{\frac{1}{2}}\left[F\left(\frac{Gd\varepsilon_y-Hd\varepsilon_z}{FG+GH+HF}\right)^2+\cdots+\frac{2d\gamma_{yz}^2}{L}+\cdots\right]^{\frac{1}{2}} \quad (15)$$

That is, we got a formula for calculating the intensity of the increment of deformation $\overline{d\varepsilon}$.

These formulas will be simplified in the flat stress state of the sheet metal in the case of symmetry around the axis z

$$r = \frac{H}{G} = \frac{H}{F}$$

And we'll get

$$\overline{\sigma} = \sqrt{\frac{3}{2}\left[\frac{\sigma_x^2+\sigma_y^2+r(\sigma_x-\sigma_y)^2}{2+r}\right]} \quad (16)$$

$$\overline{d\varepsilon} = \sqrt{\frac{2}{3}\left\{\frac{2+r}{(1+2r)^2}\left[(d\varepsilon_y-rd\varepsilon_z)^2+(d\varepsilon_x-rd\varepsilon_z)^2+(d\varepsilon_x-rd\varepsilon_y)^2\right]\right\}^{\frac{1}{2}}} \quad (17)$$

We will use these formulas to determine the effect of anisotropy in the future at a plane stress state.

Conclusion

Thus, for widely used technologies (metallurgy, mechanical engineering and other fields), using plastic potential, we have established the true relationship between stresses and plastic deformations and solved the following problems: 1) the load acts in the direction of anisotropy 2) the load acts at any angle α with respect to the x-axis direction of the cut-out plate. It was found that under certain conditions, during the process of plastic deformation of a material, its state of anisotropy changes and, therefore, in the calculation it is necessary to take into account the ratio of those or other parameters of anisotropy, rather than their absolute value.

Reference

1. Malinin N. N. Applied theory of plasticity and creep. "Mechanical Engineering", M. 1975, pp. 399.
2. Hill R. Mathematical theory of plasticity. GITTLE, 1956, p. 407.
3. T. Batsikadze, A. Kvaratskhelia, Z. Mazagaua "A short course on the theories of elasticity, plasticity and creep", Publishing House "Technical University. Tbilisi, 2014.
4. T. Batsikadze, N. Murgulia, D. Nizharadze "Derivation of the equation of the theory of fluidity using plastic potential." Scientific and technical magazine "Construction". #4(64), 2022

.DESIGNING OPTIMAL PRESSURE VESSEL DESIGNS FROM CONDITIONS OF STRENGTH

David Jankarashvili, Konstantin Iashvili, Ioseb Kakutashvili, Demur Tabatadze
Georgian Technical University, Tbilisi 0170, Georgia
d.tabatadze@gtu.ge

Abstract

An approach to optimal structures operating in the elastic stage is proposed. The paper introduces a discrete condition of equal stress for elements of a composite structure as an optimality criterion. The problem of optimal designs of a cylindrical vessel with a flat bottom under internal pressure has been solved. the required thickness parameters of the hull and bottom elements are found as a result of a convergent iterative process of direct calculations of the composite structure. Examples of calculations were performed on a computer. This method can be used for optimal designs of other types of vessels under internal pressure P.
The development of methods for designing optimal structures that satisfy various optimality criteria is an extremely important and urgent task. It is generally accepted that the optimal design is such a design if, under the action of given loads, the elastic limit is reached everywhere [5]. In this case, the structure will be equally stressed and have a minimum weight [1]. The condition of equal stress throughout the entire structure is a very strict condition and its implementation in real structures, as a rule, is not possible. Therefore, it is of interest to optimal structures when mitigating the conditions of equal stress, introducing the concept of a discrete condition of equal stress not over the entire continuum of the structure, but at individual points of each element of the composite structure.

Keywords: cylindrical shell, optimal designs, iterative process, internal pressure, elasticity.

Introduction

The development of methods for designing optimal structures that satisfy various optimality criteria is an extremely important and urgent task. It is generally accepted that the optimal design is such a design if, under the action of given loads, the elastic limit is reached everywhere [5]. In this case, the structure will be equally stressed and have a minimum weight [1]. The condition of equal stress throughout the entire structure is a very strict condition and its implementation in real structures, as a rule, is not possible. Therefore, it is of interest to optimal structures when mitigating the conditions of equal stress, introducing the concept of a discrete condition of equal stress not over the entire continuum of the structure, but at individual points of each element of the composite structure.

Main part

1Let the vessel design be given in the form of a cylindrical shell of constant thickness with a flat bottom (also of constant thickness). By dividing a given structure into elements, i.e. onto the body (1) and the bottom (2), we obtain the main system (Fig. 1). It is required to select such thicknesses of elements and that the maximum equivalent stresses in the elements differ from the permissible stresses within specified limits. This is the fulfillment of the discrete condition of equal tension.

2. To solve the problem posed, we consider the issue of determining the internal force factors along the section line of the structure into elements with fixed parameters. For this purpose we use general theorems of the theory of elasticity. The potential energy of the entire structure can be represented in the form:

$$\Pi = \Pi_1 + \Pi_2, \quad (1)$$

where Π_1 is the potential energy of the body, Π_2 - the same, bottoms.

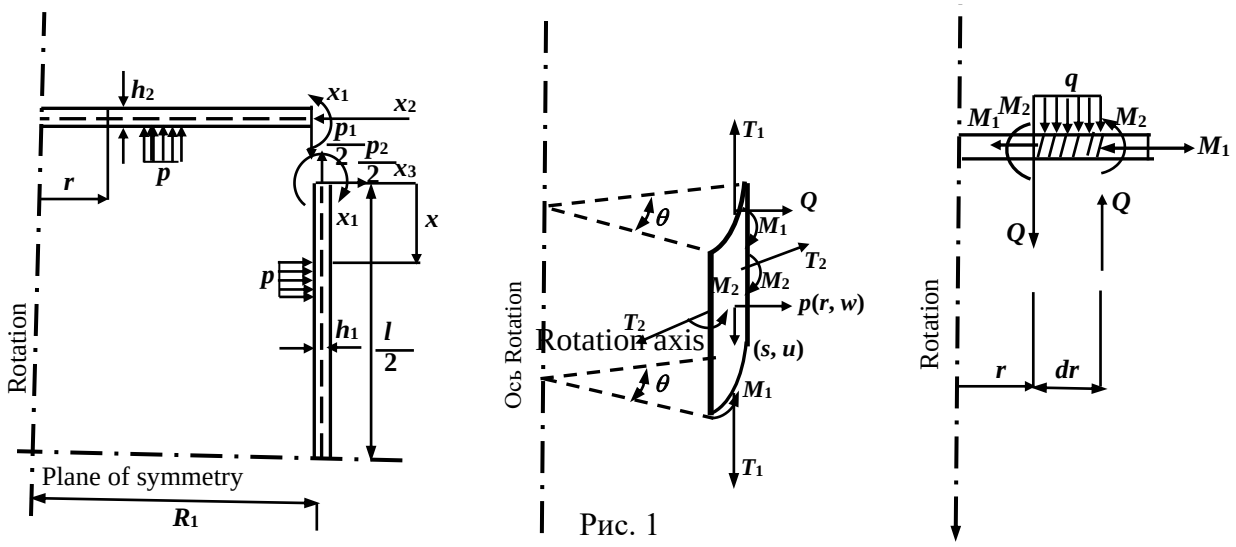

Рис. 1

According to Clapeyron's theorem, for a given system we have:

$$\Pi = \frac{1}{2} A, \qquad (2)$$

where A is the formally calculated work of external force factors on the actual displacements of points of a given system. For the main system, work A can be represented in the form $A = A_1 + A_2 + A_0$. (3)

Taking into account the accepted rule of signs (Fig. 1 a, b, c), the meanings of the works can be presented as follows:

$$A_1 = \int_L \left[\left(-\frac{dw_1}{dS} \right) x_1 + (w_1) x_2 \right] dl; \qquad (4)$$

$$A_2 = \int_L \left[\left(-\frac{dw_2}{dr} \right) x_1 + (\chi_1) x_2 \right] dl; \qquad (5)$$

$$A_p = \iint_P p[w_1(S) + w_2(r)] dF. \qquad (6)$$

3.According to the principle of independence, all movements can be represented in the following form: $-\frac{dw_1}{dS} = \delta_{11}^{(1)} x_1 + \delta_{12}^{(1)} x_2;$

$$-w_1 = \delta_{21}^{(1)} x_1 + \delta_{22}^{(1)} x_2 + \Delta_{2p}^{(1)};$$

$$-\frac{dw_2}{dr} = \delta_{11}^{(2)} x_1 + \Delta_{1p}^{(2)};$$

$$-\chi_2 = \delta_{22}^{(2)} x_2; \quad (7)$$

$$-w_1(S) = w_{p1}^{(1)} x_1 + w_{p2}^{(1)} x_2 + w_{pp}^{(1)};$$

$$-w_2(r) = \delta_{p1}^{(2)} x_1 + w_{p2}^{(2)} x_2 + w_{pp}^{(2)}.$$

From the disclosure of the principle of minimum potential energy

$$\frac{\partial \Pi}{\partial x_k} = 0 \ (k = 1, 2) \qquad (8)$$

we obtain a system of canonical equations in the form of a generalized method of forces (k = 1, 2), (9)

$$\sum_{i=1}^{2} \delta_{kl} x_l + \Delta_{kp} = 0 \, (k = 1, 2), \qquad (9)$$

Where

$$\delta_{11} = 2\pi R_1 \left[\delta_{11}^{(1)} + \delta_{11}^{(2)} \right];$$

$$\delta_{12} = \pi R_1 \left[\delta_{12}^{(1)} + \delta_{21}^{(1)} \right];$$

$$\Delta_{1p} = 2\pi R_1 \Delta_{1p}^{(2)} + \frac{p}{2} \iint_F \left[w_{p1}^{(1)} + w_{p1}^{(2)} \right] dF; \quad (10)$$

$$\delta_{21} = \pi R_1 \left[\widehat{\delta}_{21}^{(1)} + \widehat{\delta}_{12}^{(2)} \right];$$

$$\delta_{22} = 2\pi R_1 \left[\delta_{22}^{(1)} + \delta_{22}^{(2)} \right];$$

$$\Delta_{2p} = 2\pi R_1 \Delta_{2p}^{(1)} + \frac{p}{2} \iint_F \left[w_{p2}^{(1)} + w_{p2}^{(2)} \right] dF.$$

In this case, according to the reciprocity theorem of possible works, we have the following relations:

$$\delta_{12}^{(1)} = \delta_{21}^{(1)}; \ 2\pi R_1 \Delta_{1p}^{(2)} = \frac{p}{2} \iint_F [w_{p1}^{(1)} + w_{p1}^{(1)}] dF; \qquad (11)$$

$$2\pi R_1 \Delta_{2p}^{(2)} = \frac{p}{2} \iint_F [w_{p2}^{(1)} + w_{p2}^{(2)}] dF.$$

To determine the values of the coefficients of equation (9), we consider a cylindrical shell

under the action of an external load and edge internal forces.

The differential equation of a cylindrical shell under the action of internal pressure has the form [2].

$$w_1^{(IV)}(S)+4k_1^4 w_1(S)=\frac{p}{D_1}-\mu_1\frac{T_1}{D_1R_1}, \quad (12)$$

Where

$$k_1=\sqrt[4]{\frac{E_1h_1}{4R_1^2D_2}}; D_1=\frac{E_1h_1^3}{12(1-\mu_1^2)}, \quad (13)$$

μ_1-. Poisson's ratio.

We consider the shell as long, i.e. condition is met

$$\frac{l}{\sqrt{R_1h_1}}\sqrt[4]{3(1-\mu_1^2)}>1.5, \quad (14)$$

where $l-$ is the length of the shell.

In relation to the problem under consideration, the deflection function $w_1(S)$ will look like: $w_1(S)=\frac{e^{-k_1S}}{2D_1k_1^2}$

$$\left[(\cos k_1S-\sin k_1S)x_1+\frac{\cos k_1S}{k_1}x_2\right]+$$

$$\frac{PR_1^2}{E_1h_1}\left(1-\frac{\mu_1}{2}\right). \quad (15)$$

Using the function $w_1(S)$, we get the coefficients $\delta_{ik}^{(1)}$:

$$\delta_{11}^{(1)}=-\left.\frac{dw_1}{dS}\right|_{x_1=1}=\frac{1}{D_1k_1}; \quad (16)$$

$$\delta_{12}^{(1)}=-\left.\frac{dw_1}{dS}\right|_{x_1=1}=\frac{1}{2D_1k_1^2}; \quad (17)$$

$$\delta_{22}^{(1)}=\left.w_1\right|_{x_2=1}=\frac{1}{2D_1k_1^3}; \quad (18)$$

$$\delta_{21}^{(1)}=\left.w_1\right|_{x_1=1}=\frac{1}{2D_1k_1^2}; \quad (19)$$

$$\Delta_{2p}'=\frac{PR_1^2}{E_1h_1}\left(1-\frac{\mu_1}{2}\right). \quad (20)$$

4. To determine the coefficients $\delta_{ik}^{(2)}$ Let us consider the bottom of the vessel as a plate subject to transverse bending and a plane stress state.

According to [4], the differential equation of a round plate has the form:

$$\frac{1}{r}\frac{d}{dr}\left\{r\frac{d}{dr}\left[\frac{1}{r}\frac{d}{dr}\left(r\frac{dw}{dr}\right)\right]\right\}=\frac{d}{D_2}. \quad (21)$$

The deflection function in relation to this problem has the form

$$w_2(r)=\frac{(R_1^2-r^2)x_1}{2D_2(1+\mu_2}-$$

$$\frac{p(R_1^2-r^2)}{64D_2}\left[\frac{(5+\mu_2)R_1^2}{1+\mu_2}-r^2\right]. \quad (22)$$

According to [3], the differential equation of an axisymmetric plate will have the form:

$$\frac{d^4\chi_2}{dr^4}+\frac{2}{r}\frac{d^3\chi_2}{dr^3}-\frac{1}{r^2}\frac{d^2\chi_2}{dr^2}+\frac{1}{r^2}\frac{d\chi_2}{dr}=0. \quad (23)$$

Radical displacement function χ_2 will look like:

$$\chi_2=\frac{(1-\mu_2)x_2}{E_2h_2}r. \quad (24)$$

Using functions $w_2(r)$ and χ_2, we get the coefficients $\delta_{ik}^{(2)}$

$$\delta_{22}^{(2)}=-\chi_2\big|_{x_2=1}=\frac{(1-\mu_2)R_1}{E_2h_2}; \quad (25)$$

$$\Delta_{1p}^{(2)}=-\left.\frac{dw_2}{dr}\right|_{p\neq0}=-\frac{pa^3}{8D_2(1+\mu_2)}. \quad (26)$$

5. After solving system (9), the stress state in each structural element is analyzed. For each fixed section, equivalent stresses are determined, which must satisfy the forming energy criterion in the optimal design.

$$[\sigma]\geq\frac{1}{\sqrt{2}}\sqrt{(\sigma_\alpha-\sigma_\beta)^2+(\sigma_\beta-\sigma_\gamma)^2+(\sigma_\gamma-\sigma_\alpha)^2+6(\tau_{\alpha\beta}^2+\tau_{\beta\gamma}^2+\tau_{\gamma\alpha}^2)} \quad (27)$$

.

The stressed state of the shell at points on the internal and external surfaces is determined by stresses of the form:

$$\sigma_s = \frac{T_1}{h_1} \pm \frac{6M_1}{h_1^2};$$
$$\sigma_\theta = \frac{T_2}{h_1} \pm \frac{6M_2}{h_1^2}, \quad (28)$$
$\sigma_z^B = -p$ (on the inner surface),
$\sigma_z^H = 0$ (on the outer surface).

The stresses at points on the middle surface of the shell are determined by the formulas

$$\sigma_s^c = \frac{T_1}{h_1}; \quad \sigma_\theta^c = \frac{T_2}{h_1}; \quad \tau_{sz}^c = \frac{3}{2}\frac{Q}{h}. \quad (29)$$

Here

$$T_1 = \frac{PR_1}{2}; \quad M_1 = D_1 \frac{d^2w}{dS^2}; \quad M_2 = \mu_1 M_1;$$
$$T_2 = T_1\mu_1 + w_1 \frac{E_1 h_1}{R_1}; \quad (30)$$
$$Q_1 = D_1 \frac{d^3 w_1}{dS^3}.$$

For each section S_l we have $\sigma_{\text{экв}}^B$, $\sigma_{\text{экв}}^H$, $\sigma_{\text{экв}}^C$. Selected from them $\max \sigma_{\text{экв}}^l$.

$$\max \sigma_{\text{экв}}^l = \max\{\sigma_{\text{экв}}^B, \sigma_{\text{экв}}^H, \sigma_{\text{экв}}^C\}. \quad (31)$$

Of all $\max \sigma_{\text{экв}}^l$ (i = 1, 2, … ,n) is selected $\max \sigma_{\text{экв}}^l$, Where j– proximity number.

Then the coefficient is determined k_j characterizing the uneven tension of an element in relation to a given strength condition.

$$R_j = \frac{\max \sigma_{\text{экв}}^j}{[\sigma]}. \quad (32)$$

If $k_j > 1$, then the element is overloaded and it is necessary to increase the material consumption for this element.

The iterative process is carried out by correcting h_1 according to the formula:

$$h_1^{j+1} = \frac{h_1^j (k_j + 1)}{2}; \; j = 1, 2, \ldots, n. \quad (33)$$

A similar iterative process is carried out to select the thickness of the bottom h_2.

The following formulas are used to determine stresses: $\sigma_r = -\frac{x_2}{h_2} \pm \frac{6M_r}{h_2^2}$;

$$\sigma_0 = -\frac{x_2}{h_2} \pm \frac{6M_\theta}{h_2^2};$$
$$\sigma_z^B = -p; \quad \sigma_z^H = 0; \quad (34)$$
$$\sigma_r^C = \sigma_\theta^C = -\frac{x_2}{h_2}; \quad \tau_{rz}^C = \frac{3}{2}\frac{Q_2}{h_2}.$$

Here

$$M_r = -D_2\left(\frac{d^2w_2}{dr^2} + \frac{\mu_2}{r}\frac{dw_2}{dr}\right);$$
$$M_\theta = -D_2\left(\frac{1}{r}\frac{dw_2}{dr} + \mu_2 \frac{d^2w_2}{dr^2}\right); \quad (35)$$
$$Q = -\frac{p_r}{2}.$$

The iterative process for the entire structure stops, then for each element the following condition will be satisfied:

$$|k_j - 1| \le |\boldsymbol{E}|, \quad (36)$$

– given value.

6. Examples of calculations: Let a vessel under internal pressure be given p with parameters: l= 250 sm, R_1 = 50 sm, $E_1 = E_2$ = 0,981 · 2 · 10^6kn/dm^2, $\mu_1 = \mu_2 = 0{,}3$, $[\sigma]_1 = [\sigma]_2 = 0{,}981 \cdot 2000$ kn/dm^2. Need to select thickness h_1 And h_2, that $\max \sigma_{\text{экв}}^l$ reached [σ].

а) Taking p = 1 ат, $h_1 = h_2 = 1$ sm, In the process of direct calculation, we obtained results that coincided with the results given in [2].

б) Taking p = 15 ат During the iterative process, the optimal thickness parameters h_1 = 3.296 cm and h_2 = 3.345 cm were obtained. At the same time, in Figure 2 shows the convergence of the iterative process.

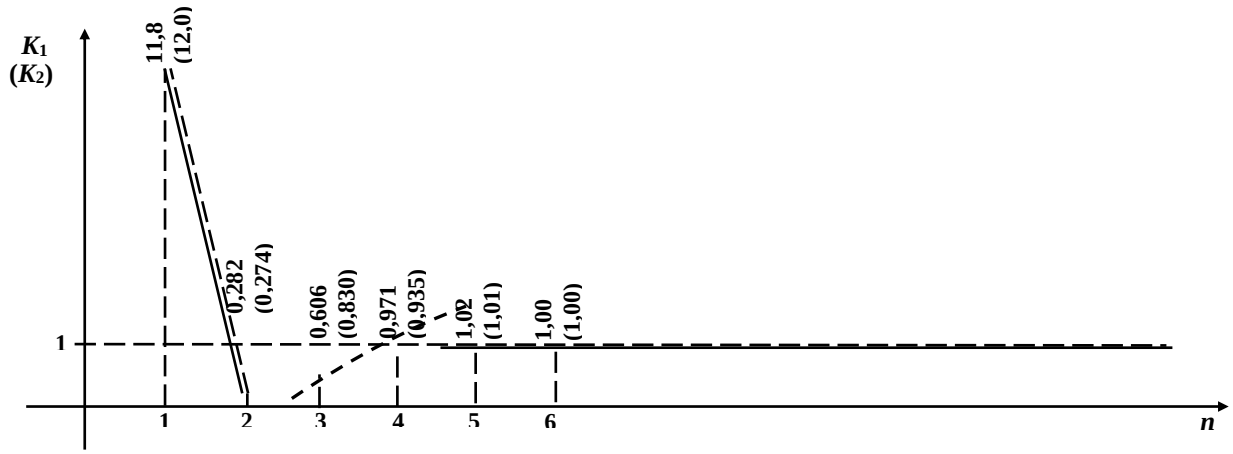

Figure 2

в) In Fig. Figure 3 shows the results of selecting optimal parameters h_1 h_2 depending on pressure. h_1 And h_2 depending on pressure.

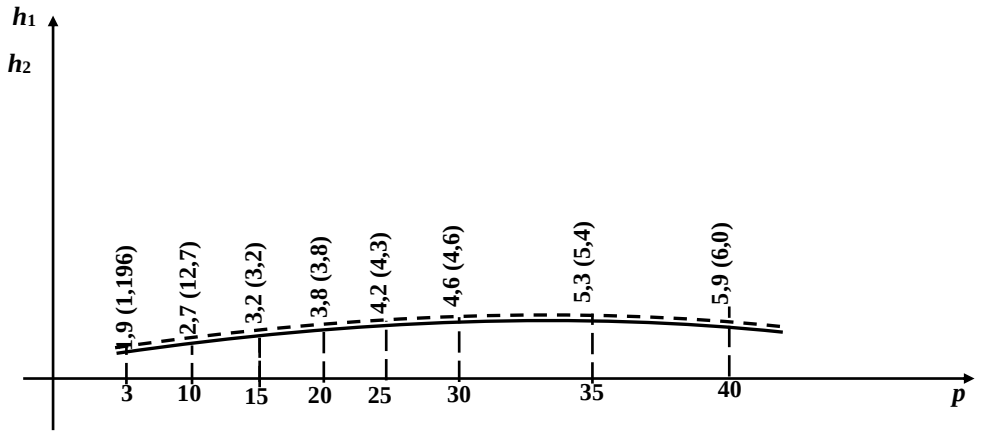

Figure. **3**

г) With parameters h_1 = 3,29 sm and h_2 = 3,34 sm, close to optimal, a direct calculation of the vessel was carried out.

S_l (sm), r_i (sm), w (sm), $M\left(\frac{\text{кГсм}}{\text{см}}\right)$, $Q\left(\frac{\text{кГ}}{\text{см}}\right)$, $T\left(\frac{\text{кГ}}{\text{см}}\right)$, $N\left(\frac{\text{кГ}}{\text{см}}\right)$, $\sigma\frac{\text{кГ}}{\text{см}}$.

In the SI system, tabulated values of internal conditions and stresses should be multiplied by the corresponding coefficients.

Table 1

lateral surface(korpus)					
Section	1	2	3	4	5
S_i	0,0000	24,332	48,664	72,996	97,328
W	$0{,}23\cdot10^{-2}$	$0{,}32\cdot10^{-2}$	$0{,}50\cdot10^{-2}$	$0{,}48\cdot10^{-2}$	$0{,}48\cdot10^{-2}$
M_1	4166,2	295,80	7,6534	1,2343	–0,222
M_2	1249,8	88,741	2,2960	0,3703	–6,681
Q_1	–450,18	8,2561	2,3302	–0,3732	$0{,}31\cdot10^{-1}$
T_1	362,66	362,66	362,66	362,66	362,66
T_2	422,21	531,92	777,33	743,79	746,39
$\sigma^{в}_{экв}$	2146,1	1506,4	218,74	209,02	209,47
$\sigma^{н}_{экв}$	1974,7	248,66	203,84	195,64	196,52
$\sigma^{с}_{экв}$	375,02	143,21	204,77	195,00	196.49

Base

Section	1	2	3	4	5	6
r_i	0,0000	10,000	20,000	30,000	40,000	50,000
W	–0,2164	–0,2006	–0,1566	–0,0952	–0,0346	0,0000
M_r	–3067,5	–2778,2	–1910,1	–463,38	1562,0	4166,2
M_θ	–3067,5	–2900,9	–2401,1	–1568,1	–402,00	1097,36
Q_2	0,0000	–75,00	–150,0	–225,00	–300,00	–375,00
N_1	450,18	450,18	450,18	450,18	450,18	450,18
N_2	450,18	450,18	450,18	450,18	450,18	450,18
$\sigma^{в}_{экв}$	1500,0	1378,6	1035,2	649,67	1024,7	2119,7
$\sigma^{н}_{экв}$	1784,6	1663,0	1314,2	853,66	931,85	1919,2
$\sigma^{с}_{экв}$	134,78	146,11	175,78	216,38	262,82	312,33

M(НМ) – on 0,0981,

$Q\,\frac{\text{Н}}{\text{М}}$, $T\,\frac{\text{Н}}{\text{М}}$, $N\,\frac{\text{Н}}{\text{М}}$ on $9{,}81 \cdot 10^2$,

$\sigma\,\frac{\text{КН}}{\text{ДМ}^2}$ on 0,981.

Conclusions

The research results showed that this approach makes it possible to optimize structures, i.e. find the required optimal parameters of the elements, satisfying the accepted strength conditions.

Reference

1. Pipkin, Rivlin. Design of high-pressure vessels of minimal weight, reinforced with inextensible threads. Applied mechanics. IL, series E, No. 1, 1963.
2. Ponomarev S.D. and others. Fundamentals of modern methods for calculating strength in mechanical engineering. Mashgiz, M., 1950.
3. Sneddon I.N., Berry D.S. Classical theory of elasticity. Fizmatgiz, 1963.
4. Timoshenko S.P., Voinovsky1-Krieger S. Plates and shells. Fizmatgiz, M., 1963.
5. Shield R. Methods for optimal design of structures. Mechanics

INTEGRATED MANAGEMENT OF WATER RESOURCES

Ketevan Gordeziani, Lasha Kavelashvili, Nikoloz Kakhidze
Georgian Technical University, Tbilisi 0170, Georgia
k.gordeziani@gmail.com

Abstract

Many processes preceded the establishment of the concept of sustainable development. In September 2015, world leaders unanimously adopted the Sustainable Development Goals. Georgia has decided to lay the foundation for their integration into national development plans and multi-disciplinary strategies. Georgia was one of the twenty-two countries that submitted the National Review (VNR) voluntarily. In order to achieve the Sustainable Development Goals, at the Political Forum on Sustainable Development in July 2016, Georgia took active measures to change the Sustainable Development Goals and Indicators in accordance with the conditions, challenges and opportunities in the country. In 2017, Georgia chose the seventeenth sustainable development goal and announced it as a national priority along with others. At the end of 2019, the process of nationalization of sustainable development goals was completed. The Administration of the Government of Georgia is the main government agency responsible for coordinating and overseeing the implementation of the national sustainable development agenda. The Sustainable Development Goals Council includes ministers of the relevant sector of the government, heads of UN agencies, representatives of the private sector and public organizations, as well as international organizations.

Keywords: Millennium Development Goals, Sustainable Development Goals, Safe Water, Water Supply Systems, Drinking Water Treatment Plant.

Introduction

Many processes preceded the establishment of the concept of sustainable development.

In September 2000, at the largest meeting of heads of state in the history of the world, the "United Nations Millennium Declaration" was adopted, the fulfillment of the goals of which was set for the period until 2015.

Millennium Development Goals (MDGs)

Sustainable Development Goals (SDGs)

Main part

Sustainable water supply and sanitation sector development programs remain one of the most pressing challenges in the world.

In 2011, ADB launched a $500 million program to help provide better water supply and sanitation (WSS) to the population of Georgia. The program included implementation of biological water treatment, awareness raising of the service and regulatory sector, staff training and operational management. Updated in 2020, the program included infrastructure and advanced technology for water treatment, network expansion, sustainable operation and maintenance. The efficiency of the state-owned water supply, which was improved under the previous program, was improved by the government's reform policy.

One of the main goals for our country is clean water and sanitation. this means that:

- Ensuring universal and equal access to safe and affordable drinking water for all people by 2030.
- By 2030, achieving access to adequate and equal sanitation and hygiene conditions for all people and elimination of open defecation.
- By 2030, implementation of integrated management of water resources at all levels, including, within the limits of capacity, through transboundary cooperation.
- Implementation of integrated management of water resources.

In this article, for example, the problems of water supply in Fasanauri township and ways to solve it are discussed.

The village of Fasanauri is located at the confluence of the Mtiuleti and Gudamakari Aragvi rivers, on the military road of Georgia, 1050 m above sea level, 47 km from Dusheti. The climate is moderately humid, with moderately cold winters and long cool summers. The average annual temperature is 7.8°C, -4.1°C in January, 18.5°C in July; Absolute minimum -30°C, absolute maximum 36°C. Precipitation 1000 mm per year. Fasanauri has an overabundance of tourists in all seasons of the year.

The type of water supply in Fasanauri township is central, self-powered. Some of the existing capital buildings are:

1. Chabarukhi - a surface water receiving structure, which is arranged by arranged by the local population. Debit 15-18 l/s. This water is not cleaned, it just flows into the reservoir. It was built in 1977. It was canceled due to the 1985 flood. In the later period, a coastal type surface water intake was organized. During the period of overflowing water, its
2. quality does not meet the standard, it is in an emergency condition.
3. Khevsha-1 - complex type, drainage and captage joint facility. Debit 11 l/s. It was built in 2005. Captage and drainage are calmated. Sanitary norms are not observed. 8-10 l/s. It spills and cannot be collected.
4. Khevsha-2 - catchment type water receiving facility. Debit 8 l/s. It was built in 2016. It is not protected sanitarily.
5. Oshpitali - captage type building. Debit 8 l/s. It was built in 1977. It does not have a chamber, there is water leakage from the walls. Sanitary norms are not observed.

Water is distributed in the territory from two reservoirs:

1. Chabarukhi reservoir - volume V=1000 m3, reinforced concrete, quadrangular, one-chamber, half covered with earth, the foundation is visible. It was built in 1977. It does not have a ventilation chamber, there is water leakage from the walls. The territory does not have a sanitary fence, guardhouse and toilet facilities.
2. Oshpiteli reservoir - volume V=75 m3, reinforced concrete, quadrangular, one-chamber, half covered with earth. It was built in 2016. Storage, chlorination and toilet buildings are located on the territory.
3. Chabarukh water treatment plant (located one hundred meters from the Chabarukh reservoir). It was built in 1977. Consists of three sections of two clarifiers and slow filters. Performance 12 l/s. It is not functioning after the flood of 1985. Today, the buildings of Salektri and Slow Filters are half destroyed as a result of the landslide and are not subject to rehabilitation.

In order to fulfill the main goal and establish a clean, safe water supply network, along with topographical and geological studies, complex studies and works were carried out.

After receiving the results of geological, hydrological, sustainability conclusions and water analyses, it was decided to rehabilitate the existing infrastructure. As a treatment plant, we selected a modern water treatment plant, which responds to the results obtained during the calculation.

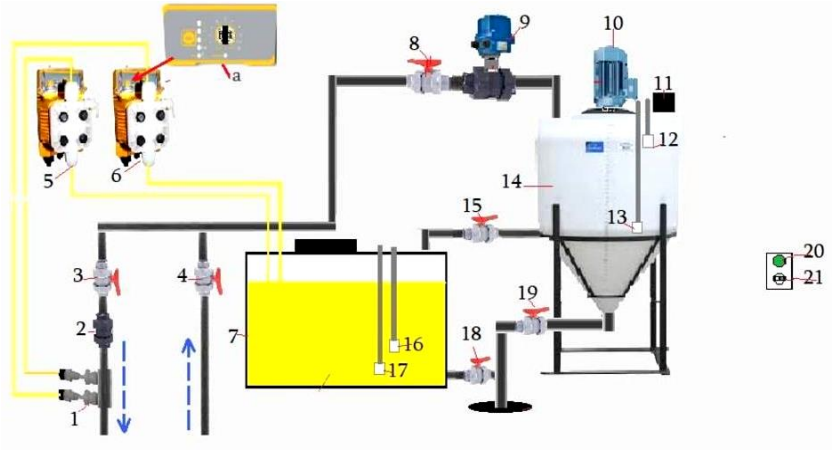

3 Conclusions

Population growth and development is increasing every year, which affects the demand for clean water. During the dry season, many regions of Georgia experience a shortage of clean water due to poor clean water management. Clean water management companies play a critical role in maintaining access to the clean water that communities need. In order to get a proper system, it is necessary to involve specialists in the field. For the example presented in the article, the following treatment plant was selected:

1. Chlorination point (injector).
2. Reverse valve.
3. Passing water valve (chlorination occurs when the hand valve is open).
4. Incoming water valve.
5. Chlorination pump-doser.

a. Pump-doser dosage regulator.

6. Spare chlorination pump-doser.
7. Hypochlorite supply tank.
8. Manual/hand valve.
9. Valve with electric actuator.
10. Mixer.
11. Hypochlorite reservoir.
12. Tank overflow valve in hypochlorite mixing tank.
13. Hypochlorite mixing tank minimum level indicator (alarm).
14. Hypochlorite mixing tank.
15. Hypochlorite hand valve coming out of a finished hypochlorite tank.
16. he hypochlorite tank alarm level indicator.
17. Level indicator sensor (emptying the hypochlorite tank).
18. Discharging valve of the hypochlorite supply tank.
19. Discharging valve for hypochlorite making tank.
20. Opening-closing button of the electric valve (functions when the hypochlorite preparation tank is not full).
21. Mixer on-off switch (functions when the hypochlorite mixing tank is full).

Hypochlorite is prepared in the following order:

1. Water valve #3, #4, and #8 are open.
2. Hypochlorite valves #15, #18 and #19 are closed.
3. Weigh and place in a separate vessel 30-31 kg of calcium hypochloride powder with a concentration of 65%.
4. Press the button #20 of the opening-closing of the electric valve #9 for no less than 3 seconds. If hypochlorite preparation tank #14 is not present, electric valve #9 will open and tank #14 will begin to fill.
5. Set the on-off switch of the hypochlorite solution #10 vortex mixer #21 to the on position. #10 mixer will only turn on when #14 hypochlorite preparation tank is filled with water.
6. Using the funnel #14, we pour the pre-weighed hypochlorite powder into the tube #11 located in the upper part of the hypochlorite preparation tank.

7. Wait for #14 hypochlorite preparation tank to fill with water (1000 L).
8. When the hypochlorite preparation tank #14 is filled with water, the electric valve #9 will automatically close and the hypochlorite solution mixer #10 will turn on.
9. A #10 vortex mixer must be run for at least one hour to dissolve the calcium hypochlorite powder at a concentration of 65% in water.
10. One hour after turning on the hypochlorite solution #10 vortex mixer, the #10 mixer will automatically turn off.
11. After about an hour, turn the on-off switch #21 of the hypochlorite solution #10 vortex mixer to the off position.
12. The hypochlorite solution prepared for chlorination of drinking water should stand for no less than 24 hours.
13. After preparing the hypochlorite solution prepared for chlorination of drinking water, we open the #15 hypochlorite tank and wait for the filling of the #7 hypochlorite supply tank.
14. After filling the hypochlorite supply tank #7, we close the hypochlorite valve #15.

Reference

1. Gao, Y.J., Li, S.J. (2019) Optimization of multiple fillers used for removal of water pollutants of large well near the river in northern China. Journal of Water, Sanitation and Hygiene for Development, 9(2): 363-373.
2. World Health Organization (2011) Guidelines for Drinking-water Quality, 4th Edition. World Health Organization, Geneva.
3. Progress towards SDG 6, in the United Nations World Water Development Report 2023: Partnerships and cooperation for water. UN Water, UNESCO, 2023.
4. Goal 6: Clean water and sanitation, KnowSDGs platform, European Commission's Joint Research Center, accessed 4 July 2023.
5. EU voluntary review on the Implementation of the 2030 Agenda for Sustainable Development, European Commission, 2023.
6. Sustainable development in the European Union: Monitoring report on progress towards the SDGs in an EU context – 2023 edition, European Commission, Eurostat, 2023.
7. Abdou AH, Hassan TH, El Dief MM (2020) A description of green hotel practices and their role in achieving sustainable development. Sustainability. https://doi.org/10.3390/su12229624

THE ARTISTIC DECORATION OF THE FASADE OF THE BUILDING IS COMPOSITE WITH WALL PANELS

Irakli Kvaraia
Georgian Technical University, Tbilisi 0170, Georgia
irakvara@yahoo.com

Abstract

The article discusses the progress of building facade finishing works using modern composite wall panels. Along with the installation of basic wall panels and arrangement of ventilated facades on the outer walls of one of the newly built schools in Tbilisi, large-scale artistic panels were also arranged in several places using the same wall panels of different colors. Such an approach, literally without incurring additional costs, made possible the high-quality artistic decoration of the facade and significantly increased the architectural attractiveness of the building. In addition, it must be noted that the wall panels were cut into simple elements (triangle, rectangle, etc.) to create an artistic panel, and then the desired result was achieved by distributing them according to a predetermined image.

Key words: building, composite, panel, wall, aluminum, fixing, installation, rivet, bracked, decoration

Introduction

In recent years, composite panels are used more and more frequently for the purpose of cladding buildings. A composite is a man-made material consisting of two or more components that provide its strength and durability. Composite panels for exterior cladding are made on the basis of various materials and are distinguished by great diversity. It is moisture-resistant, resistant to impacts and natural precipitations, withstands large temperature fluctuations, does not shrink, does not change color. It is especially important that such panels can be cut using simple tools, that is, they are very easy to process and install. Based on these properties, composite panels already compete with natural stone facing materials. In addition, with their help, it is possible to easily arrange artistic-decorative inserts (artistic panels, paintings, etc.) on the facades of the building, even using rectangular elements. Their presence makes buildings more complete from an architectural point of view. It is also important that such artistic decoration of building facades does not require special costs.

HPL (High Pressure Laminates) panels of the Austrian company "Fundermax" belong to one of the most high-quality and durable exterior cladding composite panels. It is made by pressing resin-impregnated kraft paper (wooden paper) and covered on both sides with a decorative and protective laminated layer. The mentioned panels were used in St. In order to cover the new building of the 138th public school in Tbilisi, and on its facades, four diverse artistic panels were arranged from the same material, which added special attractiveness to the school building.

Main part

The exterior walls of the monolithic reinforced concrete frame of the three-story, rectangular school building were built with ceramic bricks. The project included high-quality plastering on all four facade parts, a large part of which was to be covered with "Fundermax" HPL exterior wall panels. In addition, based on the architectural solution, in several places, as a result of cutting and installing the same facing panels into simple elements, artistic decoration of quite large areas had to be done according to a predetermined drawing.

Before the start of paving works, HPL external wall panels of different colors were brought to the site based on the contract signed directly with the Austrian company "Fundermax". The size of all of them was 4100 X 1854 X 6 mm. The main color was dark gray. There were also black, green, orange and white panels, which had to be cut into different sized elements to cover and decorate the building. For this purpose, an open workshop was organized directly on the construction site, where the mentioned panels were cut into the necessary sizes and processed. In addition, white color panels, all of the same size (2050 X 1700 X 10 mm) were factory made according to the pre-order. According to the request of the author of the project, triangular figures were pre-cut and high-quality in the factory using the laser cutting method. Panels of this type were provided to cover the windows of entrances and toilets along the entire height of the building and deaf walls in some places. Matching their color with the color of the main panels made the cladding very effective.

Finishing works have started with the installation of special aluminum brackets on the entire height of the facade walls. on which longitudinal

aluminum profiles were fixed in a vertical position with self-tapping screws (Fig. 1).

Fig. 1. Installation of aluminum brackets and beams

The configuration of the aluminum bracket embedded in the wall allowed for box-like placement of wall panels, i.e. ventilated facades, over the entire height of the building. These works were carried out using a hanging electric basket (Fig. 2). It should be noted that during the operation of the building, in order to exclude the negative influence of temperature variations on the installed wall panels, the difference in height between the elements of all sizes of the vertically placed wall panels was at least 0.5 cm. The installation of the elements of the artistic panel was carried out with similar deviations, which was mainly carried out using triangular pieces of wall panels and finally gave a diverse circular configuration.

Fig. 2. Installation of main wall panels

The main stage of finishing the facade was finished with the installation of white colored panels. Their transportation and on-site installation was carried out by means of an auto basket between the vertical profiles for fixing the wall panels, which was very easily carried out by one person (Fig. 3).

Fig. 3. Installation of figured white panels

The wall panels were cut with a special electric saw and a multi-grooved aluminum ruler provided for its movement. However, if only rectangular elements of almost the same size were used to make the main wall panels, it was necessary to make triangular or rectangular elements of different sizes and colors to make the whole picture of the artistic panel. In order to maximize the use of the wall space, the element of the required outline and size was precisely drawn in advance, and only after that the process of cutting it began (Fig. 4).

Fig. 4. The process of cutting the wall panel

The process of arranging the artistic panel involved the arrangement of triangular elements pre-cut to the required sizes in such a way that they would take the shape of a continuous circle after being installed next to each other. Several such circles formed the main image of the panel, and to fill the remaining spaces, along with triangles, other shaped elements cut from the wall panels were used.

Fastening of wall panels and their elements was carried out directly on vertical aluminum profiles with special rivets and using the appropriate tool. It should be noted that the color of the rivets was the color of the panels to be installed and was included in the factory. The installation of the largest panels required special precision and good fastening, as the process was carried out in two parts. First one side of the panel was completely finished, and then the construction of the other part began. Technologically, this process also started from the lowest part of the wall (Fig. 5).

The installation of the first triangular elements of the artistic decoration around the central point (Fig. 6) was followed by the continuation of its installation in the vertical direction and the filling of the sides (Fig. 7).

Fig. 5. Start panel installation

Fig. 6. Installation of triangular elements

Fig. 7. Installation of the panel vertically

After that, the installation of its first part was completed (Fig. 8).

The installation of the second part continued from the lower level, by connecting the triangular elements with sides of exactly the same length to the sides of the installed elements of the first part (Fig. 9).

Fig. 8. Completed first part

Fig. 9. Installation of the second part of the panel

The correct interconnection of the triangular elements intended for artistic decoration and the bordering of the received diverse paintings with

the main wall panels, i.e. putting them in a box-like frame (Fig. 10), gave the panel a finished look (Fig. 11).

Fig. 10. Arranging the frame of the panel

Fig. 11. Finished panel

The other three panels were made much faster and easier, because they took up relatively less space. Such artistic decoration significantly enriched the facade part of the building. Fig. 12 shows the panel arranged on the left side of the main facade of the building, and Fig. 13 shows the side, very effective panel together with the right panel of the main facade.

Fig. 12. The left panel of the main facade

Fig. 13. Pano on the side facade

It should be noted here that when finishing the facade with external wall panels, especially when arranging ventilated boxes, their upper parts should be covered with tin or other material required for roofing. This is necessary in order to exclude natural precipitations and their harmful effects on the outer walls of the building in this way (Fig. 14).

If there are parapets on the roof, the solution to this problem is easily implemented by covering the tin covering of the parapet on the box-shaped parts of the cladding (Fig. 15). In addition, the tilt of the tin must be directed towards the building, so that the water spills on the roof and is carried out by the existing system.

Fig. 15. A box of wall panels

Fig. 16. Covering wall panels with tin

Conclusions

1. The use of composite wall panels when finishing the facades of modern buildings greatly speeds up and simplifies the construction process. At the same time, such panels, due to their versatility, allow, without excessive costs, to arrange large-sized artistic decoration elements on the walls of the building. The presence of large areas artistically decorated on the walls of the building greatly enriches the facade and makes the whole building much more attractive.

2. When using composite wall panels for the artistic decoration of building facades, it is not necessary to cut them into complex outline elements. For this, it is enough to make straight details on the construction site using a special electric saw and a multi-groove aluminum ruler, which will then be installed according to the pre-made drawing.

3. When covering the facades of buildings with composite wall panels, it is necessary to exclude the negative effect of temperature on them and on the aluminum support elements, they should be separated from each other by at least 0.5 cm in height. A similar deviation must be maintained, in all directions, during the artistic decoration of facades with wall panel elements.

4. To protect against natural precipitation. When arranging ventilated facades from external wall panels, it is necessary to overlap them. If there is a parapet in the building, this is easily done by using tin to cover the parapet. In addition, the tin cover should be arranged in such a way that the water falling on it goes to the roof.

Reference

1. I. Kvaraia. Innovative technologies in construction. Technical University. Tbilisi. 2020. 184 pp.
2. A. Chikovani. Building materials. Technical University. Tbilisi. 2019. 156 pp.
3. I. Kvaraia. Production of natural stone cladding of the temple. Technical University. Tbilisi. 2019. 99 pp.
4. A. Chikovani, L. Klimiashvili, D. Gurgenidze. Architectural materials science. Technical University. Tbilisi. 2018. 247 pp.
5. I. Kvaraia. Modern technologies of construction production. Technical University. Tbilisi. 2018. 101 pp.
6. Z. Ezugbaia, I. Kvaraia, I. Iremashvili, N. Mskhiladze. Construction production technology. Technical University. Tbilisi. 2018. 254 pp.

PREPARATION OF MILITARY ENGINEERING TERRITORY

Levan Matsaberidze
Georgian Technical University, Tbilisi 0170, Georgia
"Military Engineering" program, third-year doctoral student. Major, Logistics of the Georgian Defense Forces IX-Class Planning Officer of the Supply Command.
levanmacaberidze@gmail.com

Abstract

The paper discusses the arrangement of the military-engineering area and its importance according to the military-engineering combat functions: mobility, countermobility and survivability. Based on these functions, the application of the Lanchester equations and the expected results during the military-engineering tactical planning process are explained. The implementation of this method in the educational field of the Defense Forces - in the Davit Aghmashenebeli National Defense Academy, in the general military center, in the military-engineering captain and platoon commander courses is an important issue. Historically fortified buildings in ancient times, the role of their construction for the protection of the population, on the example of different countries, are also discussed.

Keywords: fortification (a military structure intended for defense) built to protect a city and its population from potential aggressors.; Mobility, countermobility.

Introduction

The military-engineering arrangement of the territory has played a major role in our country for many centuries. Georgia faced great threats and challenges in the past, such as restoring territorial integrity and preserving the country's sovereignty. Against this background, different types of public units are formed to protect the country. In the past centuries, the leading role in the military engineering arrangement of the territory belonged to military engineers, as for military engineering, it originated in ancient times, in the ancient Middle East. In order to protect themselves from the enemy, people resorted to different methods, they used natural and available resources to protect the territory, such as "fortified" structures, caves, caves, etc.

Along with the development of military weapons and technologies, combat tactics and military operations are also developing. These types of moves require good planning and proper analysis. Therefore, in the future, Lanchester's system of equations will help the military-engineering units in the process of combat planning, simplify the assessment of threats and provide opportunities for accurate analysis.

Main part

During the military-engineering arrangement of the territory, it is necessary to study the terrain to arrange the obstacles, in this process, military engineers play a big role. In the process of planning combat tasks, we should use practical and theoretical possibilities. In some cases, it is difficult to make a correct analysis against a strong opponent with old-fashioned approaches. That is why military engineers can use Lanchester's equations when designing combat engineering obstacles: "mobility, countermobility, and survivability," which will aid in the planning process of combat tasks.

Mobility

The purpose of mobility operations is to support maneuver units in overcoming obstacles and maintaining movement momentum. Based on this situation, we can calculate the confrontation of the armed forces of the two sides with the Lanchester system of equations, in which one is weak and the other is strong.

$$X_1 = \sqrt{X_0^2 - \left(\frac{K \cdot X_0}{N}\right)^2} = X_0 \cdot \sqrt{1 - \left(\frac{K}{N}\right)^2}$$

Countermobility

The purpose of countermobility is to prevent the enemy's forces from moving by using engineering and natural obstacles. In this process, Lanchester's system of equations helps us determine what kind of firepower we will use to destroy the suspended enemy forces. It is calculated by the formula:

$$\frac{dR}{dt} = -\beta B$$
$$\frac{dB}{dt} = -a$$

Viability

The purpose of survivability is to protect one's forces from the enemy's direct and indirect firepower. For this, we need to calculate the amount of our own forces with this formula.

$$\frac{dB}{dt} = -aR$$
$$\frac{dR}{dt} = -\beta B$$

Historical "fortification" buildings in ancient times:

During the process of military-engineering arrangement of the territory, one of the important components is the arrangement/selection of "shelters" in order to protect the population. We must use the natural and artificial obstacles at our disposal to protect the country. Many centuries ago, Georgians began to select such places where it was difficult for a strong opponent to conduct military operations. For this purpose, settlements were built for the population in inaccessible places; In hard-to-reach places, together with location selection, settlements were fortified with various methods that protected them from the attack of enemies as much as possible, they made engineering barriers, barriers, fences, ditches and obstacles around the villages. In later periods of development, humans developed construction that brought about radical changes in military engineering. "Fortification" structures are created, which were built from the beginning using wood and stone in populated areas. Masters appeared who studied to achieve success and created various types of "fortification" structures at a high level.

The art of military construction became available and developed in the ancient centuries, a visible example of this is the ancient defensive construction around Babylon (VI-V BC), the fortification of Carthage and also the arrangement of various ancient cities; In the 1st-2nd centuries AD, the "Derband" wall stretched from the Caspian Sea to the Caucasus Range.

Fig. 1

Initially, for 500 years, the military-engineering work was carried out by classical Roman methods, which included the construction of "fortification" buildings, and then it gradually developed, and during the feudal age, the construction of wooden fortresses began, and then - stone. Castles were built on dominant points of terrain (usually on the top of a steep hill or on an impenetrable rock, often protected by a river), which provided almost impregnable shelters for the great feudal lords and their soldiers. The approach to the fortress wall was prevented by deep and wide water ditches. It was possible to cross the moat only with the help of a bridge, which was properly reinforced and protected.

Fortifications built along some state borders confirm that at that time the above-mentioned fortification was a high-level developed example of military engineering art.

The inhabitants of the ancient cities of Egypt started to build fences and walls to protect the territory from the enemy. It is known from history that in the Battle of Thermopylae (480 AD), the Greeks retreated due to the wall built on the Isthmus of Corinth. Mandrocles built a bridge over the Bosphorus, across which the Persian king Darius moved his army to Scythia Minor. One of the most interesting works of ancient military engineering was a 60-meter-high tower on wheels, raised above the walls of a besieged city, so that the soldiers in it could throw shells into the castle walls.

The largest ancient defensive structure is the Great Wall of China, which was built in c

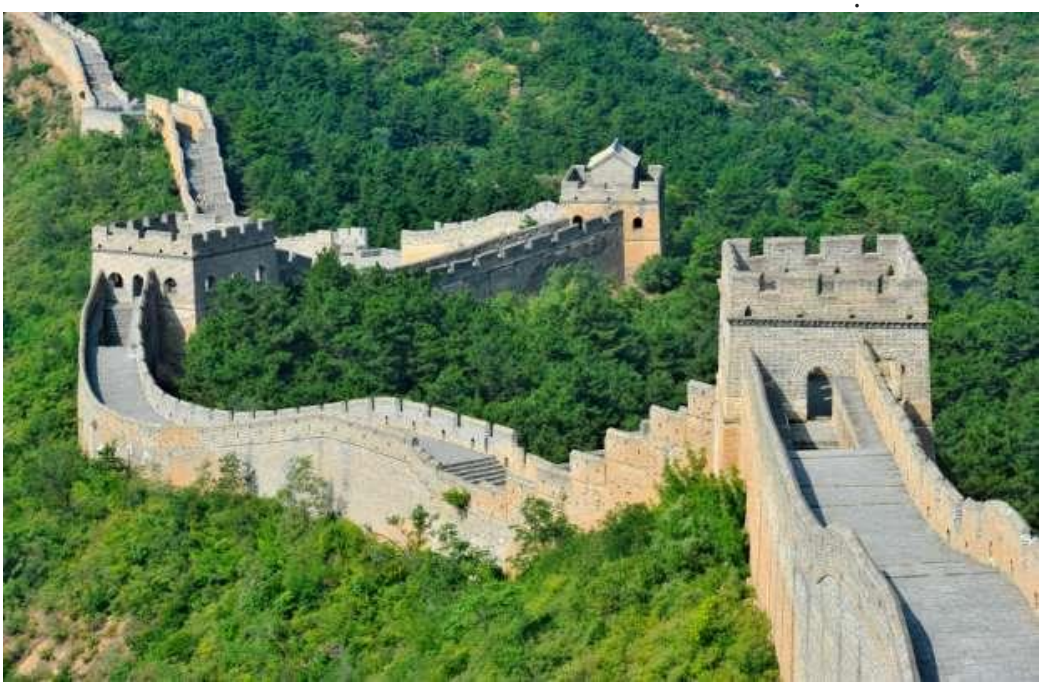

Fig. 2 The Great Wall of China

Wall sizes are different in different places. Approximate average dimensions are - height up to 7.5-8, height at the withers up to 9-10, width at the withers - up to 5.5-6, main width - up to 6.5. Towers are built in the key places of the walls. The approximate distance between the towers is 200 meters. Arrow shooting distance. Two-storied towers known as fire signal towers are also built. In the event of the appearance of an opponent, they would quickly send signals to each other by various means.

Roman soldiers were distinguished by their knowledge of surveying and engineering and combat tactics, Roman generals used military engineers to overcome obstacles on the front line of battle, they were well equipped with engineering tools that helped them to study the area, with this equipment they were good at selecting camp sites and making roads, paths and arranging bridges. The Roman engineering troops built a system of military main roads, equal to 6 m wide, with stone edges on both sides. This system had a total length of about 75,000 km and connected Rome to its colonies, while ensuring the military security of the empire.

The Romans were the preeminent military engineers of the ancient Western world, and we can still see examples of their work throughout Europe and the Middle East today. The Roman army, or military garrison towns, were protected by walls, ditches, and connected by straight military roads along which their legions could move quickly. Like the Chinese, the Romans built walls to protect their empire, the most famous being Hadrian's Wall in Britain, which is 73 miles (117 km) long and was built to protect the northern border against the Picts and Scots (Figure 3). Legions of troops and engineers built many of the greatest monuments of the Roman Empire

Fig. 3 "Hadrian's" wall.

The Byzantine Empire, India, and China continued to fortify their cities with walls and towers, while urban civilization in Europe collapsed with the fall of the Roman Empire. One of the signs of the revival of urban civilization were the castles of Motte-en-Baille. This consisted mainly of a high mound of earth (the motte) surrounded by wooden palisades, ditches, embankments (the bailey) and a wooden tower occupying the central mound. From the 11th century, they were replaced by stone fortresses, which served as military bases and administrative centers. Medieval engineers were adept at mining operations, tunneling under castle walls.

Conclusion

In conclusion, we can say that for the purpose of defense of Georgia, the issue is very urgent and this activity will increase if we take into account the above-mentioned issues. That is why

Lanchester's system of equations will enhance the military engineering planning process in the defense forces. Also, historical facts show that from the beginning there was a strong "fortification" and in the future it will continue to be a strong barricade to protect the safety of the population.

References

1. "Development of military-engineering art/business from ancient times to the present day". Tbilisi, 2022.
2. Medzmariashvili, Elguja, "Georgian military terms and definitions according to military branches". Tbilisi, 2018
3. Medzmariashvili, Elguja. "Fundamentals of Georgian military-engineering doctrine". Tbilisi, 2006.
4. https://geoarmada.files.wordpress.com/2013/01/800px-20090529_great_wall_8125.jpg

FITTING AN ELASTIC RING WITH A LOAD ON THE INTERNAL CONTOUR

Vasil Sokhadze
Georgian Technical University, Tbilisi 0170, Georgia
V.sokhadze@gtu.ge

Abstract

Considered in this article srttlr of ring under the loading does not cause the deformation of cross-section, only a change in angle. In this case, we have tensile and compressive deformations in the perpendicular direction of the cross section. Tach annular fiber of ring is uniformly tensioned or compressed and remains the annular shape; the settle is not directly proportional to loading.

Key words: ring, settle, annular extension.

Introduction

The ring rests on the supporting plane only with its outer contour; it is obvious that the reaction forces on this contour will be equal to the intensity q. The angle of inclination between the outer contour of the that the impact of the specified load causes only a change in this angle; let's denote this change $(\alpha_0 - \alpha_1)$ (Fig. 2).

Finding the relationship between load and settlement in curved parts is an urgent task in mechanical engineering, shipbuilding, and aircraft manufacturing for elastic rings; with the help of some processing, the relationship between load and settlement can be simplified. The article discusses one of the common cases of load modes on a ring.

Main part

In Fig. 1 is presented a circular ring of rectangular cross-section, the inner contour of which is subject to a load of intensity *q*, uniformly distributed over 2π radians.

ring and the support should be α_0.. The ring is so elastic

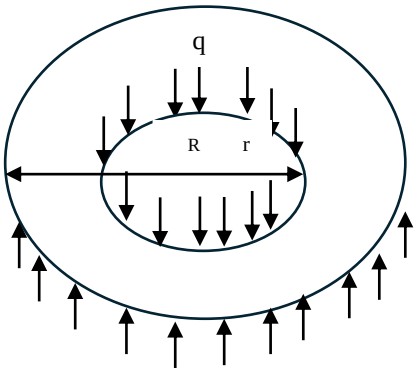

Fig. 1

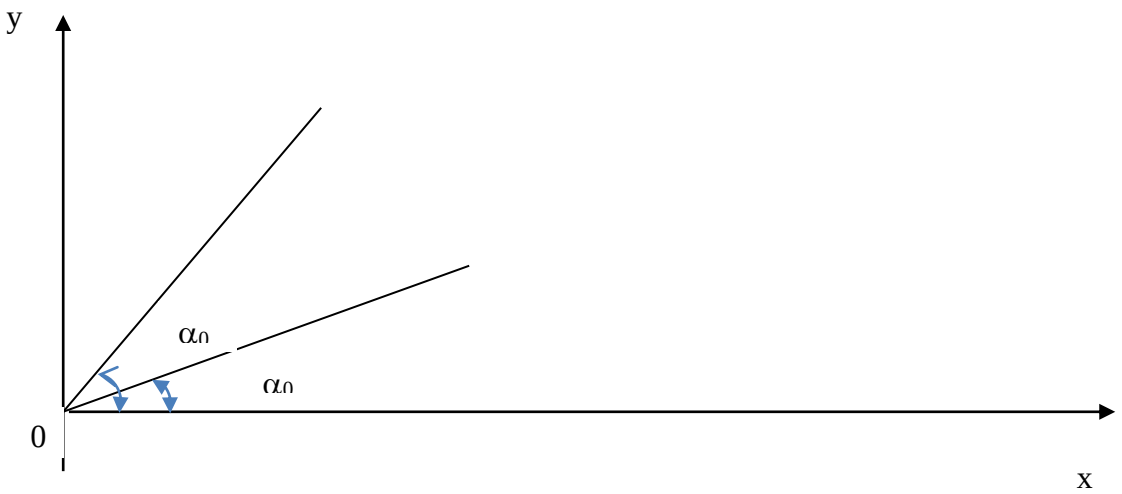

Fig. 2

Select any point on the cross section of the ring $k(x,y)$ Select any point on the ring section k_1 to a point and approaches the axis of symmetry of the ring by the next amount

$$[xcos\alpha_1 - ysin\alpha_1] - [xcos\alpha_0 - ysin\alpha_0] \quad (1)$$

Due to slight curvature and slight offset α_0 $(\alpha_0 - \alpha_1)$ The quantity is small, so

$$cos\alpha_0 \approx 1 - \frac{1}{2}\alpha_0^2 \quad sin\alpha_0 \approx \alpha_0 \quad (2)$$

$$cos\alpha_1 \approx 1 - \frac{1}{2}\alpha_1^2$$

$$sin\alpha_1 \approx \alpha_1 \quad (3)$$

From here we get the distance from the letter of change to the axis of symmetry (pay attention $\alpha_0 - \alpha_1 = \Delta\alpha$)

$$x \cdot \Delta\alpha\left(\alpha_0 - \frac{\Delta\alpha}{2}\right) + y\Delta\alpha \quad (4)$$

(4) When moving a distance, a circular elongation of the ring will occur, the relative magnitude of which will be (Fig. 3).

$$\varepsilon_1 = \frac{x\Delta\alpha\left(\alpha_0 - \frac{\Delta\alpha}{2}\right) + y\Delta\alpha}{R_0 - xcos\alpha_0 + ysin\alpha_0} \approx \frac{x\Delta\alpha\left(\alpha_0 - \frac{\Delta\alpha}{2}\right) + y\Delta\alpha}{R_0 - x} \quad (5)$$

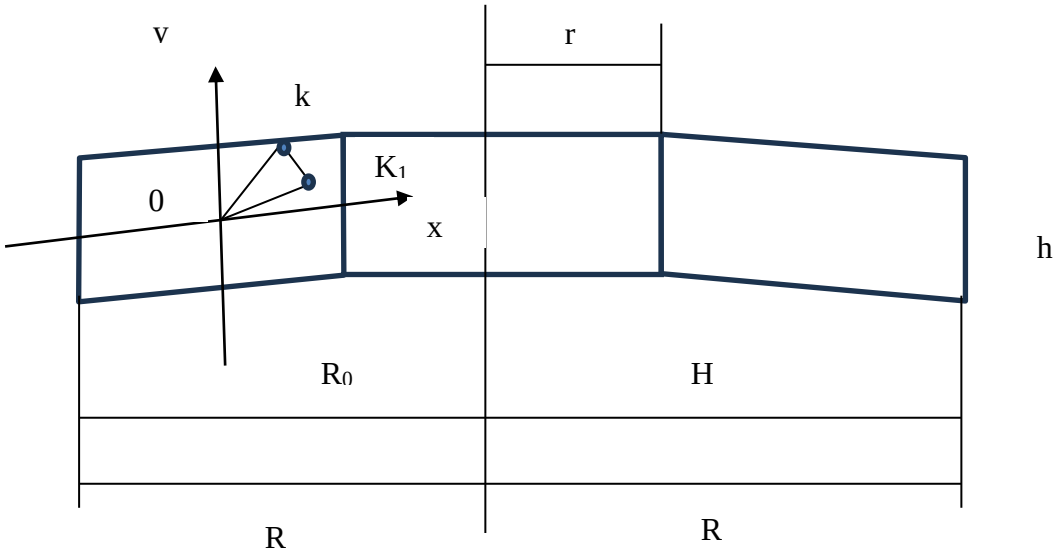

Fig. 3

normal stress in this direction

$$\sigma_1 = E\varepsilon_1 \qquad (6)$$

$$N = \int_{R_0-R}^{R_0-r}\int_{-h/2}^{+h/2}\sigma_1 dxdy \qquad (7)$$

Introduce the value of σ_1 and we get

$$N = E\int_{R_0-R}^{R_0-r}\int_{-h/2}^{+h/2}\frac{x\Delta\alpha\left(\alpha_0-\frac{\Delta\alpha}{2}\right)+y\cdot\Delta\alpha}{R_0-x}dxdy =$$

$$Eh\Delta\alpha\left(\alpha_0-\frac{\Delta\alpha}{2}\right)\left(r-R+R_0 ln\frac{R}{r}\right) \qquad (8)$$

Now let's calculate the normal forces in the section of the ring.

But it is clear that the specified load creates only bending moments and, therefore, N = 0, therefore,

$$R_0 = \frac{R-r}{ln\frac{R}{r}}$$

Let's move on to determining the moment

$$M = \int_{R_0-R}^{R_0-r}\int_{-h/2}^{+h/2}\sigma_1(xsin\alpha_1 + ycos\alpha_1)dxdy$$

$$M = E\int_{R_0-R}^{R_0-r}\int_{-h/2}^{+h/2}\frac{x\Delta\alpha\left(\alpha_0-\frac{\Delta\alpha}{2}\right)+y\cdot\Delta\alpha}{R_0-x}[x\cdot\alpha_1+y]dxdy$$

$$M = Eh\left[\Delta\alpha\left(\alpha_0-\frac{\Delta\alpha}{2}\right)(\alpha_0-\Delta\alpha)\left(\frac{R^2}{2}-\frac{r^2}{2}+2R_0r-2R_0R+R_0^2ln\frac{R}{r}\right)+\right.$$

$$\left.+\frac{h^2}{12}\Delta\alpha\cdot ln\frac{R}{r}\right] \qquad (9)$$

If you cut the ring and observe its state of equilibrium, you can easily verify that

$$2M = \frac{q}{2\pi}R\int_0^{\pi}sin\theta d\theta - \frac{q}{2\pi}r\int_0^{\pi}sin\theta d\theta$$

$$\frac{q}{2\pi}(R-r) = Eh\Delta\alpha\left[\left(\alpha_0-\frac{\Delta\alpha}{2}\right)(\alpha_0-\Delta\alpha)\left(\frac{R^2}{2}-\frac{r^2}{2}+2R_0r-2R_0R+\right.\right.$$

$$\left.\left.+R_0^2ln\frac{R}{r}\right)+\frac{h^2}{12}ln\frac{R}{r}\right] \qquad (12)$$

By numerical verification we can easily verify that when the ratio R/r is greater than one and less than 4, the following relationship will be valid:

from where

$$M = \frac{q}{2\pi}(R-r) \qquad (10)$$

That's why, we will accept

$$\frac{1}{2}\frac{R+r}{R-r}\frac{1}{ln\frac{R}{r}} \approx \frac{1}{12}ln\frac{R}{r}$$

That's why

$$q = \frac{\pi Eh}{6(R-r)^2}wln\frac{R}{r}\left[\left(H-\frac{W}{2}\right)(H-W)+h^2\right] \qquad (14)$$

in (14) $\alpha_0 = \frac{H}{R-r}$ and $\Delta\alpha = \frac{W}{R-r}$

The resulting relationship between the load intensity q and the ring friction W is nonlinear and will always depend on the H/h ratio, which is the subject of further study.

Conclusion

The resulting relationship between the load intensity q and the ring friction W is

nonlinear and will always depend on the H/h ratio, which is the subject of further study.

References

1. N. Malinin. “Applied theory of plasticity and creep. Moscow, 1975

2. Birger I. A. Round plates and rotating shells. M. Oborongis

3. T. Batsikadze, N. Murgulia, J. Nizharadze. Load-bearing capacity of a thick-walled hollow cylindrical shell under external and internal compression. Scientific and technical journal "Construction" No. 4 (19) 2016.

DETECTION OF MUDFLOWS ON ROADS IN ACCORDANCE WITH THE SCHEME OF ENGINEERING AND GEOLOGICAL ZONING OF GEORGIA

Levan Janashia
Georgian Technical University, Tbilisi 0170, Georgia
leva92leva@gmail.com

Abstract

The article discusses the issues of detecting mudfllow hazard areas on roads according to the scheme of engineering geological zoning of Georgia and the scheme of regions, districts and sub-districts. This will allow us to identify not only the mudflow hearths according to the geostructural signs, but also to detect specific mudflow hazard areas on the roads by described sign.

Keywords: Engineering geology, zoning scheme, geostructural signs, etc

Introduction

As we mentioned, in the Caucasus Georgia is distinguished by the abundance of mudflows and their diversity, posing a great danger to roads and artificial structures located on them. Georgian scientists [1] have developed maps showing the location of mudflow hearths. These data were used to identify mudflow hazard areas on the Georgian road network.

Our research has shown that the developed maps, due to the complexity of exodynamic processes, cannot accurately determine the potential location of the mudflow hearths' occurrence. In the course of the study, based on our goal, we studied the engineering and geological conditions of the territory of Georgia and identified the main geological factors causing mudflows, as well as we took into account the relief and vegetation cover.

G. Areshidze [2] divided the territory of Georgia into seven large regions according to the engineering-geological zoning scheme and geostructural features. Regions are divided into districts according to the engineering and geological features of geological complexes of rocks distributed within their borders. Some districts are divided into sub-districts according to territorial features, and a map is created (Fig.1). A table is created showing types of soils common in different regions, districts and subdistricts.

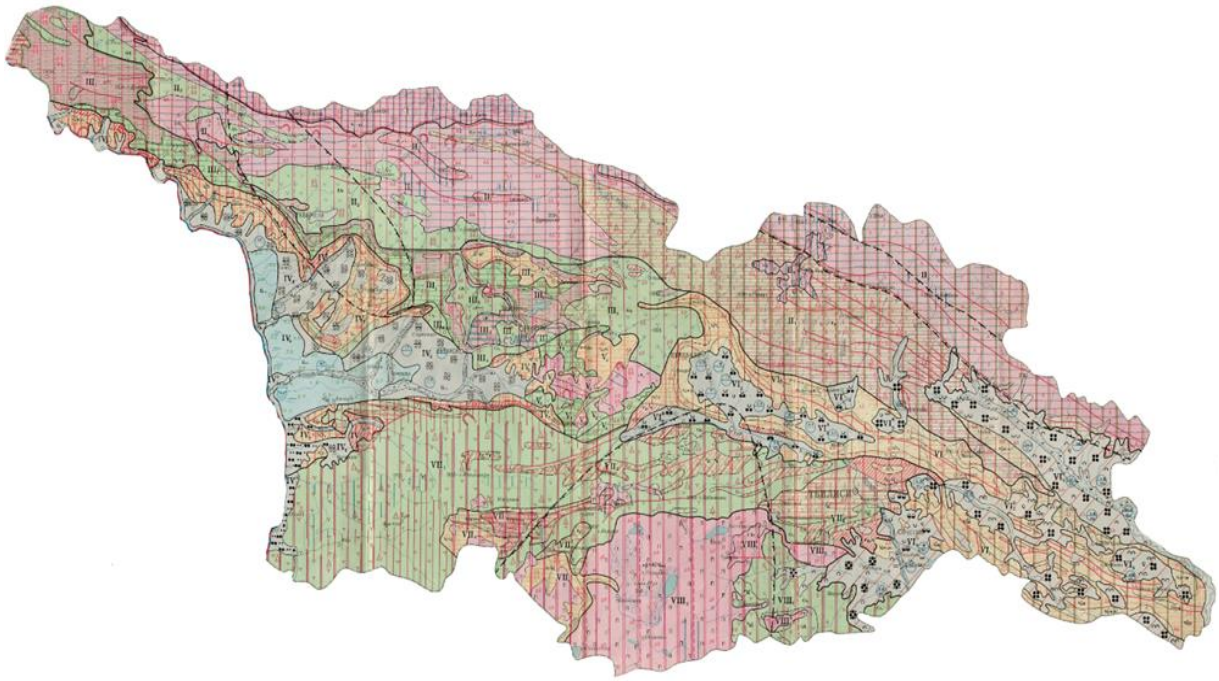

Fig.1. Engineering geological map of the territory of Georgia

Main Part

The assessment of factors developed by us is based on the analysis of existing data of the geology, relief and vegetation cover of the territory under consideration: we assessed the geological factors according to the scheme of engineering-geological zoning of the territory of Georgia of G. Areshidze [2]; We took data of the relief and flora according to the geographical atlas of Georgia [3].

The danger of mudflow in the area under discussion is assessed by us in accordance with the factors that generate mudflows. They were evaluated using intensity degrees, as well as analytical images of dangerousness.

Firstly, the degree of geological deformations is estimated by a 10-point system. These deformations are caused by weather (a large amount of precipitation per unit of time – heavy rain, low intensity but long-lasting - continuous rain, sharp temperature fluctuation throughout the day and night, wind, etc.) and are shown using D.

where: 0-2 safe;
2-4 slightly dangerous;
4-6 medium dangerous;
6-8 dangerous;
8-10 highly dangerous;

When evaluating rocks, they are conditionally selected under unfavorable circumstances, such as the steep slope of talweg of river-ravine and a small amount of vegetation on the slopes.

At the second stage, we considered how does the relief (catchment Talweg slope) affect geology, and have developed the following formula:

$$Dn=DR \qquad (1)$$

Where "n" is the slope of talweg: slight, medium and steep. Accordingly, we assigned the corresponding coefficients:

Where: Slight R=0,40;
Medium R=0,70;
Steep R=1,00.

At the third stage, we consider how does flora affect geology (the degree of vegetation development). If the grass cover is degraded, then there is a high probability of erosion and silt formation. If the grass-shrub cover is well developed, the degree of erosion is minimal; And if grassy cover and dense forest are represented together, then their erosion is less likely. Considering the above, we have developed the following formula:

$$D^{I}n=DF \qquad (2)$$

Where "^{I}n" is the degree of development of vegetation cover: sparse, medium and high. Accordingly we assigned the corresponding coefficients:

Where: Sparse F=0,90;
Medium F=0,65;
High (dense) F=0,50.

At the fourth stage, we generalized the influence of relief (slope) on geology, how does slight slope positively affect the stability of rock, and generalized the following formula, which we calculated as a percentage.

$$K\%=100-(Dn/D*100) \qquad (3)$$

Where "K" is the impact of inclination on a rock.

At the fifth stage we generalized the impact of flora (vegetation) on geology, how high vegetation has a positive effect on the stability of rocks, and developed the following formula, which we calculated as a percentage.

$$T\%=100-(D^{I}n/D*100) \qquad (4)$$

Where "T" is the impact of flora on a rock

At the sixth stage we generalized the joint influence of relief and flora and we developed the following formula, which we calculated as a percentage:

$$C\%=100-(Dn/D*100)+$$
$$+100-(D^{I}n/D*100)=K+T \qquad (5)$$

Where "C" is the combined effect of relief and flora on the deformation of a rock, considering the weather.

The above-mentioned additions are included in Table [2] of the scheme of engineering and geological zoning of the territory of Georgia, which allows us to determine: the danger zones of mudflows in accordance with the region, district and subdistrict and the degree of danger of mudflows on the roads. (Table 1) It is shown which soils are more or less dangerous for the occurrence of the

mudflows and where these soils are widespread.If the degree of slope of the river and ravine in the distribution zone is high and the vegetation cover is degraded, there is a high probability of mudflows in such areas.

Identification of mudflow hazard areas according to these signs allow us to take measures in advance and eliminate mudflow hearths. Taking preliminary measures will ensure safe operation of roads in mountainous terrain, where protection of road structures from mudflows is the most important component of operation. In addition, it is very important to assess the danger of a mudflow during the preliminary study and design of a road.

The following are the results of the formulas developed by us and 3 examples are shown:

First: Region III, District Five: (Subargillites containing pyrite and gypsum, with rare interlayers of arkosic graywacke sandstones. Sandstones on clay cement and clays in the middle of shell-limestones and conglomerates) If the given rock if it is in unfavorable circumstances (steep terrain and small vegetation cover) is estimated by us at 9 points. The above-mentioned region and district are located between Tsageri and Ambrolauri regions on the banks of the Tskhenistskali and Lajanura Rivers. The valleys of the banks of these rivers are distinguished by very steep slopes exceeding 60^0 and having moderately developed vegetation. We estimated the impact of the relief at R=1.00 and the impact of the flora at F=0.65.

We include these coefficients in our formulas: since the talweg slope of the valleys in this area is steep, 9 points will remain unchanged. Since the impact of flora is medium we put it in the formula of the influence of flora on geology (2)

F=0.65:

$$D^I_2=9*0.65=5.85$$

The medium vegetation cover in this area has reduced the degree of geological deformation from 9 to 5.85 points, making the area moderately dangerous. The positive impact of vegetation cover should be shown by the formula (4):

$$T=100-(5,85/9*100)=35\%$$

Averagely developed flora reduced the risk of mudflows by 35%.

Second: Region VII, district III, sub-district II: if a rock is in unfavorable condition (a very steep slope and a sparse vegetation cover) we estimate it as 7-point intensity. The above-mentioned region, district and subdistrict are located in the Aspindza region, at the confluence of Raqhistskali and Tcharkhaleti Rivers, mainly on the right bank of Uraveli River.

The ravines of the banks of these rivers are distinguished by medium slopes not exceeding 50^0, and highly developed vegetation. According to our estimation the impact of the relief is R=0.70, and the impact of flora is F=0.50.

We included these coefficients in our formulas. Since the Talweg inclination of the ravines in this area is medium, we have included it in the formula for determining the impact of relief on geology (1) R=0.70:

$$D_2=7*0.70=4.90$$

The medium inclination on this area has reduced the point of the degree of geological deformations from 7 to 4.90, making the area medium-dangerous. For showing the positive effect of a relief we used the following formula (3):

$$K=100-(4.90/7*100)=30\%$$

Medium inclination of a relief reduced the risk of mudflow by 30%

Since the impact of flora is significant, we can use the formula for the

The Main Rocks Common in the Territory of Georgia and Their Role in the

№	Region, Distrcit, Subdistrict	Name of the Rocks	Factors Causing Mudflows																
			Degree of Geological Deformations Assessed by 10-Point System	Impact of Relief on Geology Dn=DR			Impact of Flora on Geology $D^I n$=DF			Combined Impact of Terrain and Flora on Geology Taking into Account the Weather (%)								
			Deformations caused by weather (D) (wind, rain, temperature variations, etc.)	Catchment Talweg Slope			Degree of Development of Vegetation Cover												
				Slight R=0.40	Medium R=0.70	Steep R=1.00	Slight F=0.90	Medium F=0.65	Steep F=0.50	Slight R - Slight F	Slight R - Medium F	Slight R - Steep F	Medium R - Slight F	Medium R - Medium F	Medium R - Steep F	Steep R - Slight F	Steep R - Medium F	Steep R - Steep F	
				D_1	D_2	D_3	D^I_1	D^I_2	D^I_3	C=100-(Dn/D*100)+100-(D^In/D*100)									
1	2	3	4	5	6	7	8	9	10	11	12	13	14	15	16	17	18	19	
1	I	Porphyry-like coarse-grained granitoids, micaceous, metamorphized	1	0.40	0.70	1.00	0.90	0.65	0.50	70	95	110	40	65	80	10	35	50	
2	II_1	Hornblende quartz, clay shales, quartzites, marble lenses, highly dislocated	2	0.80	1.40	2.00	1.80	1.30	1.00	70	95	110	40	65	80	10	35	50	
3	II_2	Jasper and clayey slates with rare interlayers of sandstones and quartzites, dislocated	6	2.40	4.20	6.00	5.40	3.90	3.00	70	95	110	40	65	80	10	35	50	
4	II_3	Porphyrites and their tuff, tufobreccias, tufosandstones, tufoargillites, greywacke, dislocated	2	0.80	1.40	2.00	1.80	1.30	1.00	70	95	110	40	65	80	10	35	50	
5	II_4	Mergels, mergel micas, limestones and sandstones in turn, dislocated	8	3.20	5.60	8.00	7.20	5.20	4.00	70	95	110	40	65	80	10	35	50	
6	II_5	Granitoids, syenites, diorites,	-	-	-	-	-	-	-	-	-	-	-	-	-	-	-	-	
7	II_6	Andesite lava	-	-	-	-	-	-	-	-	-	-	-	-	-	-	-	-	
8	III_1	Massive, dolomitized, breccia-like, reefal limestones, Rarely marls and sandstones, dislocated, alternating with hard and boulder-like limestones and marls, slightly dislocated	3	1.20	2.10	3.00	2.70	1.95	1.50	70	95	110	40	65	80	10	35	50	
9	III_2	Porphyrites and their tuff, tuff breccias, tuff sandstones, tuff-argillites, dislocated greywacke	2	0.80	1.40	2.00	1.80	1.30	1.00	70	95	110	40	65	80	10	35	50	
10	III_3	Sheet argillites, arkosic and greywacke sandstones, coal layer, strongly dislocated	7	2.80	4.90	7.00	6.30	4.55	3.50	70	95	110	40	65	80	10	35	50	
11	III_4	Porphyrites, quartz porphyry, albitophyres and their tuffs, tuff breccia, tufosandstones, dislocated	2	0.80	1.40	2.00	1.80	1.30	1.00	70	95	110	40	65	80	10	35	50	
12	III_5	Subargillites containing pyrite and gypsum with rare interlayers of arkosic greywacke sandstones. Sandstones on clayey cement and clays with interlayers of coquinas and conglomerates	9	3.60	6.30	9.00	8.10	5.85	4.50	70	95	110	40	65	80	10	35	50	
13	IV_1	Subargillites containing pyrite and gypsum with rare interlayers of arkosic greywacke sandstones	10	4.00	7.00	####	9.00	6.50	5.00	70	95	110	40	65	80	10	35	50	
14	IV_2	Alteration of bluish-grey clay marls, sandstones and conglomerates on the calyey carbonate cement -carbonate clays, bluish-grey sandy clays - with thin interlayers of sandstones, microconglomerates and marls _ conglomerates on limestone calcined clay cement with rare interlayers of clay - conglomerates, sandstones, sands, clays	10	4.00	7.00	####	9.00	6.50	5.00	70	95	110	40	65	80	10	35	50	
15	IV_3	Pebblestone, sandstone and sandy fillers	8	3.20	5.60	8.00	7.20	5.20	4.00	70	95	110	40	65	80	10	35	50	
16	IV_4	Alternation of peatery, clay-like and sandy soil	8	3.20	5.60	8.00	7.20	5.20	4.00	70	95	110	40	65	80	10	35	50	

Formation of Mudflows Table 1

17	IV_5^1	The pebblestone of Abkhazia	8	3.20	5.60	8.00	7.20	5.20	4.00	70	95	110	40	65	80	10	35	50
18	IV_5^2	The sands of Colchis	8	3.20	5.60	8.00	7.20	5.20	4.00	70	95	110	40	65	80	10	35	50
19	IV_5^3	The pebblestone of Adjara	8	3.20	5.60	8.00	7.20	5.20	4.00	70	95	110	40	65	80	10	35	50
20	V_1	Coarse-grained granitoids, porphyry-like, mica-like, metamorphosed, granitoids, even-grained granitoids, gneiss, crystal shales	-	-	-	-	-	-	-	-	-	-	-	-	-	-	-	-
21	V_2	Porphyrites and their tuffs, quartz porphyries, albitophyres and their tuffs	-	-	-	-	-	-	-	-	-	-	-	-	-	-	-	-
22	V_3	Thick-layered limestones, marly limestones, marls, greywacke sandstones	4	1.60	2.80	4.00	3.60	2.60	2.00	70	95	110	40	65	80	10	35	50
23	V_4	Subargillites, clays, weakly cemented sands, sandstones on clayey and carbonate cements and conglomerates	8	3.20	5.60	8.00	7.20	5.20	4.00	70	95	110	40	65	80	10	35	50
24	VI_1	Calcareous sandstones, alternation of aleurolite clays and marl interlayered aleurolites, gray-brown clays with sandstone interlayers. Clays, sandstones and conglomerates on clay and clay carbonate cement. Conglomerates with rare interlayers of clays	8	3.20	5.60	8.00	7.20	5.20	4.00	70	95	110	40	65	80	10	35	50
25	VI_2	Pebblestone (Tiriphoni lowland)	7	2.80	4.90	7.00	6.30	4.55	3.50	70	95	110	40	65	80	10	35	50
26	VI_2^2	Clays and loams (Khashuri-Zemoavchala)	8	3.20	5.60	8.00	7.20	5.20	4.00	70	95	110	40	65	80	10	35	50
27	VI_2^3	Clays and loams (Mukhnari pit)	8	3.20	5.60	8.00	7.20	5.20	4.00	70	95	110	40	65	80	10	35	50
28	VI_2^4	Loesses and loess-like soils (Basaleti Plateau)	9	3.60	6.30	9.00	8.10	5.85	4.50	70	95	110	40	65	80	10	35	50
29	VI_2^5	Salty soils (Rustavi-Marneuli)	9	3.60	6.30	9.00	8.10	5.85	4.50	70	95	110	40	65	80	10	35	50
30	VI_2^6	Salty soils (Erdso and Tianeti pits)	9	3.60	6.30	9.00	8.10	5.85	4.50	70	95	110	40	65	80	10	35	50
31	VI_2^7	Coarse gravel, grit, sand and pebbles with sandy filler (on the Iori lowland)	8	3.20	5.60	8.00	7.20	5.20	4.00	70	95	110	40	65	80	10	35	50
32	VI_2^8	The same (on Alazani lowland)	8	3.20	5.60	8.00	7.20	5.20	4.00	70	95	110	40	65	80	10	35	50
33	VII_1	Layered and coarse-grained andesitic tuff breccias, tufosandstones, andesite coatings, tuffs, dislocated argillites, porphyrites, quartz porphyry, albitophyre and their tuffs, tuff breccias, tufosandstones	5	2.00	3.50	5.00	4.50	3.25	2.50	70	95	110	40	65	80	10	35	50
34	VII_2	Thin-layered limestones, variegated marls and argillites	8	3.20	5.60	8.00	7.20	5.20	4.00	70	95	110	40	65	80	10	35	50
35	VII_3^1	Marls, argillites, limestones, sandstones, subargillites containing pyrite and gypsum (Manglisi-Tbilisi)	9	3.60	6.30	9.00	8.10	5.85	4.50	70	95	110	40	65	80	10	35	50
36	VII_3^2	Argillites, sandstones, marls, breccias, basalts, trachytes and their pyroclastolites, gray and mottled subargillites and sandstones on limestone calcined clay cement	7	2.80	4.90	7.00	6.30	4.55	3.50	70	95	110	40	65	80	10	35	50
37	VII_4	Sandstones, conglomerates, tuffs, tuff breccias, tuff-conglomerates, andesite dacites, slightly dislocated. Lava layer of basalts, dolerites and andesite-dacite.	4	1.60	2.80	4.00	3.60	2.60	2.00	70	95	110	40	65	80	10	35	50
38	$VIII_1^1$	Granitoids, granodorites, crystal shales, phyllites, strongly dislocated (crystal massif of the ravine)	-	-	-	-	-	-	-	-	-	-	-	-	-	-	-	-
39	$VIII_1^2$	The same (crystal massif of the Loki)	-	-	-	-	-	-	-	-	-	-	-	-	-	-	-	-
40	$VIII_2$	Porphyrites, quartz-porphyry, albitophyres and their tuffs, tuff breccias	-	-	-	-	-	-	-	-	-	-	-	-	-	-	-	-
		Andesitic tuff breccias, tufosandstones, sandstones and argillites	8	3.20	5.60	8.00	7.20	5.20	4.00	70	95	110	40	65	80	10	35	50
		Porphyrites and their tuffs, tuff breccias, tufosandstones, dislocated	1	0.40	0.70	1.00	0.90	0.65	0.50	70	95	110	40	65	80	10	35	50
41	$VIII_3$	Andesite and dacite lavas of basalt dolerites	1	0.40	0.70	1.00	0.90	0.65	0.50	70	95	110	40	65	80	10	35	50

High vegetation cover on this area has reduced the point of the degree of geological deformations from 7 to 3.50, vegetation cover is shown by the following formula (4):

$$T=100-(3.50/7*100)=50\%$$

Highly developed flora has reduced the risk of mudflow by 50%

Total positive value of the medium inclination and high vegetation cover is shown by the following formula (5):

$$C=30\%+50\%=80\%$$

Medium inclination of a relief and high flora vegetation cover have reduced the mudflow risk by 80%, totally.

Third: Region V, District III: (thick-layered limestones, marly limestones, marls, greywacke sandstones) If the given rock if it is in unfavorable circumstances (steep terrain and small vegetation cover) is estimated by us at 4 points. The abover region and district are located between Kharagauly and Surami regions, on the banks of Chkherimela and Suramula rivers. The valleys of these banks are distinguished by steep slopes exceeding 70^0 and having highly developed vegetation. We estimated the impact of the relief at R=1.00 and the impact of the flora at F=0.50.

We include these coefficients in our formulas: since the talweg slope of the valleys in this area is steep, 4 points will remain unchanged. Since the impact of flora is high we put it in the formula of the influence of flora on geology (2) F=0.50:

$$D^{I}_{3}=4*0.50=2.00$$

The high vegetation cover in this area has reduced the degree of geological deformation from 4 to 2,00 points, and this area remained slightly dangerous. The positive impact of vegetation cover should be shown by the formula (4):

$$T=100-(2.00/4*100)=50\%$$

Highly developed flora reduced the risk of mudflows by 50%.

Construction of a new road on this section or rehabilitation of the existing one requires options for design decisions:

1. Active measure: if we are building a new road, it is advisable to bypass the section, afforest and terrace the slopes.

2. Passive measure: reduction of valley talweg slope by barrages.

making the area slightly dangerous. Positive effect of

The final choice of measures depends on the technical-economic comparison of options, which takes into account the total amount of construction and operation funds. This methodology is known [18] and we aren't providing details here.

Conclusion

Considering the climatic conditions of Georgia shown in the existing fund materials (in accordance with the engineering and geological zoning of Georgia), on the basis of engineering geological research works carried out over the past 3 years in different regions of Georgia it was determined which soils are dangerous for the formation of the mudflows and where these soils are developed. Thus, the mudflow hazard areas on the international and secondary roads are determined accordingly.

Reference

1. I. Qhruashvili (2014). Mudflows and methods of combating them.

2. Сидоренко, А. (1970). ГИДРОГЕОЛОГИЯ СССР Том X ГРУЗИНСКАЯ ССР. Москва, Недра.

3. Vakhushti Bagrationi Institute of Geography of the Georgian Academy of Sciences. (1992). Geographical Atlas of Georgia. Tbilisi, Education

4. Coussot, P. (1997). Mudflow Rheology and Dynamics. Iahr Monograph,1 st.

5. Sassa, K., Konagai, K., Tiwari, B., Arbanas Z., Sassa, S. (2022). Progress in Landslide Research and Technology. Volume 1 Issue 1. Springer.

6. Lorenzini, G., Mazza, N. (2004). Debris Flow. Italy, University of Bologna.

THE ROLE OF THE CABLE CAR IN CIVIL AND MILITARY PURPOSES

Tamaz Guruli

Georgian Technical University, Tbilisi 0170, Georgia
Lieutenant Colonel. Defence Forces Logistics Command Headquarters, G-2 Service Officer.
tamazguruli577@gmail.com

Abstract

The article discusses the use of portable and mobile ropeways in hard-to-reach places, their capabilities for both civil and military purposes.

The fact is that both in the past and today, engineering units and means have been widely used and will be actively used in the future in combat operations. Every day, the development of this family of military, technological improvement and improvement of various engineering tools open up great prospects for the future. In the maneuver units of the Defense Forces of our country, in order to achieve the assigned task, in order to increase mobility, along with the rapid construction of roads and bridges by engineering units, the use of portable and mobile cranes used in the defense forces of other countries is a good way to overcome land and water obstacles.

Units of the Georgian Defense Forces, depending on the current geopolitical situation or the presence of difficult terrain in Georgia, may have to participate in rescue or crisis situations, as well as conduct a full range of operations in various environmental conditions and locations. , for example, such as:

- inclined and sloping arrangement;
- valleys;
- Rivers and river basins;
- in places with different and difficult meteorological conditions;
- during natural disasters;
- location of wetlands;
- in mountainous terrain, etc., for which the logistics and engineering units of the Georgian Defense Forces must be ready to support maneuver units and carry out ropeway transport operations to perform mobility and logistics operations or enhance these capabilities.

keywords: cable car - a vehicle, aerial cable car, cabin, seat and traction equipment of a tractor, as well as a funicular, intended for the transport of passengers[1].

Introduction

Georgia's past experience and the unfolding history of wars have repeatedly shown us that the enemy in many cases went on the offensive with excessive military forces, various engineering and combat capabilities and means.

Due to Georgia's mountainous terrain, fighting often took place in difficult terrain, such as mountainous areas or valleys. Georgians were forced or tactically selected to participate in combat and operations in valleys and mountainous terrain, where timely, uninterrupted logistics and mobility were especially important. Based on today's technological capabilities, one of the best ways to travel in difficult places and in the presence of various obstacles is to use mobile or mobile ropeways for logistics operations, such as NATO (North Atlantic Treaty Organization) and implemented in the armed forces of different countries around the world.

[1] https://matsne.gov.ge/ka/document/view/2187377?publication=0

Figure 1 (source: https://www.bpn.ge/article/14987-riqe-nariqalas-sabagiro-10-dgit-mgzavrebis-momsaxurebas-sheacherebs/).

Main part

There is no doubt that in order to achieve success in the fight against the enemy, the Georgian Defense Forces must be equipped with modern weapons and equipment, as wars and military confrontations in other countries have repeatedly shown in recent years. In this regard, the Georgian Defense Forces are no exception, and they are being actively equipped with modern weapons and equipment, although the Georgian Defense Forces have not yet had any reasons to use or participate in international exercises with the armed forces. foreign state in such exercises, where they used a mobile/portable ropeway for military purposes, which, in turn, greatly facilitates the operations of transporting/transporting military personnel and logistics in time and space, having a dual purpose (for both military, and for the military). civil support) in overcoming various obstacles.

In this regard, it is possible to consider the creation of mobile and portable ropeway units in the engineering battalions of the Georgian Defense Forces, whose task is to install mobile or portable ropeways at the required time and in the required place, which, in turn, will significantly facilitate Defense Force mobility, logistics and transport/transportation operations, and civil support capacity during natural disasters.

It is necessary to study the territories of Georgia using the example of the natural disasters that occurred in Georgia in recent years. Forecasting of landslides, avalanches, landslides, possible flooding and other potentially dangerous places, indicating on the map those critical places where mobile and portable ropeways will be effectively used by the defense forces in the shortest possible time.

Figure 2

The pre-selected preparation of territory for the placement of military transport and mobile cable cars in a specific location and its use must certainly be focused on possible threats that civil society or state security may face.

Considering the mountainous terrain of Georgia, taking into account possible dangers, studying the territory and preparing it in advance for the placement of portable or mobile cable cars is a very important issue and will play a big role in the timely mobility of not only the military, but also the rescue squads of the Ministry of Internal Affairs, during logistics, during rescue, search and evacuation for military or civilian purposes, for operations.

Regarding the above issue, in Georgia we have had many sad cases, for example, the bitter outcome of the natural disaster that occurred in Racha on August 3, 2023, clearly showed us how mobile and portable cable cars will facilitate the movement of people. rescuers, evacuation of the population and victims, rescue and search operations in time and space.

It is widely known that in winter in the mountainous regions of Georgia, traveling by road during heavy snowfalls is associated with many risks and difficulties due to the danger of avalanches. Movement through avalanche-prone areas is periodically prohibited almost throughout the entire winter period and is associated with great risks; to this is added the presence of avalanche-prone and avalanche-prone areas in various places, which is no less an obstacle and danger. Also, during the rainy season in spring and river floods when glaciers melt, big problems are created and it becomes impossible to move along roads and cross the river bed. There are also frequent cases when, due to avalanches, landslides, heavy snowfalls or river floods, it is not possible to transfer rescuers, defense forces or border guards of the Ministry of Internal Affairs to the border perimeter or to a specific location. For example, taking into account the above problems and dangers, border guards during periods of heavy snowfall are forced to move to relatively flat terrain, to a place where they can carry out their service, their shifts and supplies. River overflows during the melting of glaciers or during the rainy season also create problems and the river channel becomes impossible. Accordingly, from the point of view of border perimeter control, the effectiveness of tracking and control of a specific location is reduced. There are many areas of this complexity in the border areas of Georgia and in the vicinity of the temporarily occupied territories. If you take into account the capabilities of mobile and portable lifts, it becomes clear how easily the existing problem can be solved. A mobile and portable cable car for the gradual change of personal equipment

and its logistics at an observation post of the border zone at a certain altitude will significantly facilitate the fulfillment of the task assigned by the border guards.

Figure 3

During combat operations, especially in mountainous areas, it is important that military personnel remain and will remain the main characters, since the effectiveness of soldiers is more important than their numbers. It is technical and technological means, such as portable and mobile cable cars, that will significantly facilitate movement in mountainous areas, increase mobility and logistics supply capabilities, which, in turn, is one of the necessary conditions for solving the problem. Conducting ground tactical operations in a mountainous region involves both horizontal and vertical dimensions, which in turn is a major obstacle and limiting factor in movement, transportation and various logistics operations. With the ease of use and mobile transportation capabilities of mobile or portable ropeways, both aspects can be overcome to some extent, since ropeways have the unique ability to operate at a suitable length and a certain slope, subject to certain limitations of course.

Movement in the mountains and transportation of material and technical equipment is fraught with great difficulties; in many cases it is impossible to use special ground or air means due to bad weather conditions (heavy snowfall, avalanche conditions, fog, strong wind, etc.). It is in this case and in order to reach hard-to-reach places, regardless of almost any weather and terrain (with the exception of strong side winds affecting cable cars), a mobile or portable cable car is a good way to transport logistics goods. . For example, a German-made portable cable car, which is intended for military purposes (it is also actively used to support the civilian population if necessary). Due to its simple design, ease of design and mobility, this ropeway can be used in terrains of varying complexity and gradients, as well as in international operations.

Figure 4

The German-made transport cable car is capable of transporting personal belongings, as well as cargo weighing up to 400 kilograms and of various sizes. In addition to the reception and departure stations, the transition cable car includes, in addition to various elements, support beams, which are used depending on the complexity of the location, slope and length of the cable car. Support beams can be used depending on the required height and angle of inclination.

A portable cable car has only a pulling cable and, due to the simplicity of its design, does not require a traction cable along which the cargo gondola moves using a self-propelled internal combustion engine, and also does not require traction. rope for moving loads. During towing/carrying, when the nacelle reaches its destination, the engine automatically stops and stops moving, and the internal combustion engine brakes on the nacelle are automatically applied to keep the nacelle stationary. The cable car is a type of pendulum cable car, which means that the gondola only moves in one direction rather than in a circle.

Before laying a cable car for German military purposes, Bundeswehr soldiers conduct terrain reconnaissance, collect data, calculate and study the complexity of the road with mathematical precision. The data is entered into the computer and a special program processes it. The computer program has the ability to quickly create an electronic drawing of the placement of cable car receiving stations, starting stations, as well as support beams (with calculations of the required number, distance and height) on the selected route. to a suitable location, in the form of electronic drawings, with calculations of the corresponding heights and distances. The computer produces, along with the drawing, a list of the required amount of materials for the construction of the cable car, and only after that the required amount of building materials is transported to the nearest place from where construction and installation work will be carried out. carried out by military personnel. Once the portable ropeway structure is delivered to its destination, the associated materials are physically transported to specific locations by military personnel using appropriate backpacks. At each site, the structure transport team includes five military personnel who assemble the structure upon arrival at its destination. At the same time, other groups carry out the transfer and assembly of the remaining load-bearing beams, as well as the installation of receiving and launching stations. Once the portable ropeway is ready (after carefully strengthening the supporting beams, ropes, receiving and launching stations for which ropes, winches and ground anchors are used), the first thing to do is test lowering of the gondola and internal combustion engine to check the efficiency . Only after a successful inspection does the ropeway begin to operate for its intended purpose,

allowing the military to carry out operations to transport personnel or logistics to remote or inaccessible locations very easily.

Conclusion

Based on all of the above, in conclusion, we can say that the use of mobile and portable ropeways will give border guards, rescuers and the defense forces of the Ministry of Internal Affairs of Georgia a good opportunity to increase their ability to overcome obstacles. defense force mobility and logistics to protect the sovereignty of a country or to support government agencies during natural disasters. It cannot be denied that many important issues must be taken into account in the process of installing cable cars. To successfully carry out the intended operations, military engineers must develop extensive operational plans, it is important to carefully select the exact location for placing the mobile and portable ropeway, study, test in various aspects.

The use of portable and mobile ropeways requires appropriate knowledge and experience. Its use should not be considered only in a military context. The use of bagirgzes during natural disasters to support the population is one of the important issues that will become a new challenge for the defense forces, which, given its capabilities and purpose, is a unique opportunity for Georgia, considering mountainous areas as a developing country, to strengthen defense during emergencies situations or natural disasters. Time for civilian support.

Reference

1. https://matsne.gov.ge/ka/document/view/2187377?publication=0. Last checked - 10.07.2023

ENERGY EFFICIENT VENTILATION SYSTEMS OF BUILDINGS

Alex Kopaliani, Mamuli Grdzelishvili, Solomon Goderdzishvili
Georgian Technical University, Tbilisi 0170, Georgia
ecocomfort@ymail.com

Abstract

The article discusses a recuperative ventilation system to ensure the microclimate of houses with low energy requirements (passive, zero, active, etc.). The parameters of the air supplied to the recovery unit were determined, and the process of thermodynamic air purification in this unit was investigated.

Key words: recuperator, efficiency, zero energy house, ventilation, energy efficiency, i-d diagram.

Introduction

Energy efficiency of buildings is one of the current trends in modern construction and implies the rational use of energy in buildings in order to create the most comfortable environment in them. Requirements for energy efficiency in buildings were driven by problems related to the supply of world petroleum resources that began during the First Arab-Israeli War (1948-1949), and the real energy crisis began during the Fourth Arab-Israeli War, when the Organization of Arab Countries oil exporters (OAPEC) announced an embargo on the supply of petroleum products to countries supporting Israel (USA, Canada, UK, Holland, Japan).

Since the beginning of this crisis, what practical steps have been taken, the developed countries of the world have made significant progress in the energy efficiency of buildings. Passive houses with virtually zero energy consumption were created.

Georgia is no exception in this regard. The Parliament of Georgia adopted a law [1] on the energy efficiency of buildings, according to which all new buildings planned for construction in 2029. After September 30, it must meet the requirements of a near-zero energy building. For public buildings, this date is set as September 30, 2027.

One of the important means of increasing the energy efficiency of buildings is to equip the building with an energy-efficient ventilation system.

Main part

At designing a zero-energy building, there are five basic principles that the Passive House standard takes into account:

1. Impermeability of the building;
2. Passive house windows;
3. Thermal insulation shell of the building;
4. Building structures without cold bridges;
5. Ventilation with heat energy recovery.

The first four questions on this list must be resolved in the architectural and structural part of the building, and to complete them it is necessary to use a passive house design package [2]. As for the ventilation recovery system, it should be addressed when designing building microclimate systems.

The main component of such a ventilation system is the so-called air recuperator, which separates exhaust (contaminated) air from the warehouse, instead supplying the warehouse with clean air from the environment (Fig. 1). The main element of this device is a heat exchanger, which in winter takes heat from the warm air in the room and transfers it to cold air supplied into the room from the environment. In summer, on the contrary, cold accumulates. There are many types of recuperators: plate, rotary, enthalpy, etc. The amount of heat recovered in the recuperator in winter is sufficient to heat a house with almost zero energy consumption and to cool it in summer. Thus, such a ventilation system eliminates the need to use a heating device or air conditioner in the compartment.

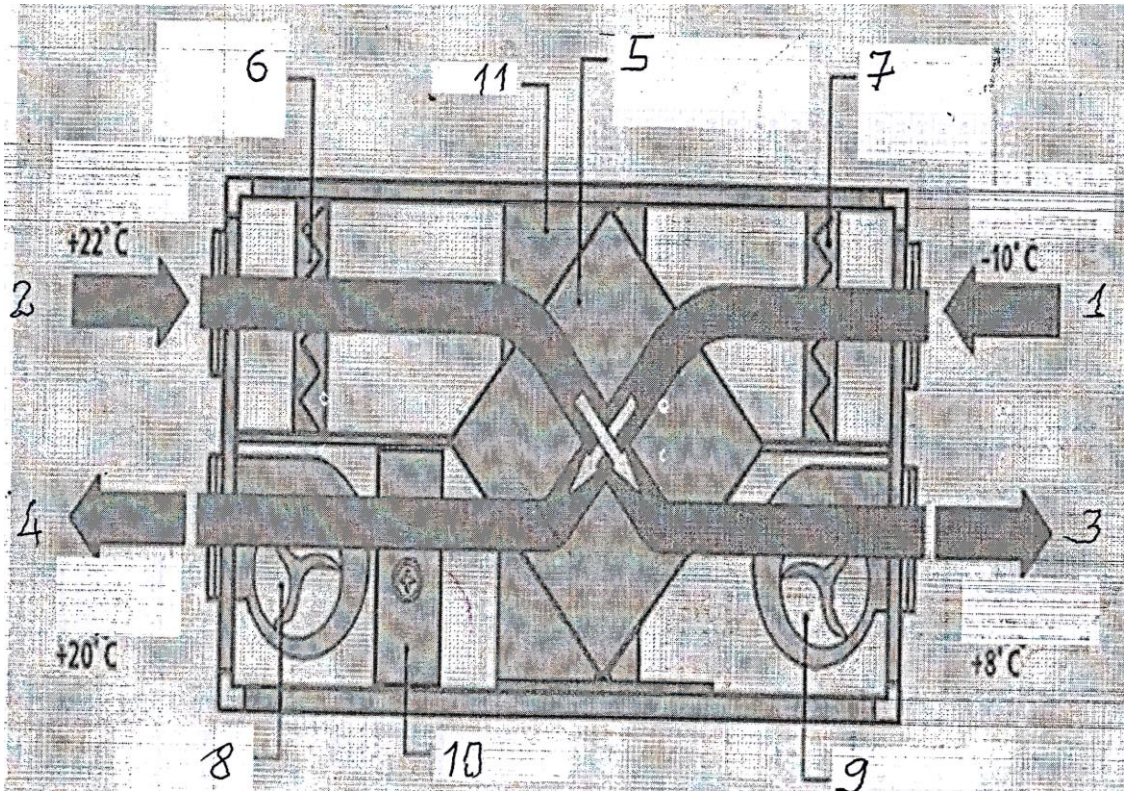

Fig. 1 - external air, 2 - supply air, 3 - exhaust air, 4 - supply air, 5 - recuperator, 6 - supply filter, 7 - supply filter, 8 - supply fan, 9 - exhaust fan, 10 - radiator, 11- bypass

An important feature of the recuperator is its efficiency. It shows how much the recuperator can heat the supply air compared to the ideal option. The ideal option is when the supply air is heated to the supply air temperature. In practice, such a case does not exist, and in fact the supplied air is heated to some intermediate temperature (t_{del}). At this time, the efficiency of the recuperator is calculated using the formula:

$$\eta = \frac{t_{sup} - t_{ext}}{exh - ext}, \quad (1)$$

where t_{sup} – is the supply air temperature after the recuperator; t_{exh} - is the exhausted air temperature and it is equal to room air temperature (t_r); t_{ext} – is the design outdoor temperature. Formula (1) takes into account the apparent heat transfer process in the recuperator. When the mass transfer process is considered along with heat exchange in the recuperator, it is better to use the enthalpy efficiency of the recuperator:

$$\eta = \frac{i_{sup} - i_{ext}}{i_{exh} - i_{ext}} \quad (2)$$

i_{sup} – is the supply air enthalpy kJ/kg; i_{exh} - is the enthalpy of exhausted air (i_{int}) kJ/kg; (i_{sup})- Outdoor air enthalpy kJ/kg

Enthalpy. This is the physical heat contained in the air, the dry part of which is equal to 1 kg, and its values are taken accordingly from the i-d diagram.

Using formulas (1) and (2), two main parameters of thermodynamic air treatment can be calculated: supply air temperature.

i_earth - enthalpy of supplied air in kJ/kg; i_gats - enthalpy of intake air

(i_in) kJ/kg; (i_gar) - enthalpy of outside air, kJ/kg.

Enthalpy. This is the physical heat contained in the air, the dry part of which is equal to 1 kg, and its values are taken accordingly from the i-d diagram.

Using formulas (1) and (2), two main parameters of thermodynamic air treatment can be calculated: supply air temperature.

$$t_{sup} = t_{ext}(t_{int} - t_{ext})t_{sup}\eta \quad (3)$$

and enthalpy

$$i_{sup} = i_{ext} + (i_{int} - i_{ext})\eta. \quad (4)$$

Naturally it is implied that t_{del}=t_{sh} end $i_{exh} = i_{ext}$

In this formula, η is an important value of the recuperative ventilation system, the efficiency of the recuperator, and it varies in a wide range η=0.3÷0.97; for houses with practically zero energy consumption, this value is taken equal to $\eta \geq 0.75$. The Table shows the temperatures of the air supplied at the outlet of the recuperator, depending on the temperature of the outside air at the inlet to the recuperator, with the recuperator efficiency η=92%.

Table 1

$T_{g,}$°C	-23	-15	-10	-5	0	25	30	35
t_{del}°C	18,9	19	19	19	19,5	22,3	22,9	23,4

As can be seen from this table, in recuperative ventilation systems in zero energy homes, thermal comfort can be established without any heating and air conditioning systems. When installing recuperative ventilation systems, you should strive to ensure that the quantities of supply and exhaust air entering the recuperator are equal. Otherwise, an imbalance in the amount of recovered heat (mass) will arise, which will violate the specified parameters of thermodynamic air treatment, therefore, when determining the temperature and enthalpy of the supplied air, it is necessary to make appropriate amendments to the formulas. (3)–(4). If we look at formulas (1) and (2), we will see that the numerator indicates the amount of heat absorbed by the air supplied to the recuperator, and the denominator indicates the amount of heat transferred by the exhaust air, when the values of the supply and exhaust air are equal. In general, these formulas are also written as follows:

$$\eta = \frac{G_{sup} \cdot .C(t_{sup} - t_{\partial ext})}{G_{\partial \flat} \cdot (t_{exh} - t_{ext})} \quad (5)$$

or

$$\eta = \frac{G_{sup} \cdot (i_{sup} - i_{ext})}{G_{exh} \cdot (i_{exh} - i_{ext})}, \quad (6)$$

where C is the heat capacity of air and is equal to 1 kJ/kg·deg. when Iron = G-d. Formulas (1)-(2) are accepted as a special case for Gland. The temperature and enthalpy of the supply air are calculated using the formulas:

$$t_{sup} = t_{ext} + a(t_{int} - t_{ext})\eta \quad (7)$$

$$i_{sup} = i_{ext} + a(i_{int} - i_{ext}), \quad (8)$$

where

$$a = \frac{G_{exh}}{G_{sup}}.$$

It is the correction that must be calculated in advance when Gland ≠G. The i-d diagram below (Fig. 2) shows the thermodynamics of air in a recovery ventilation installation ??? in winter. 1-2. And 1-3 correspond to the process of air cooling and drying in the apparatus in summer conditions. During periods 1'-2' and 1'-3', only air heating and combined processes of intravenous heating and humidification are used.

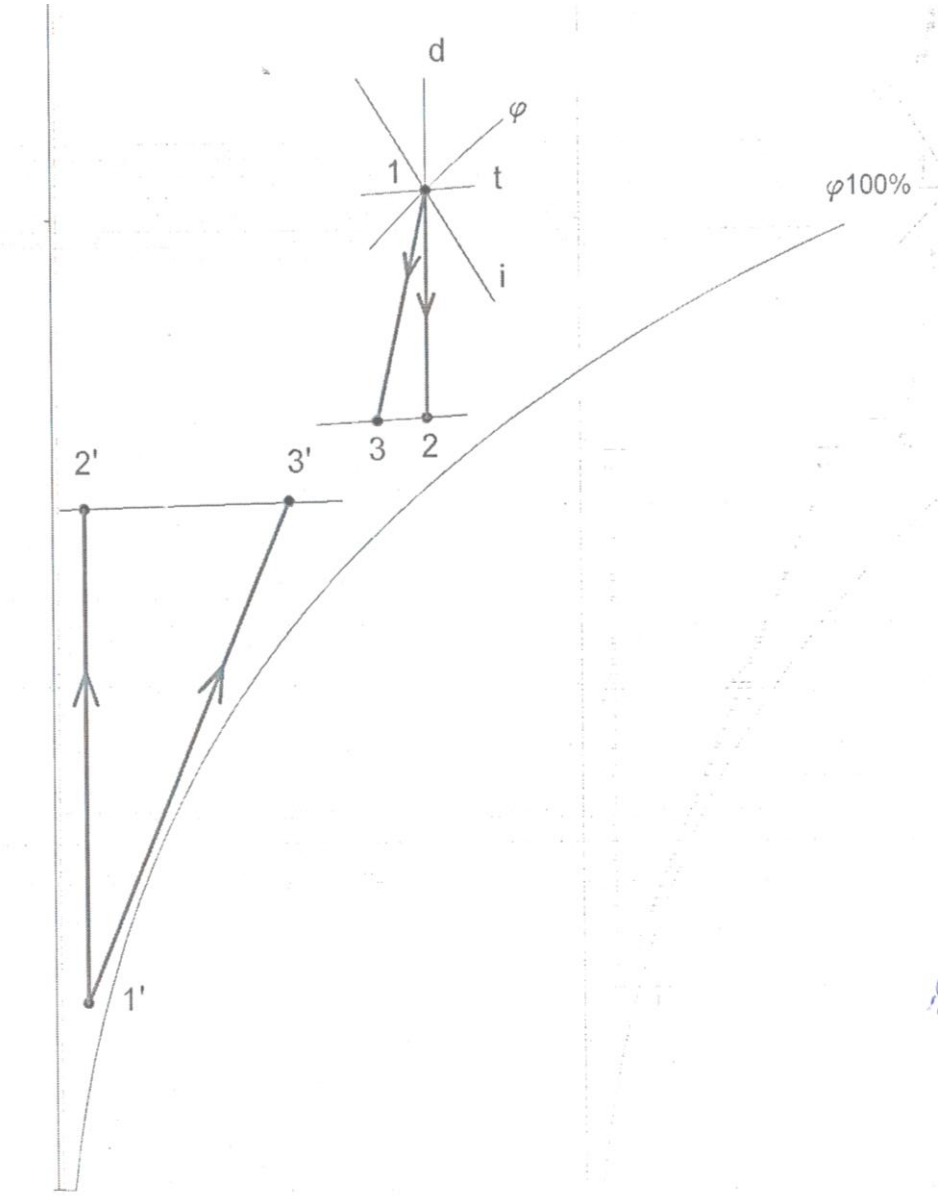

Fig. 2. Image of the process of thermodynamic air treatment in the recuperator on the i-d diagram. Points: 1 - external air in summer, 2-3 - supply air after the recuperator; 1" - external air in winter; 2'-3' - supply air after the recuperator in winter.

If in traditional central air conditioners the main elements are radiators, air coolers and sprinklers, then in recuperative ventilation systems all these elements are replaced by one heat exchanger - a recuperator. On the i-d diagram we set the parameters of the air supplied to the storage facility, based on the construction of the thermodynamic air treatment process. This process is common to all types of buildings (energy efficient, passive, net zero energy, etc.).

Since in houses with low energy consumption there is no room for either heat supply or heat loss, the recuperator is quite sufficient to ensure the thermal comfort of the room, and at this time ter=tsh. Along with determining the supply air temperature, it is necessary to determine the relative humidity of the air in the room (φ) so that the operating point corresponding to the calculated parameters of the air in the room is in the so-called comfort zone.

The comfort zone (Fig. 3) determines the combination of air temperature and humidity in the room at which a person does not experience thermal stress

.

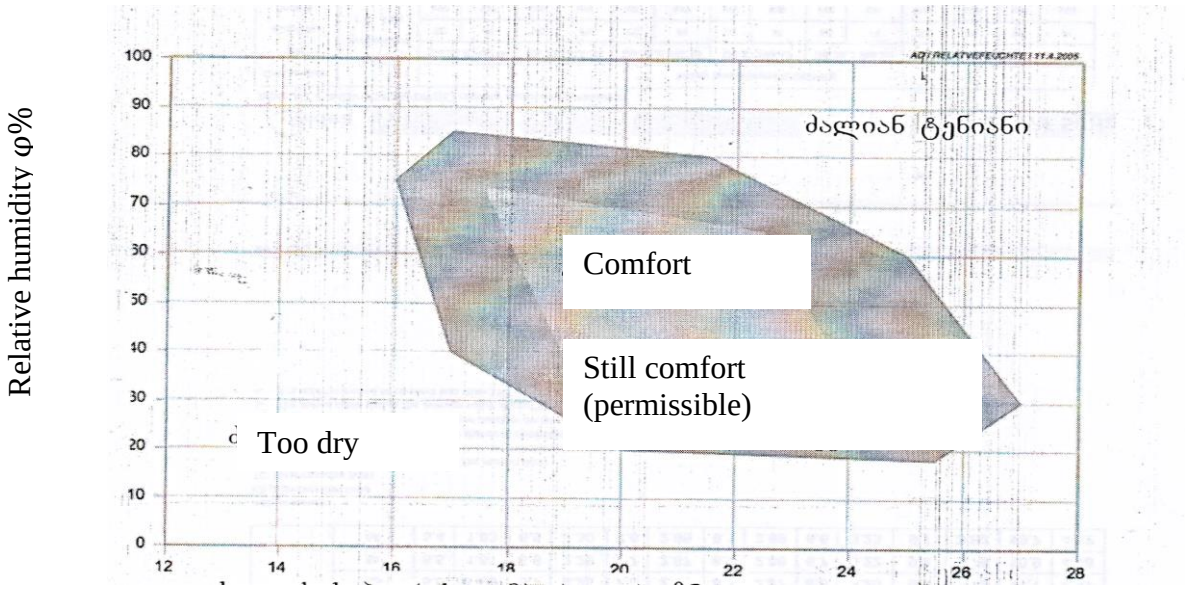

Fig. 3. Thermal comfort table

If there is an excess or lack of heat in the warehouse, then in accordance with the current temperature and humidity conditions in the warehouse, the assimilation process takes place.

$$\epsilon = \pm \frac{\Sigma Q}{\Sigma W}\ kJ/kg\ . \qquad (10)$$

With its help, we must determine the parameters of the supply air in the compartment and carry out additional measures to ensure the necessary parameters of the supply air.

Conclusion

The organization of recuperative ventilation systems in houses with low energy consumption (passive, zero, active, etc.) is an important condition for increasing energy efficiency and ensures maximum thermal comfort in buildings without heating and air conditioning systems.

Reference

1. Law of Georgia on Energy Efficiency of Buildings, No. 5900 SS, 05/21/2020.,
2. Passivhaus -Projektierungspacet, PHPP Version 10 (2021)
3. Reference book. 13330.2012 – Thermal protection of buildings, Moscow. 2012

IMPACT OF ANISOTROPY OF SOIL PROPERTIES ON SLOPE STABILITY

Giorgi Lutidze, Kote Iashvili, Nina Areshidze, Giorgi areshidze
Georgian Technical University, Tbilisi 0170, Georgia
george.pato@gmail.com

Abstract

In construction-related engineering geology, the oversight of soil property anisotropy is a frequent occurrence. This oversight often leads to unforeseen consequences, impacting both construction processes and subsequent building operation. This article predominantly delves into the impact of two forms of soil property anisotropy on overall slope stability: structural anisotropy and lithogenic anisotropy within the slope massif. The first type of anisotropy directly influences immediate slope stability, while the second type pertains to the formation of the soil's deformation horizon, crucial for the long-term stability of the slope.

Key words: anisotropy of soil properties, slope array, slope stability assessment, immediate slope stability, long-term slope stability.

Introduction

Introduction Assessing slope stability stands as a primary objective when designing construction within landslide-prone areas. [1] One pivotal phase in evaluating slope stability involves schematization, entailing the creation of a mathematical model. This process comprises generalized and specialized approaches. Generalized schematization entails simplifying the representation of a complex natural object, balancing between limited scientific understanding and the available information's quality. Specialized schematization involves refining the conceptual model into a specialized (geomechanically) framework, aiming for maximum simplification while retaining essential accuracy. Justifying schematization choices remains a critical task in constructing and describing a mathematical model, frequently employed in engineering studies. [2]

Specialized schematization involves several distinct stages: Firstly, it involves structurally schematizing the inclined ground array. This step delineates the foundational structure of the slope under study. Secondly, it encompasses the schematization of soil properties. This facet determines the anticipated behavior of the soil array during modeling. Lastly, it involves the condition-based schematization of the slope itself—modeling the object to ascertain its stability status. This final determination of stability, whether "stable" or "unstable," hinges on the predefined criteria set by the soil properties.

The crux of slope stability assessment lies in understanding the interplay between soil property heterogeneity and slope orientation. There exists a discernible alignment between identified heterogeneity and slope direction, forming a crucial ratio. The term "anisotropy" encapsulates this non-uniformity and unevenness in ground properties, which vary based on direction.

In essence, 'anisotropy' pertains to the coordinate system within which the properties of rocks in the Earth exhibit 'anisotropic' traits. An important distinction lies between linear anisotropy, observed within the Cartesian coordinate system, and curvilinear anisotropy, which emerges, for instance, in cylindrical or spherical coordinate systems. If symmetry isn't established, such as in defining 'anisotropy,' an unspecified coordinate system is employed, resulting in the treatment of 'anisotropic' rocks as heterogeneous.

Anisotropy generally refers to the specific coordinate system wherein rocks under investigation showcase anisotropic attributes. This classification distinguishes between linear and curvilinear anisotropy [3]. When symmetry isn't established, leading to the utilization of an undefined or inaccurate coordinate system, the characterization of anisotropic ground as non-uniform becomes prevalent.

Clearly, an accurate depiction of the geological structure and soil properties in the geomechanically soil model guarantees closer alignment between numerical values derived

from slope stability analysis and real-world conditions. Describing simpler geological structures with straightforward soil models poses little challenge. However, in the case of complex geological formations, often characterized by soils exhibiting anisotropic properties, utilizing an inadequate calculation model might prove insufficient and lead to inaccuracies when applied to real scenarios.

Main part

An analysis of the anisotropic properties within the soil array encompassing the slope identifies two discernible types of anisotropy [4]. The first type emerges from inherent characteristics present in the constituent soils shaping the slope, while the second type evolves from the development of inhomogeneity in their properties due to specific field stresses exerted on the slope massif. Consequently, when evaluating slope stability, it becomes pertinent to consider two forms of anisotropy (non-uniformity) influencing the slope's stability:

I. Natural dispersion of ground properties anisotropy within the massif (structural or lithogenetic). Formation of anisotropic conditions, shaping geotechnical horizons in the slip zones during the main deformation process within the massif.

The first type of anisotropy, characterized by property variations based on direction, should be analyzed within the Cartesian coordinate system, while the second type pertains to the cylindrical system. Naturally, the slope array is typically modeled using the Cartesian coordinates, where the second type manifests as inhomogeneity. This second form of anisotropy, described within the cylindrical coordinate system regarding soil properties, can also be termed a non-uniform slope array within the Cartesian coordinates, emerging during the progression of the landslide process.

The emergence of the second type of anisotropic conditions results from the alteration of the initial slope array structure, accompanied by changes in soil composition and properties. This transformation occurs concurrently with the development of maximum shear stresses within the boundaries of the sliding zone. A decline in the slope stability coefficient is evident, primarily due to the formation of a slip zone characterized as a geotechnical horizon of significant deformations (representing the second type of anisotropy or inhomogeneity), which notably impacts long-term stability.

Simultaneously, incorporating the anisotropy of soil properties (the first type of anisotropy) into slope stability modeling allows for immediate assessments of slope stability.

To assess the impact of soil property anisotropy on numerical slope stability analysis, a series of standard calculations using the Morgenstern-Price method were conducted using the GeoStudio software developed by GEO-SLOPE (International) [6]. Four scenarios were considered:

1. Anisotropic representation (first type).

2. Isotropic representation using soil physico-mechanical properties in the layer's natural direction for calculation.

3. Isotropic representation using soil physico-mechanical properties perpendicular to the layer's direction for calculation.

4. Anisotropic representation (Type I) alongside the formation of a horizon of primary deformations (Type II) within the slope array.

calculation option	Stability coefficient (m-p* method)	circular Cylindrical surface radius M	Total area of potential landslide projection m2	slope condition
1	1.793	150.244	4958.31	Stable
2	1.704	148.632	4724.16	Stable
3	2.063	149.122	4823.35	Stable
4	1.009	150.214	4958.41	Marginal equilibrium condition
1 under seismic loading	1.092	197.071	685.72	Marginal equilibrium condition

All other conditions, including technogenic groundwater loads, remained constant across all options. For the first option, a supplementary report on seismic loads was generated based on pseudo-static analysis.

An inconsistency arose concerning the ratio between vertical and horizontal acceleration coefficients in calculating slope stability under seismic effects. Measurements revealed a prevalence of horizontal acceleration over vertical acceleration. Notably, in our case, the vertical detector for seismic impact wasn't utilized, and a maximum magnitude of 0.3 was applied for seismic horizontal acceleration."

The results of the numerical assessment of the slope model, considering anisotropy's influence, are presented in the table. It's evident that the minimum anticipated landslide deformations and the lowest Km values for slope stability (without considering changes in soil properties within the primary deformation zone) occur when anisotropy is disregarded, and the soil's physico-mechanical properties align with parallel layering in the soil massif. However, if the slope features differing conditions in soil layering, evaluating its physico-mechanical properties as parallel layering would be erroneous, as it fails to accurately depict the engineering-geological scenario.

The anticipated landslide deformations increase slightly (by approximately 2%), and the maximum coefficient of slope stability is observed in calculations where the soil's physico-mechanical properties were determined perpendicular to the identified layering (as per the third option).

*M-P - Morgenstern-Prysa [7] method

However, it's important to note that determining the soil's physico-mechanical properties perpendicular to the pavement in all cases for slope stability assessment would be inaccurate. This approach leads to a significantly inflated Km value compared to the actual engineering-geological conditions.

In scenarios where soils are horizontally layered, conducting a numerical analysis considering soil property anisotropy is acceptable for a more accurate slope stability assessment. When considering the first type of anisotropy using the initial calculation option, the coefficient of stability obtained is marginally higher than that derived from calculations based on properties determined in accordance with the laying pattern. However, it notably diminishes (by approximately 15%) compared to values obtained using properties determined perpendicular to the laying pattern.

It is particularly noteworthy that the assessment of slope stability, taking into account the anisotropy of soil properties, showed the maximum volumes of expected landslide deformations. Thus, anisotropy affects both the reference slip plane and the value of the ratio stability coefficient.

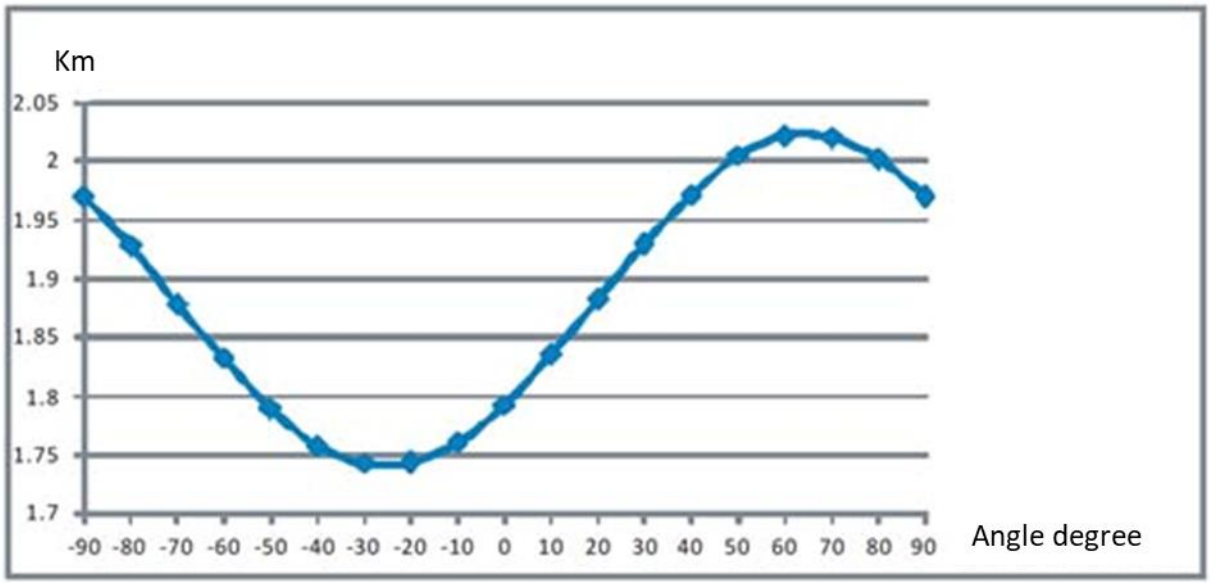

fig. 1. Dependence of the slope stability coefficient on the angle of inclination of the anisotropic plane.

Negative angle - inclination of the plane of anisotropy in the direction of the slope,
positive - in the opposite direction

Considering the seismic impact within the numerical analysis and factoring in the anisotropy of soil properties (first type), additional calculations revealed the potential for instantaneous stability loss when the seismic impact surpasses 8 points.

Furthermore, the outcomes from the numerical analysis investigating slope stability considering non-uniformity (anisotropy of the second type), specifically the fourth calculation option, are intriguing. In this scenario, during the formation of the geotechnical horizon zone of primary deformations, the slope's long-term stability significantly diminishes, transitioning from a stable state to a limited equilibrium. There's a high probability of a landslide process occurring.

conclusion

The comprehensive evaluation of the slope stability model, considering the influence of soil property anisotropy, indicates its impact on both the positioning of the sliding reference surface and the slope stability coefficient. Introducing the first type of anisotropy conditions into the geomechanical calculation scheme demonstrates relatively higher values (around 5%) compared to those obtained from the physical-mechanical properties aligned with the laying pattern. Conversely, there is a notable reduction (approximately 15%) in the stability coefficient values when utilizing properties determined perpendicular to the laying. Simultaneously, calculations incorporating the first type of anisotropy reveal the maximum anticipated volumes of landslide deformations.

When considering the immediate stability of the slope model, the activation of the landslide process is contingent upon a seismic impact exceeding 8 points on the MSK-64 scale. However, the slope's long-term stability is influenced by the creation of inhomogeneities within the sloping massif (the second type of anisotropy), associated with slip zone formation. These inhomogeneities significantly diminish the slope's long-term stability, shifting the primary factor for the landslide process development away from seismic impact.

Referencs

1. Фоменко И.К. Математическое моделирование напряженного состояния инженерно-геологического массива, сложенного анизотропными горными породами: автореф. геол.-минер. М., 2000. 24 с.
2. 5. Фоменко И.К., Захаров В.С.,

Самаркин-Джарский К.Г., Сироткина О.Н. Учет сейсмического воздействия при расчете устойчивости склонов // Геориск. 2009. №4. С. 50-55.

3. Hoek E., Carranza-Torres C., Corkum B. Hoek-Brown failure criterion
4. //Proceedings of the North American Rock Mechanics Symposium.
5. Toronto, 2002. V 1. P. 267-273.

6. Li A.J., Merifield R.S., Lyamin A.V. Stability charts for rock slopes based on the Hoek-Brown failure criterion // International Journal of Rock Mechanics and Mining Sciences. 2008. V. 45. № 5. P. 689-700.

7. Z. Gwishiani, T. Khmelidze , A Brief Vocabulary of Civil Engineering Terms, Publishing House "Technical University", 2023, Tbilisi, Georgia, pp.18 (Georgian)

8. Stability modeling with SLOPE/W. 2007 Version. An Engineering Methodology: 4th Edition. GEO- SLOPE International Ltd., 2008.

9. Morgenstern, N.R., and Price, V.E. 1965. The analysis of the stability of general slip surfaces. Géotechnique, 15(1): 79-93.

STRONGTHENING OF THE LOAD-BEZRING WALLS OF THE OLD BUILDING BY TORQUE-RETORTING METHOD

Irakl Kvaraia
Georgian Technical University, Tbilisi 0170, Georgia
irakvara@yahoo.com

Abstract

The article discusses the progress of strengthening the external load-bearing walls of the old building during the reconstruction process. Over time, all buildings require urgent reconstruction works to extend their useful life. At this time, a thorough study of the physical condition of the load-bearing structures and the correct planning and implementation of the strengthening-strengthening works of the entire building are of particular importance. In recent years, in order to strengthen the old building, along with the reinforcement of windows and door openings with steel angular profiles, it is more and more common to completely cover the outer and inner surfaces of the wall with reinforcing mesh. If in the early years, after the use of nets, such surfaces were mainly covered with plaster, modern machinery allows for the easy use of the torqueretting method for this purpose. As a result of torcreting, the cross-section of the walls and, accordingly, their load-carrying capacity increases.

Key words: building, window, wall, armature, anchor, framework, grid, concrete

Introduction

In the beginning of the 70s of the last century, the three-story brick school building underwent several renovations. Mainly, the facade part of the building was restored with plaster and its subsequent painting. Similar work was carried out inside the building, but no strengthening work had been carried out so far, therefore, despite the rather long period of operation, the building looked visually satisfactory, and no serious damage was noticed inside the building. Based on the new regulations adopted in the country, it was considered appropriate to study the condition of the building that is more than half a century old. As a result of comprehensive examination of the foundation and load-bearing structures, it was determined that it was definitely necessary to carry out strengthening works of the external load-bearing walls. The brick walls, which over the years were most affected by the intense impact of natural precipitations, in many places could not meet the load-bearing capacity conditions envisaged by the project.

Such categorization, together with the physical condition of the walls, was also caused by the fact that the said building was designed for the impact of a 7-point earthquake at the time. Subsequently, due to the transition to 8-point calculation in almost the entire territory of Georgia, the existing walls could not meet the increased requirements of seismic resistance. In order to strengthen the outer load-bearing walls, it was decided to frame all the existing windows and door openings in 100 mm equal steel angular frames. And in order to increase the bearing capacity of the walls themselves, on the inner and outer surfaces of the walls, it was necessary to attach factory-made reinforcement nets. It was decided to use the torqueretting method for high-quality performance of the vertical surfaces of the wall covered with reinforcing mesh, reliable concreting and strengthening works.

Previously, the mentioned method was mainly used in mining construction, in the concreting of tunnel arches and walls, but now it has become widespread in the construction and reconstruction of all types of construction objects. This was facilitated by the production of new types of equipment needed for torque-retting, which are distinguished by their ease of operation.

Main part

The strengthening of the external load-bearing walls of the old building began with the complete removal of the plaster layer on its external and internal surfaces. The mentioned works included the cleaning of the walls, both from the remnants of the plaster and from the layer of exhausted fermentation revealed in the brick stack. The mentioned works were carried out using electric demolition machines. A hanging electric basket or an auto basket was used for perfect treatment of any part of the external walls. After removing the plaster layer, the brick surface was treated using

special metal brushes. Special attention was paid to this process not by chance, because in this way, the areas cleared to the appropriate level significantly increase the adhesion between the old brick wall and the newly laid concrete after filling with shotcrete concrete. Fine-grained, high-class concrete, under high pressure during the torque-recrete process, easily reaches all vulnerable places and significantly increases the load-bearing capacity of the walls.

The final stage was the strengthening of window and door openings with steel angles. They were installed directly at the workplace. The edges of the opening on the entire perimeter, both from the inside and outside of the wall, were covered with steel angles, which were then connected to each other with 10 mm thick metal sheets, and a powerful reinforcement system was created by means of a spatial frame (Fig. 1).

Fig. 1. Fig. 1. Reinforcement of window openings

Reinforcement of reinforced concrete coils connecting the outer wall with all the inner walls was done by arranging similar frames in the corridors. In this case, the spatial frame was created by installing angle brackets in the corners of the coil and the support column. These corners were connected to each other with steel sheets (Fig. 2).

Fig. 2. Reinforcement in the corridor

After the openings were strengthened, factory-made reinforcing meshes were attached to the walls. For this, they used 12 mm diameter reinforcing anchors, which were placed in pre-drilled holes across the width of the wall (Fig. 3).

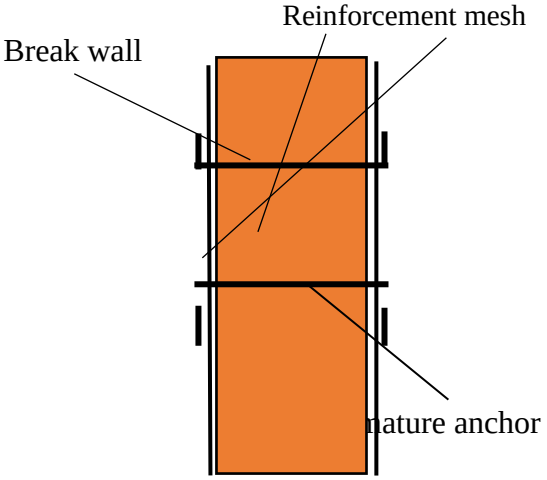

Fig. 3. Grid arrangement scheme

8 mm diameter reinforcement nets made by spot welding (size 200 X 200 mm) were delivered to the site in an unfolded state, easy to move and install (Fig. 4).

The dimensions of said nets were 6000 X 2000 mm, but often, especially for fixing them on the inner walls, it was necessary to cut the nets. This operation was carried out directly on the site, and before installation, the reinforcement meshes were cut to the desired dimensions using angle cutters.

Fixing of the nets on the inner surface of the wall on the curved parts of the ends of the anchors was carried out by means of an anchor. The bending of the anchor heads also allowed the rebar mesh to be firmly fixed on the outer surface. Also, by using a folding guide, the nets could be easily tied together in all directions, which was done by hanging electric baskets (Fig. 5).

Fig. 4. Reinforcement grids

Fig. 5. Installation of nets with a hanging basket

It should be noted that the welding of the ends of the nets to the reinforcing steel angles of the window and door openings was carried out by arranging a seam of at least 50 mm. In the event that the rods of the mesh reinforcement did not allow their full fusion with the angles, then they resorted to the extension of the rods of the mesh reinforcement. On the extension rod, a rebar rod of the same diameter was fixed on top with a clamp. so that the length of the welding seam connecting the frame to the corner was not violated (Fig. 6. and Fig. 7).

Fig. 6. Mesh on the inner surface of the wall

Fig. 7. Weld the grid to the corner

After window and door opening reinforcement frames, external load-bearing walls with reinforcement nets, internal and external surfaces were completely covered and all connecting nodes were arranged, the vertical walls were concreted using a special torque-creting machine (Fig. 8).

Fig. 8. Torque-creting machine

New aluminum windows installed before the start of torquing work were securely wrapped with cellophane in order to protect them from damage. In order to ensure the high-quality performance of the torque-creting process, concrete application was carried out in three stages (Fig. 9):

Fig. 9. Torcreting process

- In the first stage, the space between the cleaned brick wall and the reinforcement grid was filled (Fig. 10);

Fig. 10. Torcreting stage I

- in the second stage, the reinforcement mesh was completely or partially covered, which was easily visible (Fig. 11);
- The third stage required special precision, because it meant applying a protective or finishing layer and the verticality of the concreted surface had to be preserved as much as possible (Fig. 12).

It should be noted that the smoothness of the surface obtained as a result of torcreting the facade part of the building is not of great importance. In some cases, the existing chaotic structure is even more acceptable for their further dyeing (Fig. 13).

Fig. 11. Torcreting stage II

Fig. 12. Torcreting stage III

Fig. 13. Outer surface of the wall

In the case of the internal wall surface, the situation is radically opposite, because despite great efforts, it is impossible to achieve smoothness of the concreted surface. To achieve this goal, high-quality plaster can be applied with the help of leveling beacons. In addition, gypsum-cardboard or other types of paving tiles are arranged on the torcreted surface. This requires the installation of additional profiles and the thickness of the torcrete surface increases by 10 - 15 cm, which is not always advisable (Fig. 14).

Fig. 14. Plasterboard on the inner wall

It should also be taken into account that the reinforcement steel elements must be covered with anti-corrosion paint before their installation, because then only the visible surfaces can be painted, and a large part remains exposed under the concrete layer.

Conclusions

1. During the execution of the work of strengthening the external load-bearing walls of the old building by the torquereting method, it is most effective to arrange spatial frames using

steel angles on the window and door openings. In addition, it must be connected with them by welding the reinforcement nets placed on the inner and outer surface of the wall.form of box-shaped ventilated systems, covering their upper parts with tin or other similar materials, in order to protect them from the harmful effects of natural precipitation;

2. Before starting the work of strengthening the load-bearing walls of the building with steel elements and reinforcement grids, it is necessary to clean and treat the surface of the existing wall as high as possible in order to maximize the adhesion to the torque-reinforced concrete. It is also necessary to cover the steel elements with anti-corrosion paint, because then only the visible parts can be painted and a large part remains unprotected;

3. It is impossible to obtain smooth surfaces during concreting of walls by the shotcrete method, which creates special difficulties in arranging the inner surfaces of the walls of the building. It is most appropriate to correct the mentioned problem by applying high-quality plaster on the torcreted surface. In addition, gypsum-cardboard or other types of facing wall panels can be used, but in this case the facing layer increases significantly, which is not always acceptable.

Reference

1. I. Kvaraia. Seismic protection systems in construction and their arrangement. Technical University. Tbilisi. 2023. 126 p.;

2. I. Kvaraia. Covering poorly built walls with torqueretting. Scientific and technical magazine "Construction" #3 (59), 2021. p. 18-21;

3. I. Kvaraia. Elimination of damage and defects identified during the construction process. Technical University. Tbilisi. 2017. 100 pp.;

4. Z. Ezugbaia, I. Kvaraia, Sh. Bakanidze, I. Iremashvili. Technology of construction processes. Technical University. Part 2. Tbilisi. 2016. 274 p.

5. I. Kvaraoa. Strengthening and strengthening works under extremely limited conditions during construction and reconstruction. Technical University. Tbilisi. 2016. 100 pp.;

LIMIT LOAD-CARRYING CAPACITY AND PLASTIC HINGES

Jumber Nizharadze, Manana Arabidze
Georgian Technical University, Tbilisi 0170, Georgia
j.nizharadze@gtu.ge

Abstract

Using the limit load-carrying capacity method provides a convenient opportunity to calculate structures in the plastic stage**.** According to this method, the destruction of the structure corresponds to the moment when plastic hinges appear in it.

On this basis, using the principle of virtual work, calculation schemes have been drawn up for relatively simple structures, equations were derived and calculation formulas were obtained: for a beam fixed at two ends, a flat frame with various scheme options, and for oval and round rings.

Key words*:* virtual work, plastic hinge, plastic bending moment, breaking load

Introduction

In modern construction practice, in mechanical engineering, shipbuilding, aircraft and rocketry, in the process of structural calculations, the emphasis is mainly on the limit load-carrying capacity method, which makes it possible, while ensuring reliability, to make maximum use of materials created by innovative technologies. The following work is devoted to these issues.

Main part

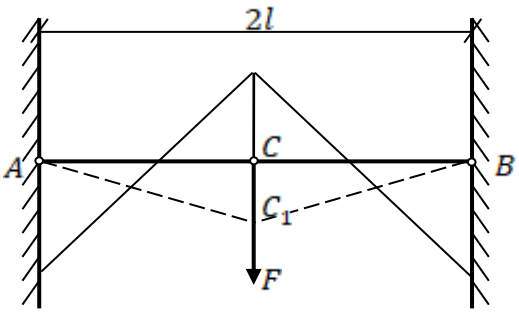

C – plastic hinge

Fig. 1

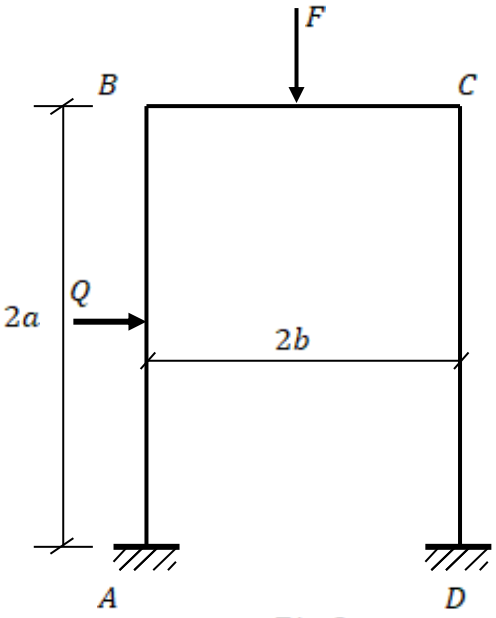

Fig. 2

Let's start our discussion by looking at relatively simple structures. Figure 1 shows a beam made of a homogeneous material, rigidly fixed on both sides, with a force F acting in the middle of the span. From the diagram of the moments, it is clear that their maximum values are found in the fastening sections and in the middle of the span. Therefore, with increasing force F, plastic deformations are obtained precisely in these sections. When over the entire area of all these three sections the material is in the plastic stage, then even the smallest increase in load will cause a significant continuous increase in deflection.

The behavior of a rigid-plastic material in the created situation is interesting. For example, the deflection will be zero until all the indicated three sections completely enter the plastic stage (the parts of the beam located between these sections remain rigid). The beam operation scheme can be compared to a system composed of two rods, which is created by three plastic hinges (these two rods rotate relative to the hinges). This scheme makes it possible to study the load-carrying capacity of a beam using the principle of virtual work. According to this principle, at the moment the maximum load capacity is reached, the power

Let's complicate the task. Let's look at the frames. In general, when calculating complex structures, through accumulated experience and experiments, the position of plastic hinges is established, the existence of which turns the

which the external force F develops when working at a unit speed from top to bottom is equal to $F \times 1$. It should be noted that this work of plastic deformation is released in the hinges in the form of thermal energy. The rotation speed of each part will be $1/l$. Let us denote by M_{pl} the value of the moment that causes plastic deformation along the entire section of the hinge. Then at points A and B the rate of dispersion (the rate of dissipation will be M_{pl}/l. And at point C will be twice as much. That's why

$$F \cdot 1 = \frac{4M_{pl}}{l} \qquad (1)$$

As can be seen from the consideration, this formula is valid only when the maximum load capacity is reached. At this moment, force F from point C will move to point C_1. To achieve this, the lengths of bars AC and BC must be changed appropriately. However, this design will not be a mechanism in the concepts used by a mechanical engineer, for the reason that the connections between the rods are still rigid.

structure into a mechanism, and then the load that causes destruction is calculated. And in this case, it is necessary to use the principle of virtual work.

Consider the following pro

blem: Figure 2 shows a flat frame with a load scheme and corresponding dimensions

.

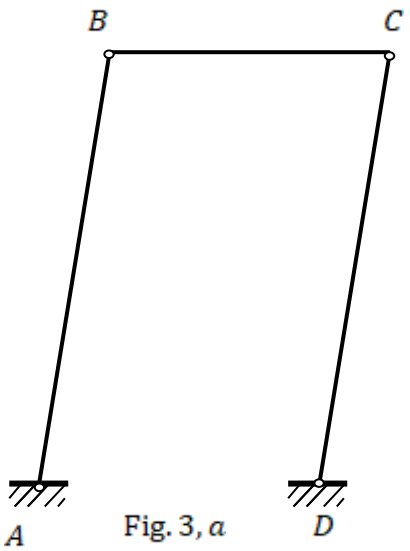

Fig. 3, *a*

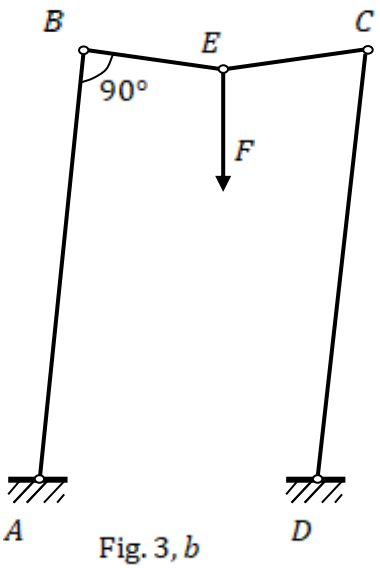

Fig. 3, *b*

Figure 3 shows common deformation schemes and possible mechanisms. Based on these options, it will be necessary to determine the maximum loads.

1) First version: scheme 1 (Fig. 3, a). The horizontal force moves at unit speed. Let's make an equation:

$$Q \cdot 1 = \frac{M_A}{a} + \frac{M_C}{a} + \frac{M_B}{a} + \frac{M_D}{a} = \frac{4M}{a} \quad (2)$$

It is obvious that $M_A = M_B = M_C = M_D = M$. Note also that at points B and C, i.e. in plastic hinges the moments are equal and are M.

2) Second version: scheme 2 (Fig. 3, b). In this case, the equation will look like

$$Q \cdot 1 + F\frac{b}{a} = \frac{M_A}{a} + \frac{2M_E}{a} + \frac{2M_C}{a} + \frac{M_D}{a} = \frac{2(K+2)M}{a} \quad (3)$$

Where $M_E = K \cdot M$.

K - the multiplier has the following physical content: as experiments have shown, to create a plastic hinge in a horizontal frame rod it is necessary K times greater moment than in vertical rods. Meaning K determined in each particular case in accordance with the geometry of the structure and load.

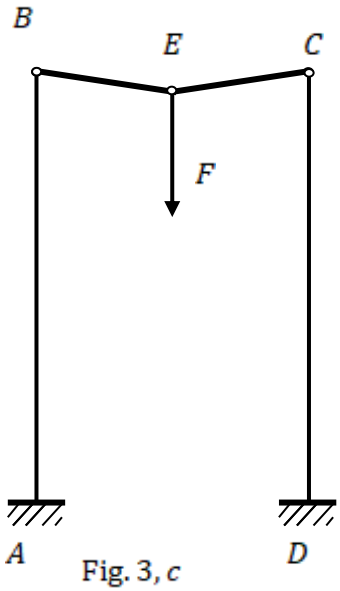

Fig. 3, *c*

Now let's compare these four options discussed above and choose the version where the force F is the smallest between horizontal and vertical loads. Let's establish a quantitative relationship, e.g. $Q = n \cdot F$. Let's go to the numbers. Let's say $Q = 2 \cdot F$, $K = 1{,}5$ and

As you can see, we need to rely on the second version, i.e. $F = \frac{1{,}4M}{A}$, since with this value of F the destruction of structures is sure to happen.

A similar approach can be successfully applied to oval and round rings too. As is known, such forms are used in various

3) Third version: scheme 3 (Fig. 3, c). It is assumed that the force F moves vertically from top to bottom with unit speed and the appropriate equation is drawn up.

$$F \cdot 1 = \frac{M_B}{b} + \frac{2M_E}{b} + \frac{M_C}{b} = \frac{2(K+2)M}{b} \quad (4)$$

4) Fourth option: scheme 4 (Fig. 3, d). By the same reasoning we get

$$Q \cdot 1 = \frac{M_A}{a} + \frac{2M_C}{a} + \frac{M_B}{a} = \frac{4M}{a} \quad (5)$$

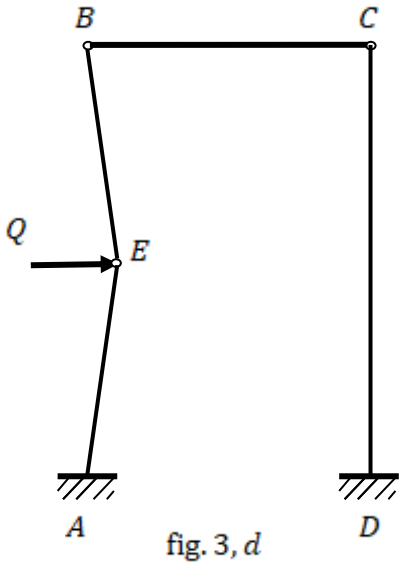

fig. 3, *d*

$\frac{b}{a} = 3$,

then from the options considered above we obtain the following values of F

1) The first version: $F = \frac{2M}{A}$

2) The second version: $F = \frac{1{,}4M}{A}$

3) Third version: $F = \frac{1{,}67M}{A}$

4) Fourth version: $F = \frac{2M}{A}$

branches of mechanical engineering, aircraft manufacturing, shipbuilding, rocket science, etc. Figure 4 shows oval a) and round b) rings. The oval ring is symmetrical about line AB. Consider the case of pure bending (Transverse forces do not act). Let us find the value of breaking load. Suppose that when

fracture begins, plastic hinges occur at points A, B, C_1 and C_2. Consider that point A is stationery and point B moves along line AB with unit speed. AC_1, C_1B, BC_2 and C_2A is a chain composed of four elements, with one instantaneous center BC_1. Elements AC_1 and C_1B rotate respectively with speeds ω_1 and ω_2 (points C_1 and C_2 must be equidistant from A and B), then

$$D \cdot B \cdot \omega_2 = 1 \quad \omega_2 = \frac{1}{DB} \quad (6)$$

and

$$D \cdot C_1 \cdot \omega_2 = A \cdot C_2 \cdot \omega_1 \quad \omega_1 = \frac{DC_1}{AC_2} \cdot \omega_2$$

and

If M is the total plastic bending moment, then

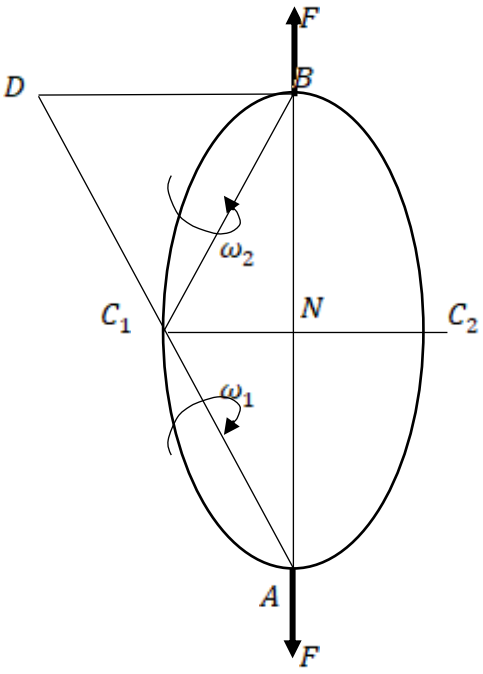

а)

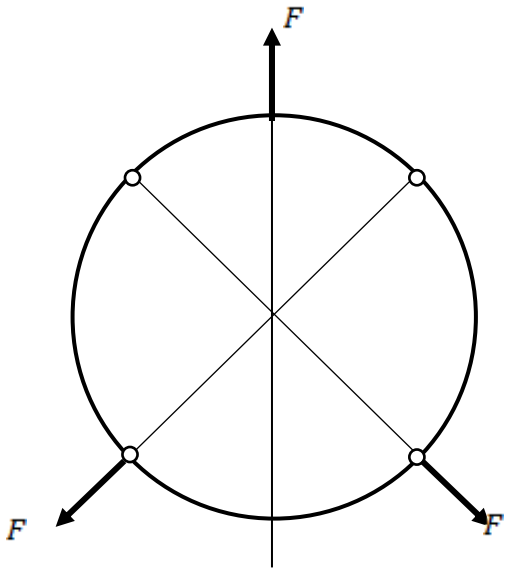

б)

Fig. 4

$$F \cdot \frac{1}{2} = 2M(\omega_2 + \omega_1);$$

$$\frac{F}{4M} = \frac{DC_1 + AC_1}{AC_1} \cdot \frac{1}{DB} = \frac{1}{C_1 \cdot N} \quad (7)$$

Based on this

$$\left(\frac{F}{4M}\right)_{min} = \left(\frac{1}{C_1 \cdot N}\right)_{max} \quad (8)$$

i.e. hinge C_1 is formed at the point, which is farthest from the line AB. Let's consider a round ring as a special case of an oval ring, but let's complicate it with a load scheme. On the figure 4 shown inclined to each other at an angle $\frac{2\pi}{3}$ three equal forces F, which emanate from the center of the ring. That's why

$$F = \frac{4Mctg\frac{\pi}{3}}{R} \quad (9)$$

Where, R is the ring radius. In such a case, 6 hinge form at the same time (according to the load scheme). Such a scheme suits well with the experimental data.

Conclusion

The problems of determining the limit load-carrying capacity in the case of the existence of plastic hinges for simple-type structures that are widely used in practice have been studied. The principle of virtual work has been used. For several special cases, the values of force factors corresponding to the limit state have been determined. Load capacity loss factors and corresponding load values have been determined.

Referencs

1. Малинин Н. Н. Прикладная теория пластичности и ползучести. «Машино-строение», М.1975 г. стр. 411.

2. Хилл Р. Математическая теория пластичности. ГИТТЛ, 1956, стр. 409.

3. *T.Batsikadze, A.Kvaratckhelia, Z.Madzagua,* A Short Course in Theories of Elasticity, Plasticity and Creep", Publishing House "Technical University", 2014, Tbilisi, Georgia

4. *T.Batsikadze, N.Murgulia, J.Nizharadze,* Derivation of the equations of creep theory using plastic potential, Scientific-Technical Journal "Building" № 4(64), 2022

5. T. Batsikadze, N. Murgulia, J. Nizharadze. "The use of plastic potentials in yield theory" #1(65), 2023.

STUDY OF DAMAGE QUALITY OF TAO-KLARJETI TEMPLES

Maya Chanturia, Giorgi Mamardashvili
Georgian Technical University, Tbilisi 0170, Georgia
m.chanturia@gtu.ge

Abstract

Tao-Klarjeti area is rich in monuments of Georgian architecture. This area has been under Turkish jurisdiction for centuries and our temples are neglected and neglected. The passage of time, earthquakes, various atmospheric events or human vandalism have greatly damaged them. The aim of the paper is to propose the arrangement of the designed seismic damping structural system in a temple for which it will be more effective.

Key words: earthquake, dome, temple, recovery-restoration.

Orthodox Christian churches, are a symbol of our nation's identity and spiritual strength. Cultural heritage is a nation's window into the historical past. That's why it needs to be treated and protected. It is known that Georgia is located in a seismically active zone, which is why earthquakes are frequent here. This natural event for centuries damaged our church monasteries, the restoration and strengthening of which was and is very important both for our ancestors and for our generation. Unlike ordinary buildings, during the restoration and deepening of cultural heritage monuments, we must take into account its constructive uniqueness. Its strengthening should be done with great clarity. Tao-Klarjeti is the richest in monuments of Georgian cultural architecture. The purpose of this paper is to visually examine the degree of destruction (damage) of the existing temples there. This study was conducted based on photographs from the Internet and various used literature, for which several temples were selected. These are: Bana, Oshki, Ishkhani, Khandzta [1,2,3,4]. The restoration of architectural monuments was also ongoing during previous centuries. Since the middle of the last century, a specific scientific theory of the restoration of architectural monuments has been formed, which was founded at the first international congress of architecture and technical specialties in Athens, which was held in 1931, where the "Restoration-Restoration Charter" of the Italians, based on G. by Giovannini, presented their views. In 1964, at the Second International Congress, issues were discussed about the need to determine the need for restoration of architectural monuments; The first attempt to perfect the theory of restoration was attributed to the French scientist Paul Leon, who formulated concrete methods of restoration of monuments (1938), based on N. Balanos' restoration of the architectural monuments of the Acropolis of Athens demonstrated that restoration could serve several purposes. Alonza Riegl (1903) of the Austrian Empire pointed out that there are different methods of restoration of architectural monuments, and that they should be used accordingly. The eminent Italian scientist Amborgio Annoni argued that one cannot use the same method during the restoration of different monuments. He claimed that the restoration of architectural monuments is an extremely difficult process, it is specific, sometimes even the restorers themselves have a hard time imagining the goal and task of restoration.

Discussion

Bana Cathedral is an original and unique monument of Georgian architecture. It is a central domed temple, which was surrounded, the remains of which are still preserved today. After Tao-Klarjeti became a part of the Ottoman

Empire, Georgian Christian churches found themselves in a deplorable state. During the Russo-Turkish war in the 19th century, the Turks used the temple as a fortress, which made it a terrible target for Russia. This further damaged this magnificent temple. It can be seen from the pictures that the dome of the temple has collapsed, there is no longer a dome neck. The railings on the walls are cracked. None of the 8 columns that supported the dome have survived, the wall on one side has completely collapsed. In terms of restoration and strengthening, the situation here is very difficult. My dissertation cannot deal with these difficulties. Here, perhaps, the conservation method will be more useful than restoration.

Fig. 1. **Bana**

Oshki represented the Episcopal Church; It is a cross-domed temple with a free dome. For a long time, the existence of Oshki was shrouded in fog for Georgians; Only in 1902, when Ekvtime Takaishvili traveled to Tao-Klarjeti for the first time and accurately described the state of the monument, its existence became known.

Oshki is currently in a deplorable state; If its restoration-strengthening is not done in time, it may collapse (Fig. 2.); Especially since this shoulder is in the zone of high seismic activity. The main load-bearing structures of the temple, including the dome, still exist, although they appear to be quite damaged. As can be seen from the pictures, the dome's neck has not yet lost its stability, although the arched roof of the western arm has completely collapsed (Fig. 2). With the intervention of the World Organization for the Protection of Monuments, an agreement was reached between the Tukul and Georgian sides regarding the restoration of Oshki by the Georgian side. The seismic damping system developed by us can be used in the restoration of this temple.[5]

Fig. 2. Oshki - facade, dome, western arm

Ishkhan - the temple built by Grigol Khandzteli and his disciples, namely Saba Ishkhaneli. Outwardly, it seems to be the best preserved, however, after a detailed inspection, we will discover the damages that are numerous in the temple and which, like other temples, require immediate help. The temple is an elongated cross-domed building (Fig. 3). The dome is badly damaged, with a fairly wide crack running radially from the cleat to the support ring. The throat of the dome is also damaged; The arched (vaulted) roof of the elongated western arm has been completely collapsed. It is subject to restoration-strengthening.

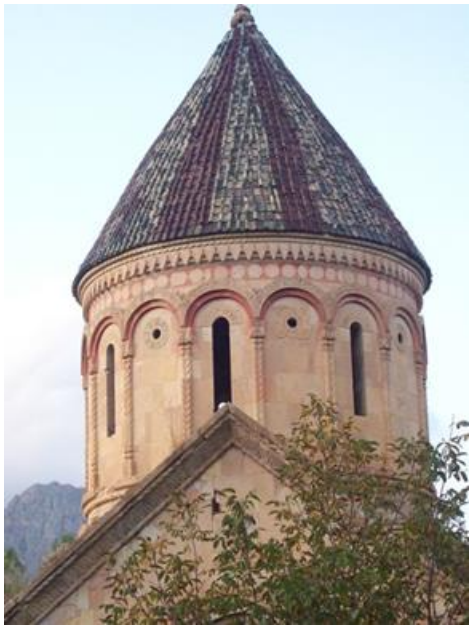

Fig. 3. Ishkhan - the throat of the dome, the altar, the dome from below

Khandza - the main temple is in the shape of an inscribed cross - it is a cross-domed temple (Fig. 4). Its dome rested on the walls of the apse on the east side, and on two piers on the west side, the remains of which have only survived. The pictures taken before 2007 show that the dome still existed (Fig. 4), and in 2010 - the dome has collapsed (Fig. 4). However, the neck of the dome is visible, on which, in case of restoration of the temple, it is possible to arrange a new dome. In this case too, it is possible to use the seismic suppression system developed by me.

Fig. 4. Khandza

As the above studies show, the main reason for the damage of our historical monuments in Tao-Klarjeti, along with the passage of time, is strong earthquakes. This event for centuries damaged our churches-monasteries, the restoration and strengthening of which was and is of the utmost importance both for our ancestors and for our generation.

Unlike ordinary buildings, during the restoration and deepening of cultural heritage monuments, we must take into account its constructive uniqueness. Its strengthening should be done with great clarity. The purpose of this work is to use seismic protection measures in the restoration of domes of damaged temples. Our ancestors used anti-seismic measures during the construction of temples from time immemorial. An example of this is the "swallow tail", or the use of stone blocks in dry stacking. They arranged the frames mainly at the neck of the dome or shell, where one structural part ends and the other - the dome or shell - begins, because there is a change in stiffness. It is this place that is dangerous during seismic impacts. The goal of our work is to restore the damaged dome of the temple and to equip it with seismic protection measures so that its authenticity is not violated. For this purpose, a computer calculation model was created, the spatial calculation of which was performed using the finite element method using the computing

complex "LIRA SAPR-2016". In general, the purpose of a seismic protection system is to reduce the seismic acceleration transmitted from the ground to the building. In our case, the cross-domed temple is structurally divided into two parts - the under-dome (cross) part and the dome itself. The function of the dampers placed between them is to reduce the seismic acceleration transmitted to the part of the dome.[5].

The constructional solution of seismic damping systems is as follows: a reinforced concrete grooved belt is arranged on the support ring, which is also the binder of the arches. Metal sheets will be anchored in the groove, on which the damper is mounted: rubber-metal (widely used in viaducts and overpasses in the places of support of the Mali structure) and spring. The throat of the dome is connected to the damper by a valve. Holes are made in the throat of the dome (shown in the diagram below), in which metal anchors are placed to limit vertical movement. As far as is known, this type of construction has not yet been used in practice, so it is a novelty.

Rubber-metal dampers of the new seismic suppression system were used for seismic isolation. The Seismic Isolating Rubber Bearing consists of alternating laminations of thin rubber layers and steel plates (shims), bonded together to provide vertical rigidity and horizontal flexibility.

Vertical rigidity assures the isolator will support the weight of the structure, while horizontal flexibility converts destructive horizontal shaking into gentle movement.

Rubber-metal dampers, as well as spring-type dampers, may be arranged in the structure arranged in the throat of the dome of the temples under construction. Based on their positive and negative characteristics, as well as the calculation, it should be decided which of these types of dampers we will choose for temples (Fig. 5).

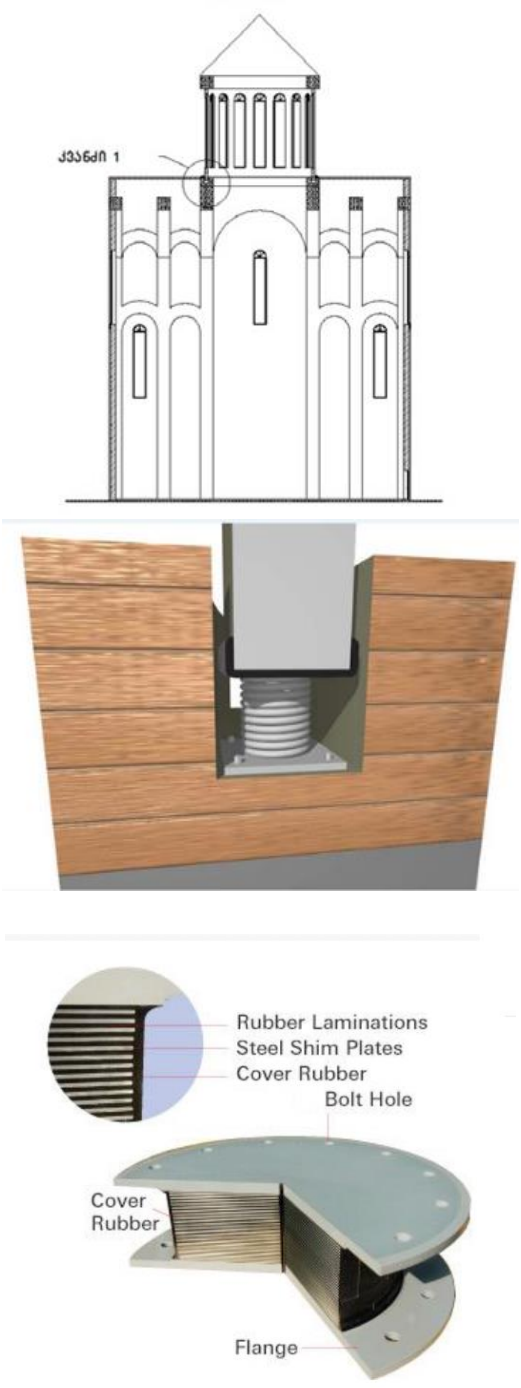

Fig. 5. temple slit; Seismic Isolating Rubber

Conclusion

As the analysis of the results of strong earthquakes shows, the contact zone between the under-domed part of the temple and the dome is the most damaged and often becomes the cause of the collapse of the dome. Tensile stresses caused by seismic impact in this zone are several times higher than the calculated tensile resistance of the stone (brick) pile. Therefore, it is possible to specify the purpose of our proposed dampers - to reduce as much as possible the value of seismic bending moments in the mentioned contact zone, which will minimize the value of tensile stresses.

References

1. Beridze Vakhtang, "Ancient Georgian Architecture" - volume, 1974; (Georgia)

2. Khoshtaria D., "Churches and monasteries of Klarjeti", Tbilisi, 2005 (Georgia)

3. Khmelidze T., Kifiani G., Khmelidze K., Vanishvili, "Monuments of Georgian Architecture". "Universal" publishing house, Tbilisi 2018, 202 p. (Georgia)

4. Silogava V., «Oshki X century. Memorial Temple", Vol. 2006, ISBN 99940-890-6-4; (Georgia)

5. Mamardashvili G., Lebanidze A., "Anti-seismic measures in Georgian architectural monuments", 2nd international symposium "Seismic resistance and engineering seismology", collection of reports. p. 161-163. (Georgia)

KINETIC AND THERMODYNAMIC CONDITIONS OF THE REBINDER EFECT

Nino Ptskialadze

Georgian Technical University, Tbilisi 0170, Georgia.
ptskialadzenino@yahoo.com

Abstract. An important peculiarity of the Rebinder bond breaking in a solid body and energy compensation of adsorption-broken bonds. This undoubtedly requires three conditions: the presence of surface-active substance in the pre-disintegration zone, that is, the active substance should immediately follow the growing crack; The chemical or physico-chemical interaction of the active substance must be witnessed at the moment of disconnection; In a plastic material, the tension at the crack tip should be at least a certain value, that is, it should not relax quite quickly as a result of plastic deformation, and for brittle bodies, it should not be more than that which ensures disintegration without the participation of an active medium.

Key words: Surface-active substances, kinetic condition, thermodynamic condition, surface diffusion, Rebinder effect.

Introduction.

The Rebinder effect refers to the effect of the environment on the mechanical properties of solid bodies, which leads to a decrease in the surface energy of solid bodies at the boundary between their phases with the environment. Rebinder and his students have studied the reduction of the energy and strength of solid bodies in a surface-active environment on many systems: metal mono- and polycrystals, which are in contact or have their surface covered with a thin layer of more malleable metals; on covalent crystals; on ionic mono- and polycrystals of metals, such as salts, oxides, hydroxides, rock, which are in contact with water, aqueous solutions of surfactants and electrolytes; on graphite; on molecular mono- and polycrystals of organic compounds (naphthalene, anthracene and others), on thermoplastic polymers in contact with organic effect is the unity of time and place of two acts: liquids of different polarity and their aqueous solutions, etc.

An important step in the study of the thermodynamic basis of the Rebinder effect is related to the development of the idea that the surface energy of a solid body and hence its strength should be reduced when it comes into contact with liquids close to it in molecular nature. Such a surface-active environment for metals is represented by liquid, more soluble metals; for ionic crystals - solutions of ionic compounds (salts, oxides, hydroxides) and also water; For molecular organic crystals and polymers - organic liquids close to them in polarity. These representations of Rebinder became the basis of large-scale, multi-year research, which on the one hand demonstrated the universal thermodynamic nature of the Rebinder effect, and on the other hand revealed its strongly expressed specificity, That is, the property that this effect is manifested only under certain thermodynamic, kinetic and structural conditions. Initially, when experiments were conducted on polycrystalline materials, all polycrystalline grains had the same chemical composition. But many alloys, rock, building and composite materials contain a conglomerate of grains of different chemical composition. Therefore, grain boundaries have different natures. The boundaries formed by substances of the same composition are called cohesive, and the boundaries formed by the contact of grains of different composition are called adhesive. .

Main part.

Much of the work in studying the kinetics of fission crack development in the presence of an active environment has been done on metallic systems. Typically, the rate of crack growth in a layer was measured in tension or bending. The

contact condition and the supply of the liquid active phase to the growing crack were varied. For metal systems, they were able to vary the viscosity of active fluids. Consider typical cases. 1. A small drop on a large metal plate. flat uniform tense: When creating a condition, a crack in the plate is formed below the drop and grows from it on both sides. The volume of the crack practically immediately becomes larger than the volume of the drop and it sinks into the crack. In the wake of the enlarged crack, the further spread of the liquid is carried out through its flow, in the form of a wetting film on the cracked walls. Because polycrystals were used in the studies, and the cleavage in them usually occurred at the grain boundary, the crack surface possessed a fairly large roughness. Therefore, even at a significant edge angle, when solid metal is wetted with liquid, the liquid metal flows freely along the crack walls. As the crack grew, the film thickness decreased, its flow viscosity resistance increased, and the crack growth slowed down. At the same time, the liquid metal was absorbed into the crack walls, which would also contribute to the thinning of the liquid film and slowing down the growth of the crack. According to the experimental data, the crack growth rate in the presence of active melt and the creep rate of the melt on the free surface, the theoretical qualitative dependence of the current length of the crack l(t) on the time t and the mass of the droplet of the final length L is derived:

$$l(t) = (3mf/2d\eta\delta k)^{1/2}t^{1/2}$$

$$L = 2{,}56\,(C_0D^{1/2})^{-2{,}5}(f/\eta\delta k)^{1/2}(m/2a)^{3/5}$$

where η is viscosity; δ - liquid phase density; a – plate thickness; k ≈ 10 – coefficient for all sizes, considering the profile of the liquid layer near the spreading front; C_0 – solubility of liquid metal in solid; D – volumetric diffusion coefficient; f – the driving force of the flow process on the crack walls; f= kσsv -(σlv +kσsl), where k is the coefficient of density, and indices s, l, and v belong to solid, liquid, and gaseous phases according to the value of interphase energy σ. Some results of the study, which demonstrate a fairly good agreement between theory and experiment, are presented in Fig. 1 and 2.

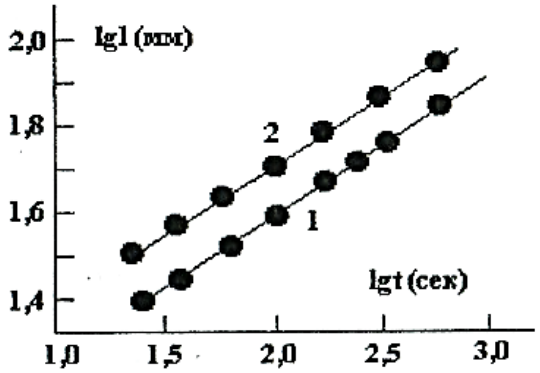

Fig. 1. Kinetics of crack growth in bending in a 1.85 mm thick zinc plate in the presence of 10 mg (1) and 40 mg (2) of mercury droplet.

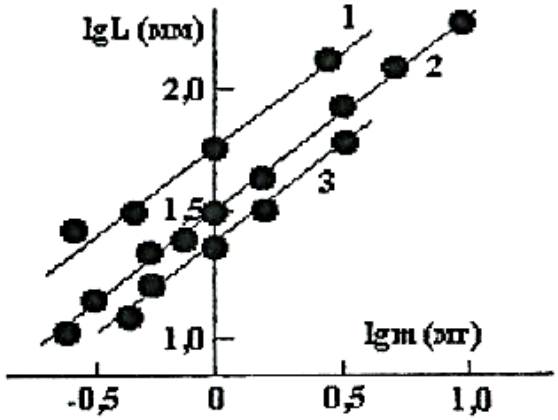

Fig. 2. Dependence of the maximum length of the crack on the mass of mercury drop of different thickness of zinc plate 1- 0.8; 2 – 1.8; 3 – 3.0 mm when bending

An important material in the study of the development of cracks in aluminum alloys,

when a drop of mercury is applied locally, is given by U. In the joint works of Rostocker and his collaborators. All of the sources mentioned above state that at higher loads, when the crack appears under the drop and begins to propagate, the crack begins to branch, with the earlier the higher the modeled stress. If the stress exceeds the strength of the material without the surface-active medium, then further cracking occurs without its participation.

2. Diffusion-migration kinetics. There was another type of kinetics, which ensured the presence of surfactants in the predisintegration zone, by impregnation of the cylindrical sample through surface diffusion in the medium, which is the surfactant for the given solid body. The maximum speed of jamming, at which the environment stopped working, was recorded. Investigated steel 45 in a solution of methyl iodide CH_2I_2 propyl spira. Methyl iodide softens steel cutting regardless of the concentration of the solution in the range of 5-50%, while propyl alcohol is practically inactive. The critical shear rate, which is not related to viscosity, confirms its invariable value in iodine solutions, in substances that differ sharply in viscosity, such as glycerin, ethylene glycol, propyl alcohol. The study of the dependence of the critical speed on the temperature, carried out on different surface-active substances for steel, allowed us to obtain the values of the activation energy and the pre-exponential multiplier in the kinetic equation, which describes the migration speed of the surface diffusion of the active substance in the dissolution zone:

$$V_c=V_0 \exp(-U_a/RT$$

The obtained data are presented in Table 1

Table 1.

V_0 and V_c values of the surface diffusion of active substances in the decomposition zone during steel 45 penetration, calculated according to the temperature dependence In $V_0(1/T)$

Active environment	V_0, m/sec	U_a kJ/mol	Temperature interval, k	Velocity interval cm/s
I_2	600±200	19,8±2,2	290-315	17-30
C_2H_5Br	9±1	10,0±1,0	270-320	18-25
$C_6H_{13}I$	9±1	10±1,0	270-320	18-25
C_6H_5I	12±2	10,5±1,2	270-320	18-25
CH_2I_2	1,2±0,2	5,5±0,8	290-330	13-17
CH Br_3	0,8±0,2	4,7±0,8	290-330	14-19

As can be seen from the table, the studied process is characterized by a very low value of energy activation, which indicates the delivery of surface-active substance by diffusion. In principle, two diffusion mechanisms are possible: gas Knudsen diffusion and surface diffusion. Knudsen diffusion appears less reliable, as a result of the dependence of the critical cutting speed on changes in the concentration of active substances in the medium and on the type of solvent, which may cause changes in gas flow parameters.

Boundary Kinetics. Different crack initiation kinetics occur when crack development is facilitated by a chemical reaction that has a sufficiently large activation energy and bond breaking time significantly exceeds the migration or flow of active substances into the cleavage zone. Such a situation is more clear and studied in the case of decomposition, crack growth or cracking in materials containing siloxane bonds and deformed in water, water vapor or polar liquids: glass,

quartz, sand, mountain rocks. In early works, dedicated to the dissolution of quartz materials under the influence of water, the action of water is explained by the fact that there is a concentration of stress in the tip of the crack and the solubility of the material is increased; Therefore, the crack grows as a result of local dissolution of the strained material. Such disintegration of glass and other materials in water has been attributed to stress corrosion cracking.

Charles and Hilling investigated the dependence of the crack growth rate of water-wetted quartz on the tensile stress at different temperatures. The energy of the activation process calculated by the Arrhenius equation was found to be 85 kJ/mol. An equation describing the experimental results was presented:

$$V = V_0 \exp[E + \sigma V * - \gamma V_m/\rho]RT$$

where V – crack growth rate; V0 – pre-exponential multiplier; E – activation energy, extrapolated to zero tension; γ-interphase energy; Vm – molar volume; ρ – radius of curvature and σ – tensile stress at the crack tip. On the one hand, very soon Bernstein's extensive and multifaceted research determined that the crack growth at its tip is not caused by the solubility of the material in tension, but by the mechanical activation of the hydrolytic cleavage of the siloxane bonds in accordance with the reaction

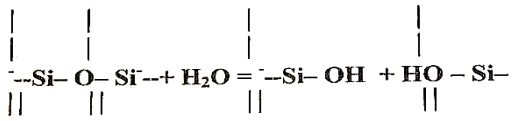

As a result of the breaking of siloxane bonds in the solid, which is responsible for propagating the crack over one interatomic distance. The activation energy of decomposition as well as the activation energy of quartz hydrolysis were found to be the same and equal to Charles, 85 kJ/mol. Thus, it was confirmed that mechanical stress in solid bodies significantly accelerates the chemical reaction of breaking chemical bonds. However, this statement can be thoroughly reformulated as follows: a chemical reaction facilitates the breaking of bonds, during which significant compensation of broken bonds takes place. If this is the case, it follows from a big difference, e.g.

The heat of wetting of pure and hydroxylated quartz surfaces by water, indicating a significant decrease in surface energy. Thus, at least for this system, the terms "Rebinder effect" and "stress corrosion" are completely equivalent.

A large series of studies on the development of cracks in glass in contact with water and steam was carried out by Wiederhorn. Tests were conducted on flexible glass plates. Some typical results of this paper are approximated by the author with Eq.

$$V = A.p^n \exp(-E/RT + \nu\sigma/RT$$

where A and n are constants; p – elasticity of water vapor; E – activation energy; ν-activation volume; σ-tension, four characteristic areas can be distinguished on this graph: I- crack development in water, which maintains a linear shape in a polylogarithmic scale in a wide range of speeds from one centimeter per day to one centimeter per second; II-similar performance of samples in the atmosphere of water vapor of different partial pressures; III- the transition of the graph in the zone of independence of the crack growth rate with the applied stress, which proves that the limited stage of the process is the transport of the active substance to the crack tip. And finally, IV - in which cleavage occurs practically without the participation of an active environment.

Many researchers have tried to determine the absolute magnitude of the surface tension of crystallites. The author set a goal to study the influence of the surface energy of a crystal

(calcite, rock salt, gypsum, quartz) on its mechanical and other properties, to reduce the surface tension of the crystal by introducing a surface-active substance into the environment, which forms a Gibbs-Langmurray layer at the boundary. The minimum force (P), which is required to populate the crystal, is reduced three times, four times and more by addition of surface-active substances (organic acids, alcohols, soap, etc.). By carrying out direct measurements of adsorption on a given crystal powder and conducting work on splitting along th e mesri, for example on wind, the author demonstrated the possibility of quantitative calculation of the sought effect; The explanation of the latter, as the author thinks, lies in the reduction of the connections of the elements of the surface frames by means of the adsorption of surface-active molecules. Also, when a surface-active substance (eg in water solution) is applied to the crystal, the strength of the crystalline crystal is greatly reduced, i.e. the amount of the smallest effort required to break the integrity - to scratch the surface. Maybe this effect is partially explained by turpentine, camphor and others. For use in glass drilling and cutting.

Volumetric study of the effect of physical adsorption of organic surface-active substances on the hardness of crystals, using the method of pendulum sclerometry, showed a significant effect of reducing the hardness. The hardness H was determined according to the amplitude A of the oscillation of the pendulum based on two points of the test crystal:

$$H = A_0 / (d A / d\tau)_0 = \tau_0$$

where τ_0 – the section on the time scale, which is cut by the arms of the amplitude curve of the pendulum oscillation at the starting point. Gypsum, calcite, barite, graphite crystals were investigated; Solutions of organic acids in water and non-polar solvents - vaseline oil were used as surface-active medium. In accordance with Rebinder's well-known rule, "polarity balance", effective adsorption of surface-active substances was observed at phase boundaries with different polarities: polar ionic crystals at the boundary with non-polar graphite hydrocarbon, non-polar graphite with water. The concentration dependence of the strength reduction H0– H (c) was found to be a symbiotic correspondence of the adsorption isotherm, and the maximum sign of the strength reduction corresponds to the saturated adsorption layer. As the adsorption according to Gibbs is unambiguously related to the reduction of the surface energy, these experiments directly show the reduction of the strength (durability) of the crystals as a result of the reduction of their surface energy at the expense of adsorption. Experiments conducted on the splitting of calcite crystals in surface-active substances and the splitting of crystals showed similar results, and with plastic materials - metals - another form of the Rebinder effect was detected: adsorption plasticization, manifested by the reduction of plastic deformation and plastic splitting. It was also found here that the maximum of the plasticizing effect is observed at the concentration of surface-active substances, which provides a saturated monomolecular layer. This phenomenon was further developed to perfect the explanation of the pressure treatment of metals. As surface-active substances for mountain rocks, with their ionic-covalent bond and ion exchange properties, some ions in water solution, predominantly multi-charged, with specific adsorption properties were found. This made it possible to implement an extensive program of using strength reducers in drilling.

An important stage in the study of the thermodynamic basis of the Rebinder effect is related to the development of the idea that the

greatest decrease in the surface-active energy of a solid body and, accordingly, a decrease in its strength should be expected when it comes into contact with a liquid that is close to it in molecular nature. Such a surface-active environment for metals is represented by liquid, easier to melt metals; for ionic crystals - melt and solutions of ionic compounds (salts, oxides, hydroxides), as well as water; For molecular organic crystals and polymers – organic liquids close to them in polarity. These representations of Rebinder became the basis of a large-scale, multi-year study, who have demonstrated, on the one hand, the general thermodynamic nature of the Rebinder effect, and on the other hand, its strongly expressed specificity, i.e., the property to be manifested only in strongly expressed thermodynamic, kinetic and structural conditions. Later, this situation was expanded and filled with ideas about the possibility of realizing the Rebinder effect of the chemical interaction of a solid body with the environment, under the conditions of a small value of the free energy generated by surface connections.

Conclusion.

Direct measurement, reduction of quantitative relationships of the surface energy of a solid body as a result of adsorption, wetting or other interaction with its environment, is a difficult problem to solve, first of all, it is practically impossible to measure the work of forming a new surface in a thermodynamic reversible process in a solid body. However, in some cases, it was possible to obtain fairly reliable data with the help of the methods used to measure the surface energy of a solid body (method of splitting crystals according to N.V. Obreimov, zero creep of Taman-Udin, measurement of the dihedral angle formed on the grain boundary surface, etc.). These methods are applicable to only a narrow category of materials and conditions. So, the splitting method is applicable only for such crystals, which are characterized by a perfect meser character, although there was an attempt to use them for glass, and the zero creep method - only for thin foils and threads, which are characterized by a special "bamboo-like" structure and only at high, pre-melting temperatures. The interpretation of the data in terms of thermal poisoning of the channels at the grain boundaries is complicated by the need to take into account the anisotropic free energy – which is different for different crystallographic directions. In the surface-active environment, these difficulties often increase significantly, so various indirect methods have been widely developed, which allow to predict with a good accuracy the strength reduction of the given material in the surface-active environment.

Reference

1. Alexeev A.D., Feldman E.P., Vasilenko T.A. Alteration of methane pressure in the closed pores of fossil coals. Fuel, 79(2000);
2. Lortkipanidze M.M. Technical diagnostics and non-destructive control. Kyiv. 2000. №3;
3. Pertsov N.V., Lortkipanidze M.M., Jojua T.A. Models and mechanisms of reversible creep of solids in surfactants. Collection of works of the International Scientific School «Vibrotechnology-2002» on mechanical processing of dispersed materials and media. Odessa. 2002;
4. Lortkipanidze M. The phenomenon of delayed reversible deformation of solids in surfactants. Part 1. Silicate materials//Energy 2002. №2. Tbilisi;
5. Lortkipanidze M.M., Jojua T.A. The influence of porosity on the strength of concrete and polymer-concrete // Energy. №4(24). 2002. Tbilisi;
6. Lortkipanidze M.M. Reversible creep of organic materials//Energy. №4(24). 2002. Tbilisi.

Davit Gurgenidze - 60 The Standard of the Exemplary Rector of the Era (A Leader Born for Building the University)

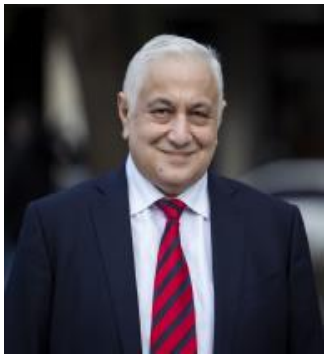

Davit Gurgenidze, an engineer-hydraulic technician and Honored Builder of Georgia, served as the Dean of the Faculty of Civil Engineering at the Georgian Technical University for four years. He holds the esteemed title of Academician in the Georgian National Academy of Sciences and is a member of the Presidium of the Academy. Additionally, Academician David Gurgenidze serves as the Chairman of the Permanent Conference of Rectors of Georgia and is a full member (academician) of the Engineering Academy of Georgia, as well as a member of the Georgian Energy Academy (Academician).

Moreover, he holds memberships in the Scientific Advisory Council of the Parliament of Georgia, the European Council of Construction Engineers (ECCE), and the World Council of Construction Engineers (WCCE). Academician Gurgenidze is an honorary member of the Georgian Society of Civil Engineers and has received honorary doctorates from institutions such as Egiazarov Institute of Water Problems and Hydrotechnics (Republic of Armenia), Bialystok Technical University (Poland), National Aviation University of Ukraine, and National University of Architecture and Construction of Armenia.

Recognitions of his contributions include the Order of Honor for his dedication to student education and youth development. The "International Fund of Journalists" awarded him the "Golden Wing" for his exceptional charity work and philanthropy. He has also received the State Order of the Republic of Lithuania - "Merit to Lithuania" - Knight's Cross. In recognition of his efforts in promoting Italian language and culture in Georgia, Academician Gurgenidze was honored with the Dante Alighieri gold medal and diploma by the Dante Alighieri Society in Rome. The presidium of the Georgian Culture Foundation conferred upon him the honorary title of laureate of the Ekvtime Takaishvili Prize and a bronze medal. Furthermore, he is awarded the Giorgi Nikoladze Medal by the Georgian Technical University.

Academician Gurgenidze is a prolific author with over 105 scientific works, including 2 inventions, 7 monographs, 7 manuals, 5 auxiliary manuals, and 1 encyclopedic dictionary (volume V). He has supervised the defense of 10 doctoral theses and is currently involved in coordinating several international grant projects.

His tenure as the leader of the Georgian Technical University is dedicated to the construction, development, and progress of the University. Despite facing challenges, Academician Gurgenidze is successfully implementing reforms that enhanced the university's recognition in the South Caucasus and globally. Under his leadership, the English-language undergraduate program in Biomedical Engineering obtained international ABET accreditation, showcasing the positive impact of his strategic initiatives.

Academician Gurgenidze is playing a crucial role in expanding the university's cultural and sports activities, fostering a sense of tradition and success among the students. Notably, he revitalized the public theater-studio "Modinakhem," allowing GTU students to showcase their talents on both national and international stages.

His efforts in deepening cooperation with renowned institutions such as CERN, KEK, J-Parc, FERMILAB, and other leading European research centers have facilitated

significant advancements in science and international collaboration for scientists and students at the University.

Academician Gurgenidze's leadership has resulted in a growing interest among potential students, leading to an increase in enrollment. His support has elevated the motivation of students, aligning the educational process with European standards. Elected as the rector of the Georgian Technical University in 2020 by the Academic Council of GTU, Academician Gurgenidze has tirelessly devoted his energy and passion to transformation of his alma mater into a European university.

Endowed with qualities befitting a leader, Academician Gurgenidze exemplifies the virtues of a teacher through his energy, friendship, and courage. He serves as a role model for many with his intelligence and generosity. His organizational talent and large-scale thinking, characteristic of a scientist, have propelled the University to new heights.

As Academician Davit Gurgenidze celebrates his 60th birthday, we extend our congratulations and best wishes. May he continue to exhibit courage, inexhaustible energy, and contribute to the longevity, professional success, and happiness of his family. We express gratitude for his dedication to the Georgian Technical University and our country. May he steadfastly uphold the scales of characteristic truth, exemplifying nobility in all endeavors.

Sincerely,
Georgian Technical University, Faculty of Civil Engineering,
The Editorial Board of the Magazine "Construction",
"Theoretical and Applied Mechanics National Committee of Georgia,"
"Union of Mechanics of Georgia"

Zurab Gvishiani - 60

Today there is a shortage of people in Georgia. It is all the more necessary to bring the professional activity and human kindness of each family member to the fore. Our jubilee is the dean of the Faculty of Civil Engineering of the Georgian Technical University, Professor Zurab Gvishian, who turned 60 years old this fall. In 1985, he graduated from the Polytechnic Institute of Georgia and was awarded the qualification of an engineer-hydraulic technician. For years, he worked in the Ministry of Agriculture, in the design institute "Saksakhtskalprojekti" in various positions. He was a graduate student of the Scientific-Research Institute of Hydrotechnics and Reclamation of Georgia and a senior scientist-collaborator of the Department of Natural Catastrophic Events. In 1994, he defended his dissertation on the topic "Investigation of the physical-mechanical indicators of torrential flows" and was awarded the scientific degree of Candidate of Technical Sciences. In 1998, he was awarded the scientific-pedagogical title of docent of the Agrarian University of Georgia, specializing in hydraulic engineering and reclamation construction. In 2004-2015, he was the founder and rector of "Georgian-British University of International Law and Management" LLC. 2020-2021, he was the acting dean of the Faculty of Construction of the Georgian Technical University. From 2021 until now, he has been elected to the position of the Dean of the Faculty of Civil engineering of GTU.

I met Mr. Gvishiani at the Georgian Technical University. From the first meeting, he made an amazing impression on me as a professional, uncompromising, and tireless person. He is a great fan of students and employees. This was evident in the business situation and in the evenings related to the days of the Faculty of Civil engineering. While on a business trip abroad, he constantly takes care of presenting the Faculty of Civil engineering of the Georgian Technical University in a dignified manner. Working next to him and under his direct guidance helps not only me but also many of my colleagues in their professional and career advancement. Mr. Gvishiani has a great family. He is an exemplary husband and father. His family is connected with the Georgian Technical University. His wife, Mrs. Marina Mghebrishvili, is a senior researcher and the learned secretary of the Institute of Water Management named after Tsotne Mirtskhulava. Son - Vakhtang, deputy dean of the Faculty of Energy of GTU in the matters of science and international relations.

On behalf of a large family of builders, I would like to congratulate Mr. Gvishiani on a remarkable date and sincerely wish him good health, endless energy, and success in his professional activities, so that he may continue to work with his usual attitude for the benefit of our country and the Georgian Technical University.

Georgia Technical University, Faculty of Civil Engineering,
The Editorial Board of the Magazine "Construction",
"Theoretical and Applied Mechanics National Committee of Georgia,"
"Union of Mechanics of Georgia"

Scientist, Teacher, and Engineer

Merab Dzidziguri, a well-known road construction specialist in Georgia, crossed the 80-year mark. He belongs to the group of meritorious specialists who have been working humbly but enthusiastically for ten years and are leading their professional activities perfectly.

M. Dzidziguri was born in 1942 in Yaneti village of Samtredia district in a family of teachers. His father Shalva went to the front before the birth of his son and never came back. After graduating from high school, M. Dzidziguri served in the Soviet army, after demobilization in

1959-65 he studied at the Polytechnic Institute of G eorgia, majoring in "motorways".

In 1967-70, he studied in post-graduate studies under the guidance of the famous Georgian scientist and teacher Vlasi Goglidze. Even then, his many positive qualities were revealed: ambitious, dedicated to work, with original ideas, a young scientist. He was a leading member of the group developing the theory of road composite phenyls. In his scientific articles and candidate thesis, for the first time in the former USSR, the theory of composite road phenyls developed at a high scientific level was reflected. After defending his thesis, M. Dzidziguri worked as a docent at the Polytechnic Institute. For years he was the learned secretary of the Faculty of Transport. Generations of Georgian Megzeve engineers who have completed 50-70 years remember well the lectures-seminars conducted with deep knowledge of his work, his principles and at the same time fair rigor in assessing students' knowledge. Along with pedagogical work, M. Dzidziguri was engaged in active scientific activities. His areas of interest were the theory of calculation of rigid and semi-rigid road panels and the use of local materials. Together with the well-known road specialist Otar Diasamidze, he was the first in the USSR to use the finite element method in the calculation of road surfaces, which was widely reflected in the scientific and technical periodicals of the USSR and abroad.

Separately, M. Dzidziguri's fundamental work "Road Construction Materials" should be mentioned, which is the only one in the literature published in the Georgian language in this field. All types of inert or binding materials used in road construction are widely presented in the work, their physical-mechanical properties and chemical composition are described, the perspectives of creating and introducing new materials are shown. The monograph is written in excellent Georgian language, along with deep scientific analysis, it is presented in a simple and understandable way. Since 1988, M. Dzidziguri has been on practical work. For years, he headed the largest road construction department in Tbilisi, which, thanks to his efforts, was transformed into a powerful joint-stock company "Road Company Tbilisi" in 1992. Under his leadership, Mtkvari left and right bank highways, Tsotne Dadiani Street, Guramishvili Avenue, Tbilisi-Airport Expressway and many other road objects in Tbilisi and its surroundings were built and repaired. M. Dzidziguri repeatedly represented Georgian Megzeve specialists abroad. For years, he participated in the US program "Sabit", which was dedicated to the problems of introducing new techniques and technologies in the advanced countries of the world.

To this day, he actively works as a scientist and consultant in the theory of road construction, participates in solving engineering problems, shares his rich life and professional experience with young colleagues. Creates a new monograph dedicated to road construction materials,

Where modern achievements in the theory and practice of creating and inventing original road construction materials will be widely covered.

The Society of Roadmen of Georgia, the Presidium of the Roadmen's Association, his colleagues, friends and former students, the editors of the "Mshenebli" magazine sincerely congratulate Mr. Merab Dzidziguri on his jubilee meeting, and express their wish that he will spend many more years for the development of road construction in Georgia.

Georgian Travelers Society,
Presidium of the Association of Travelers Stu
Traffic Department Collective, friends and colleagues.
Editorial office of "Building" magazine.

Is published in the prepared by author's format.